



**Politecnico  
di Torino**

Master's Degree Course in  
Mechanical Engineering

Master's Thesis in Mechanical Engineering

# **Systematic approach to the design of additively manufactured products**

Guidelines definition for a suitable trade off

**Supervisor:**

Prof. Eugenio Brusa

**Co-supervisors:**

Prof. Cristiana Delprete

Ing. Lorenzo Giorio

**Candidate:**

Filippo Mazzoni

April 2022



# Acknowledgements

My academic journey came to an end and I am really satisfied about it. There have been both easy and tough periods and from both of them I had the opportunity to learn and grow. Politecnico has been a severe teacher especially at the beginning but, time after time, I learned to appreciate it and if I could go back I would take the same choices. Now I know that one day at a time, being able to set the first things first and having the courage to change when circumstances require it, I can reach my goals and be proud of the results I get.

I would like to start by thanking my thesis supervisors professors Eugenio Brusa and Cristiana Delprete. They guide me in giving the right direction to the analysis that I did. They encouraged me by appreciating the extensive literature research that I did and the methodological approach that I applied. Then, they gave me precious suggestions on how to add a value to the many information that I found and how to express them properly through my work. This thesis is the result of the constant cooperation without which, today, I would not have been able to approach additive manufacturing systems with such a wide view.

Today I can say that I am who I am thanks to my parents, my sister, my grandparents (and also my grand-grandmother), my uncles and my cousins that have always been there. You are my roots and my pillars and there are no trees that can grow up without their roots nor houses that can stand without foundations.

I would like to thank my friends from wherever they come, both the “friends of a lifetime” and those that I had the opportunity to meet during my living in Torino. Thanks to all of you today I have a big bag full of precious memories!

To the person that surprised me coming to Torino after 7 years that we haven't seen each other. Our paths took different directions and then we met again. You believed in me whenever I was not able to do so. You have always been by my side. You gave me the opportunity to enlarge my family with other beautiful members and to share my life with you. I hope that you feel loved at least half of what I feel!

I wish us all to keep sharing moments and memories together!

*A door has just been closed but others will open soon!*



# Summary

The purpose of this thesis is to investigate the influence of the design parameters on the characteristics of the final component, providing guidelines that can help the engineer in the design of additively manufactured components. The analysis is limited to two additive manufacturing techniques (selective laser melting and electron beam melting) and to three types of alloys (Al-alloys, Ti-alloys and Ni-alloys).

The initial identification of all the parameters is described in the introduction. After an extensive literature research, the various characteristics, methods, and approaches have been classified under different categories: models/approaches, process parameters, defect types, production techniques, materials, properties, and inspection techniques. Then, the production process has been investigated from its early design stages to the final manufacturing phase. The analysis has been carried out in three steps.

In *Step 1: Material selection* the designer will find the properties and the related standards useful to characterize the raw powder, and a description of aluminium, titanium and nickel alloys, with a focus on the main issues related to their manufacturability through AM techniques. In addition, it can be found an introduction to more recent solutions related to the choice of the raw powder such as: powder additives, compositionally graded materials and hybrid materials.

*Step 2: approaching topology optimization* wants to give a basic idea of what is a topological optimization. The examples provided have been classified under two categories: macro and micro topology optimization. The macro-topology optimization refers to analysis performed on the whole component, while the micro-topology optimization to those focused on the improvement of unit cells composing the lattice structure.

*Step 3: Tuning parameters* explores the manufacturing phase and aims at providing guidelines consisting in suggestions, analysis of the trends, process windows and ranges of parameters and properties, that can be used as a reference or as a measure of comparison in design or experimental activities. In the first part the typical microstructures resulting from additively manufacturing aluminium, titanium and nickel alloys are briefly described. The most important part is devoted to the parameters-properties relations. The factors related to material, part design, process-machine and environment,

scanning, melt pool and heat treatments are analyzed individually to understand their influence on mechanical and geometrical properties, defects and porosity.

Then, brief remarks related to AM economics are reported. In the final part a case study is explored. The guidelines provided along the previous three steps are used to apply a reverse engineering approach to an aerospace bracket manufactured in Ti6Al4V alloy via selective laser melting.



# Contents

<b>List of Figures</b>	<b>XIII</b>
<b>List of Tables</b>	<b>XIX</b>
<b>Introduction</b>	<b>1</b>
AM market trend . . . . .	3
Intercepting the need and identifying the requirement . . . . .	4
A step back: AM features . . . . .	5
Models/Approaches . . . . .	5
Data elaboration models . . . . .	5
Process models . . . . .	8
Commercial process control solutions . . . . .	8
Process parameters . . . . .	10
Scanning strategy . . . . .	14
Defects . . . . .	15
Materials . . . . .	15
Properties . . . . .	15
Inspection techniques . . . . .	18
Scanning technologies . . . . .	21
Standards . . . . .	22
File formats . . . . .	23
Classification method . . . . .	25
Pathway definition . . . . .	29
<b>I Design</b>	<b>31</b>
<b>Step 1: Material selection</b>	<b>35</b>
Powders . . . . .	37
Types of powders . . . . .	37
Traditional powders . . . . .	37
New types of powders . . . . .	41

Powder analysis . . . . .	42
Powder additives . . . . .	44
Compositionally graded materials . . . . .	44
Hybrid materials . . . . .	45
Other solutions . . . . .	46
<b>Step 2: approaching topology optimization</b>	<b>47</b>
Topology optimization and how it works . . . . .	48
Topology optimization approaches . . . . .	50
Macro-topology optimization . . . . .	51
Micro-topology optimization . . . . .	52
<b>II Manufacturing</b>	<b>55</b>
<b>Step 3: Tuning parameters</b>	<b>59</b>
Production techniques . . . . .	61
Materials microstructure . . . . .	62
Titanium alloys microstructure . . . . .	62
Nickel alloys microstructure . . . . .	63
Aluminum alloys microstructure . . . . .	65
Parameters-Properties analysis . . . . .	66
Material factors on properties . . . . .	69
Material factors on mechanical properties . . . . .	74
Material factors on ductility and hardness . . . . .	74
Material factors on geometry and defects . . . . .	75
Material factors - Guidelines . . . . .	76
Part design factors . . . . .	78
Part design factors on mechanical properties . . . . .	78
Building orientation on mechanical properties . . . . .	78
Lattice type on mechanical properties . . . . .	79
Part design factors on mechanical properties - Guidelines . . . . .	84
Part design factors on geometry and defects . . . . .	86
Building orientation on manufacturability and surface characteristics . . . . .	86
Support structures on manufacturability and defects . . . . .	90
Part design factors on lattice geometry and defects . . . . .	92
Part design factors on geometry and defects - Guidelines . . . . .	93
Process-machine and environmental factors on properties . . . . .	95
Scanning factors . . . . .	97
Scanning factors on mechanical properties . . . . .	98
Scanning factors on mechanical properties - process windows . . . . .	105

Scanning factors on hardness . . . . .	106
Scanning factors on porosity . . . . .	112
Scanning factors on porosity - Process windows . . . . .	121
Scanning factors on geometrical properties and defects . . . . .	122
Melt pool analysis . . . . .	125
Heat treatments . . . . .	132
Heat treatments on mechanical properties, ductility and hardness	132
Heat treatment on porosity, geometry, and defects . . . . .	140
Defects . . . . .	144
<b>AM economics</b>	<b>147</b>
<b>Case study - reverse engineering approach</b>	<b>151</b>
<b>Conclusion</b>	<b>157</b>
<b>Bibliography</b>	<b>163</b>



# List of Figures

1	Hystorical evolution of Traditional manufacturing and Additive Manufacturing [3]. . . . .	2
2	Number of on-line research results per year [4]. . . . .	2
3	Publications per year [5]. . . . .	2
4	AM market growth and forecast [6]. . . . .	3
5	AM market distribution [7]. . . . .	3
6	Classes used to classify various aspects. . . . .	5
7	Classification of the Data elaboration models (Adapted from [11]). . . . .	6
8	Classification of the Process models (Adapted from [18]). . . . .	9
9	Classification of the Commercial software solutions. . . . .	9
10	Process parameters. . . . .	11
11	In-process parameters. . . . .	12
12	Sub-classification of process parameters. . . . .	13
13	Examples of common scanning strategies. At bottom: (a) raster, (b) bidirectional, (c) offset-in, (d) offset-out, (e) fractal postmanufacturing processing. . . . .	14
14	Defects list and classification. . . . .	16
15	Metal alloys most commonly studied. . . . .	17
16	Properties most commonly studied. . . . .	17
17	Inspection techniques. . . . .	19
18	3D point cloud data and Sensor-Based Process techniques. . . . .	20
19	Scanning technologies. . . . .	21
20	Metrology standards. . . . .	22
21	Data formats. . . . .	23
22	Data formats. . . . .	24
23	Production technique - Cell type. . . . .	26
24	Data elaboration models/approaches - Material. . . . .	27
25	Design parameters - Properties. . . . .	28
26	AM manufacturing steps. . . . .	30
27	Materials selection. . . . .	36
28	Number of material products for the main AM production techniques (2020) [24]. . . . .	37

29	Metal products available for each year [24]. . . . .	38
30	Cost of Ti at different production phases [32]. . . . .	39
31	Ti-6Al-4V UTS, YS and elongation for different production techniques [21]. . . . .	40
32	Ni-alloys weldability [33]. . . . .	41
33	Topology optimization approaches. . . . .	47
34	Topology, shape and size optimization [51]. . . . .	49
35	a) TO basic algorithm [23]; b) 2-level TO algorithm [52]. . . . .	49
36	Manufacturing phases. . . . .	57
37	List of design parameters and properties. . . . .	60
38	AM techniques and methods [68]. . . . .	61
39	Evolution of polymer 3D printing hardware revenues from use in professional environments: 2017 vs. 2027. . . . .	61
40	Ti-6Al-4V phase diagram [28]. . . . .	63
41	Ni-alloys for PBF [33]. . . . .	64
42	Al-Si phase diagram [72]. . . . .	65
43	Legend of the colors used in Figure 44. . . . .	66
44	Design-Properties table alloys classification. . . . .	68
45	Material factors on properties. . . . .	69
46	a) PSDs for fine and coarse powders, b) agglomerates of fine and coarse powder [95]. . . . .	71
47	Powder analysis revealing: a) powder satellites (arrows) and powder sphericity (circles), b) PSD, c) inner gas pores, d) SEM images [105]. . . . .	73
48	Hardness of the Nb-alloy with addition of Mo and Zr before and after HT [38]. . . . .	74
49	a) defects size and density and b) surface roughness for fine and coarse powders and different building locations. [95]. . . . .	75
50	Part design factors on mechanical properties. . . . .	78
51	Tensile properties of Ti6Al4V for SLMed and EBMed specimens, for different sizes and orientations (dashed rectangles refer to wrought alloys) [83]. . . . .	80
52	Stress-strain curves for different unit cell types (AlSi12Mg, uniaxial compression tests) [98]. . . . .	81
53	(a) cubic Ti6Al4V lattice structures failures modes, mode 1 SLM (b) and EBM (c), mode 2 EBM (d), mode 3 EBM (e), 45° brittle lattice failure for EBM (f) (g) (h) [80]. . . . .	83
54	Collapse of lattice specimens (SLMed in AlSi10Mg) for BCCZ (a) and BCC (b) [81]. . . . .	84
55	Part design factors on porosity, geometry and defects. . . . .	86
56	Effects of EDM wire cutting and heat treatment on upskin and downskin surface flatness (SLMed Ti6Al4V) [74]. . . . .	87

57	Effects of building orientation on the upskin and the downskin surface flatness [74]. . . . .	88
58	$R_{sm}$ and the staircase effect [74]. . . . .	88
59	Sloping angle effect on $R_a$ for upward a) and downward b) surfaces [90].	89
60	Effect of build angle on $R_{sm}$ for profiles perpendicular a) and parallel b) to the weld tracks [74]. . . . .	90
61	Effect of back and forth scanning strategy on $R_{sm}$ [74]. . . . .	90
62	EBM vs. SLM surface finish [83]. . . . .	91
63	Ti6Al4V and AlSi12Mg SLMed lattice struts manufacturing constraints. Legenda: L = many defects, M = some defects, H = successfully manufactured. a) strut diameter vs. build angle, b) strut diameter vs. span [98].	92
64	SLMed AlSi12Mg lattice struts build angle on surface roughness [98]. .	93
65	Process-machine and environmental factors on properties. . . . .	95
66	Effect of $N_2$ shielding gas (SG) and filled build chamber (BG) on stress-strain curve for SS 316L [93]. . . . .	96
67	Scanning factors on mechanical properties. . . . .	98
68	SLMed AlSi10Mg lattice specimens under compression. Stress-strain curves for different (150-400 W) laser powers at fixed (7000 mm/s) scanning speed a) and for different scanning speeds (1000-7000 mm/s) at fixed (400 W) laser power c). Maximum stress vs. laser power at fixed scanning speed (7000 mm/s) b) and maximum stress vs. laser scanning speed at fixed laser power (400 W) c). Effective and specific normalized strength vs. laser power at fixed scanning speed (7000 mm/s) e) and f), and for different scanning speeds (1000-7000 mm/s) at fixed (400 W) laser power g) and h) [96]. . . . .	100
69	SLMed AlSi10Mg specimens. UTS dependence upon laser power, energy density, hatch spacing and scan speed for as-built and machined specimens a). Yield strength dependence upon laser power, energy density, hatch spacing and scan speed b) [13]. . . . .	101
70	SLMed Al6061 specimens. UTS dependence upon laser power, energy density, hatch spacing and scan speed for as-built and machined specimens a). Yield strength dependence upon laser power, energy density, hatch spacing and scan speed [13]. . . . .	102
71	a) energy density vs. compressive yield strength (CYS) and ultimate compressive strength (UCS), b) porosity vs. CYS and UCS [97]. . . . .	103
72	Mechanical properties at room temperature of SLMed Ti6Al4V specimens [16]. . . . .	104
73	Scanning factors on mechanical properties. . . . .	106
74	SLMed as-built AlSi10Mg specimens. Effects of laser power, energy density, hatch spacing and scan speed on micro-hardness along the X direction a) and along the XY plane [13]. . . . .	108

75	SLMed AlSi10Mg specimens. Main effects (laser power, scan speed and hatch distance) and interaction plots for hardness (HB) [102]. . . . .	109
76	DMLSed AlSi10Mg specimens. Energy density on hardness, identification of a processing window ( $h_d$ : hatching distance) [104]. . . . .	109
77	SLMed as-built Al6061 specimens. Effects of laser power, energy density, hatch spacing and scan speed on micro-hardness along the Z direction a), and along the XY plane b) [13]. . . . .	110
78	SLMed as-built Alloy 718 specimens. Effects of laser energy on hardness [94]. . . . .	111
79	Scanning factors on porosity. . . . .	112
80	SLMed TiB <sub>2</sub> /AlSi10Mg samples. Scan speed vs. relative density for different raw powders [30]. . . . .	113
81	Energy input (J) vs. porosity for 90° (a) and 35.26° (b) inclination (OL = weld overlap) [108]. . . . .	114
82	SLMed AlSi10Mg lattice struts. a): laser power vs. area fraction of porosity at fixed scan speed (7000 mm/s). b): scan speed vs. area fraction of porosity at fixed laser power (400 W) [96]. . . . .	114
83	Energy density vs. porosity for constant 200 W laser power, 600-1260 mm/s scan speed and 30-120 $\mu$ m hatching distance (SLM, Ti6Al4V) [97]. . . . .	116
84	Scanning strategies for EBM (a) and SLM (b) Ti6Al4V manufactured specimens [83]. . . . .	116
85	a) Porosity vs. scanning factors for SLMed Ti6Al4V samples. b) Porosity vs. scanning factors for EBMed Ti6Al4V samples ( b1) and b4) result from Taguchi experimental factors) [106]. . . . .	117
86	Dependence of porosity on laser power for 870, 1000 and 1200 mm/s scan speed at 3 hatching distances: a) 0.05 mm, b) 0.08 mm and c) 0.11 mm (SLM, Hastelloy X) [92]. . . . .	119
87	Optical microscopy images for different laser exposure time ( $\mu$ s) and point distance ( $\mu$ m) with relative values of the laser energy input ( $J/mm^3$ ) (SLM, Alloy 718) [94]. . . . .	120
88	Scanning factors on geometrical properties and defects. . . . .	122
89	Dependence of the strut diameter on: a) laser scanning speed (power = 400 W); b) laser power (scan speed = 7000 mm/s). Nominal diameter = 300 $\mu$ m [96].	123
90	Design parameters on melt pool morphology. . . . .	125
91	Melt pool on properties. . . . .	125
92	a) Schematic of the thermal phenomena occurring during L-PBF process [17]. b) Vertical section of the melt pool with nomenclature [136].	126
93	A) Gaussian distribution of heat for laser spot diameter of (a) 50 $\mu$ m, (b) 100 $\mu$ m, (c) 150 $\mu$ m and (d) 200 $\mu$ m. B) Melt pool temperature vs. laser spot diameter for various scan speed at 150 W laser power (SLM, 316L SS) [116]. . . . .	127

94	Melt pool temperature vs. laser power for various scan speed at 80 $\mu\text{m}$ spot diameter (SLM, 316L SS) [116]. . . . .	128
95	a) energy density vs. width of the scan track and b) energy density vs. height of the scan track for 3 different specimens (DMLS, AlSi10Mg) [104].	129
96	Interactions between the electron beam and the powder: a) spattered molten jets and b) smoking [15]. . . . .	130
97	Focus offset vs. melt pool shape [15]. . . . .	131
98	Heat treatments on mechanical properties, ductility and hardness. . . .	132
99	Effect of heat treatments (Table 10) on properties of AlSi10Mg SLMed samples for different aging times at 177 $^{\circ}\text{C}$ along Z and XY directions: (a) and (d) YS; (b) and (e) UTS; (c) and (f) elongation (from [137]). . . .	134
100	Compressive stress-strain curves for as-built and heat treated Ti6Al4V lattice specimens (4 mm cell size)[123]. . . . .	136
101	Tensile stress-strain curves for EBMed Ti6Al4V specimens after various heat treatments [125] . . . . .	136
102	Effect of heat treatment temperature on (a) hardness and on (b) lattice parameter of $\gamma$ phase of L-PBF Inconel 718 [131]. . . . .	139
103	Heat treatments on mechanical properties, ductility and hardness. . . .	140
104	(a) effect of the heat treatment on the surface waviness at nanoscale [74]. Effect of chemical etching (30 min) on porosity (b) and surface roughness (c) (Ti6Al4V). [75] . . . . .	141
105	Effects of heat treatments on the length and amount of cracks for PBF Alloy 718 [12]. . . . .	142
106	Effects of HT temperatures on sub-surface principal stresses for L-PBF Inconel 718 (from [131]). . . . .	143
107	Defects on mechanical properties . . . . .	144
108	Defects on porosity. . . . .	144
109	Fracture path and defects comparison for $\text{TiB}_2/\text{AlSi10Mg}$ and AlSi10Mg [73].	145
110	Cost of per unit of parts produced with conventional and additive manufacturing [1]. . . . .	147
111	Complexity vs. cost for conventional and additive manufacturing [139].	148
112	Tensile test results for material characterization [138]. . . . .	151
113	Original (left) and optimized (right) designs [138]. . . . .	151
114	EBM (a) and SLM (b) AMed aerospace bracket. Surface roughness of the EBM (c) and SLM (d) parts. Defects detection from tomographic analysis of EBM component (e), dimensional control on the SLM bracket (f) [138].	152
115	Powder size and spot size ranges for SLMed Al, Ti and Ni alloys [73, 76, 74, 80, 81, 83, 89, 91, 92, 30, 96, 97, 13, 98, 99, 101, 102, 104, 105, 75, 87, 14].	159
116	Laser power, scanning speed and hatch spacing ranges for SLMed Al, Ti and Ni alloys [73, 76, 74, 80, 81, 83, 89, 91, 92, 30, 96, 97, 13, 98, 99, 101, 102, 104, 105, 75, 87, 14]. . . . .	160



# List of Tables

1	Titanium, Aluminum and Iron properties. . . . .	38
2	Powder properties, measuring methods and standards. . . . .	43
3	Macroscopic topological optimization approaches. . . . .	51
4	Microscopic topological optimization approaches. . . . .	52
5	Powder properties for Ti6Al4V fine and coarse powders (from [95]). . .	71
6	Powder sizes for different materials. . . . .	72
7	Young's moduli and $\sigma_{\max}$ for BCC to BCCZ cell types in AlSi10Mg (elaborated from [81]). . . . .	81
8	Scanning factors on mechanical properties - process windows. . . . .	105
9	Scanning factors on porosity - process windows. . . . .	121
10	Heat treatments (from [137]). . . . .	132
11	Heat treatments on mechanical properties - process windows for AlSi10Mg (elaborated from [91] and [137]). . . . .	133
12	Heat treatments on mechanical properties for Ti6Al4V alloy. . . . .	137
13	Heat treatments on mechanical properties - process windows for L-PBF Inconel 718 and DED Inconel 625 (elaborated from [130] and [120]). . .	139
14	Effect of HIP and chemical etching on surface finish (EBM, Ti6Al4V) (elaborated from [125]). . . . .	141



# Introduction

Additive manufacturing (AM) is a formal term that includes many different production techniques as expressed by Diegel et Al. [1]:

*”Additive manufacturing (AM) encompasses a range of technologies that allows physical components to be made, from virtual 3D models by building the component layer-upon-layer until the part is complete.”*

Adding material layer-by-layer is the basic principle of all the AM production methods as stated by Gibson et Al. [2]:

*”The key to how AM works is that parts are made by adding material in layers; each layer is a thin cross-section of the part derived from the original CAD data.”*

Modern Additive Manufacturing first appeared in the mid-20th century and it slowly developed in the following decades (Fig. 1). Its initial success has been due to the reduced time needed to produce a single piece or a small number of pieces, this is why it is also called rapid prototyping (RP) or rapid manufacturing. This definition is, especially today, not very appropriate since the parts produced are very often final parts that can directly satisfy many purposes and are not only prototypes. 3D printing is the most popular definition given to the various additive manufacturing techniques and it better reflects how the manufacturing process works [2]. Starting from a 3D CAD virtual model the material is added layer-by-layer, as opposite to traditional manufacturing where the material is removed from an initial bulk piece until the wanted shape is obtained [1].

AM can hence be more suitable than traditional manufacturing in many applications. The difference do not rely only on the on the practical method adopted to produce a component, but should be also considered during the design phases starting from its early stages. The different approaches and methods adopted cover different areas of what is called *Design for Additive Manufacturing (DfAM)* [4].

Recently the efforts to exploit its full potential are increasing very rapidly and this can be easily perceived doing an on-line research (Fig. 2) or looking at how many publications related to AM have been published during the last years (Fig. 3).

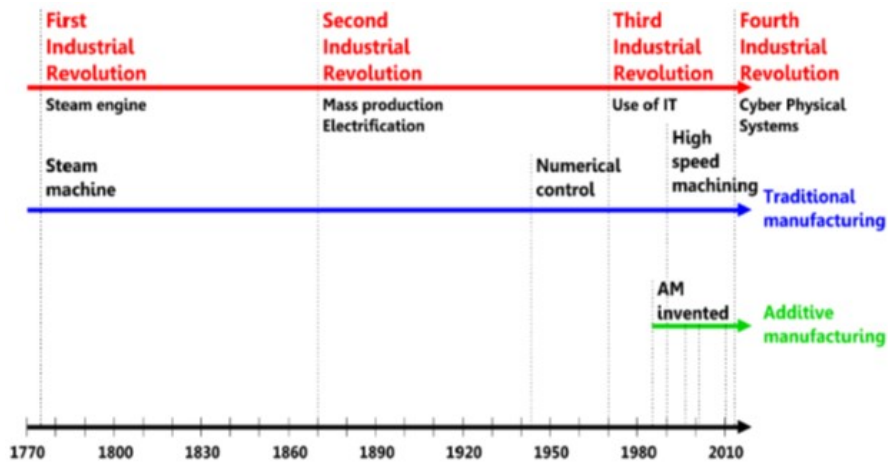


Figure 1: Historical evolution of Traditional manufacturing and Additive Manufacturing [3].

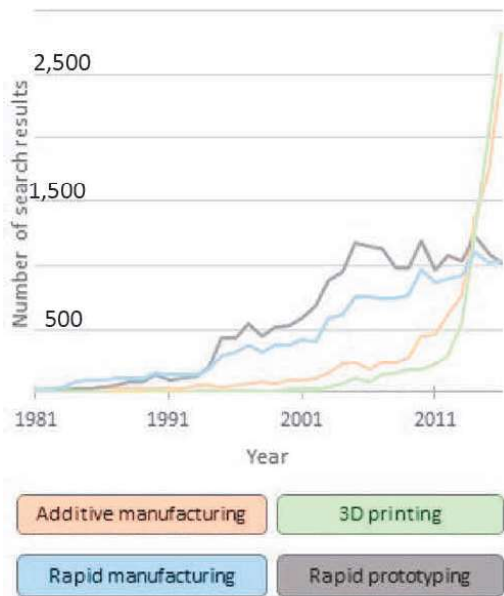


Figure 2: Number of on-line research results per year [4].

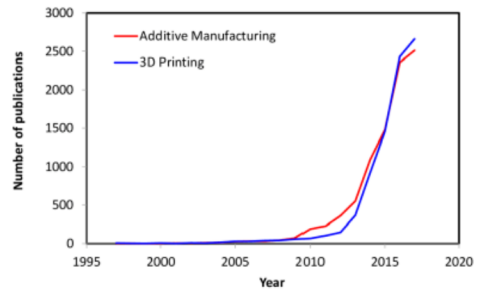


Figure 3: Publications per year [5].

## AM market trend



Figure 4: AM market growth and forecast [6].

In recent periods AM manufacturing market has experienced a very strong growth like never before. Around 2010 AM was increasing at an annual rate of 33% and kept increasing until today with an impressive market size of more than 20 billions in 2020 [8]. Despite of the fact that the implementation of AM in many sectors could be slow, the number of experts and researchers is increasing and the market related to AM is also expected to grow even more in the future (Fig. 4) [6]. Moreover, AM covers many production sectors such as industrial, medical, automotive and electronics (Fig. 5), and the expected technological improvements will reduce costs of 60% in the in the next 2-3 years and of a further 30% in the following years. Such a vast reduction of costs together with a wide applicability of AM production processes will induce a further boost to the expansion of AM [142].

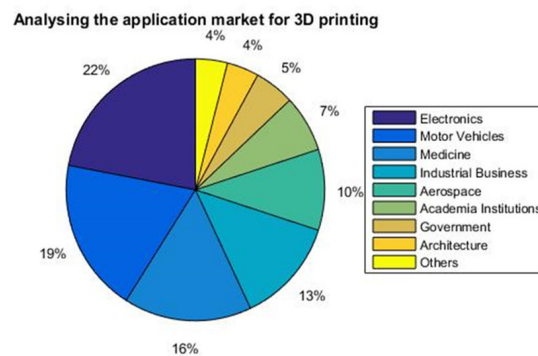


Figure 5: AM market distribution [7].

## Intercepting the need and identifying the requirement

Additive Manufacturing removes many limits to the design allowing to realize geometries that are practically impossible to obtain with traditional manufacturing. This higher design freedom implies a higher complexity.

Dealing with this novel and disruptive technology also means that many areas are under research. As showed before the efforts on this way are increasing and many resources are put in place to investigate all the possibilities that AM can offer since there are aspects that still have to be better enlightened.

For example, talking about traditional manufacturing, when an engineer has to deal with certain requirements and constraints he can be confident of well assessed standards, thanks to which the best choice among many options can be made, looking for a trade-off between weight, costs, reliability, performance and many other factors. The engineer can rely on well assessed standards and be sure that the part produced will satisfy, inside certain ranges of uncertainty, the initial requirements of the project.

Despite the fact that AM is experiencing a huge development, as previously showed, there are also some barriers to a wider adoption of this technique. The lack of standards leads to uncertain results. Even if different models to predict the behavior of the final part are present in literature, still the behavior of the final product cannot be foreseen with enough accuracy, and this obviously represents a big obstacle to a wider adoption of AM [10].

Starting from these considerations the following need has been identified:

*Foresee the behavior of the final product from its early design stages*

Satisfying this need is then of fundamental importance but definitely not straightforward. Starting from the same raw material, in case of additively manufactured metal parts from the same metal powder, does not guarantees that the final behavior will be the same.

The behavior of a component highly depends on the characteristics of the material, hence on its microstructure which is made of different elements such as texture, grain size and degree of anisotropy. During the production process the metallic powder used as precursor undergoes very high thermal gradients that contribute to the final microstructure [11].

Understanding the connections between the parameters used to tune the machine, the microstructure and the properties is then crucial to satisfy the previous need.

Thus, the following requirement can be identified:

*Understand "design parameters-properties" relations*

Nevertheless, a step back is required before looking for these relations. The parameters characterizing the AM process have to be identified and classified and, only after that, their relationships with the properties of the produced part can be inspected.

## A step back: AM features

After an extensive research in literature ([1][2][10][11][13][14][15][16][17][18][19]) the following aspects have been selected (Fig. 6).

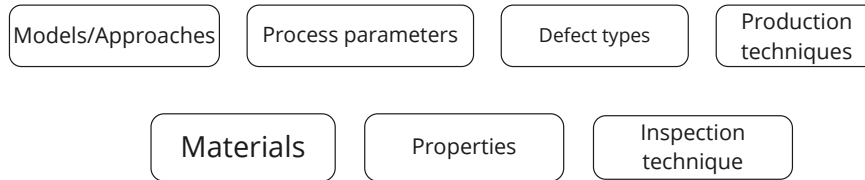


Figure 6: Classes used to classify various aspects.

In the following sections each one of these categories (Fig. 6) will be explored.

### Models/Approaches

This category focuses on the statistical models adopted to analyze data and to the software used to simulate the production process and so to estimate the results.

A further division in three groups have been made:

- Data elaboration models
- Process models
- Commercial process control solutions (software)

### Data elaboration models

The elaboration of the data obtained experimentally is a key point to assess the relations between the variables studied and the results obtained. Many publications focus only on a limited number of parameters and study their effects on the final results. This represents a limitation considering that if other factors, not taken into account, change, also the reliability of such experiments fails. In other words, the results obtained could be applicable only to particular experimental conditions and if these conditions change it might be necessary to restart the experiments from the beginning.

One possible solution to this issue is to conduct extensive experimental campaigns so that the effect of many variables can be studied under varying boundary conditions. The outcomes would then surely be more reliable but the costs would increase of a very big amount.

So, the choice of the appropriate statistic method becomes fundamental when looking for optimal parameters that could be possibly generalized to more than one specific case [11].

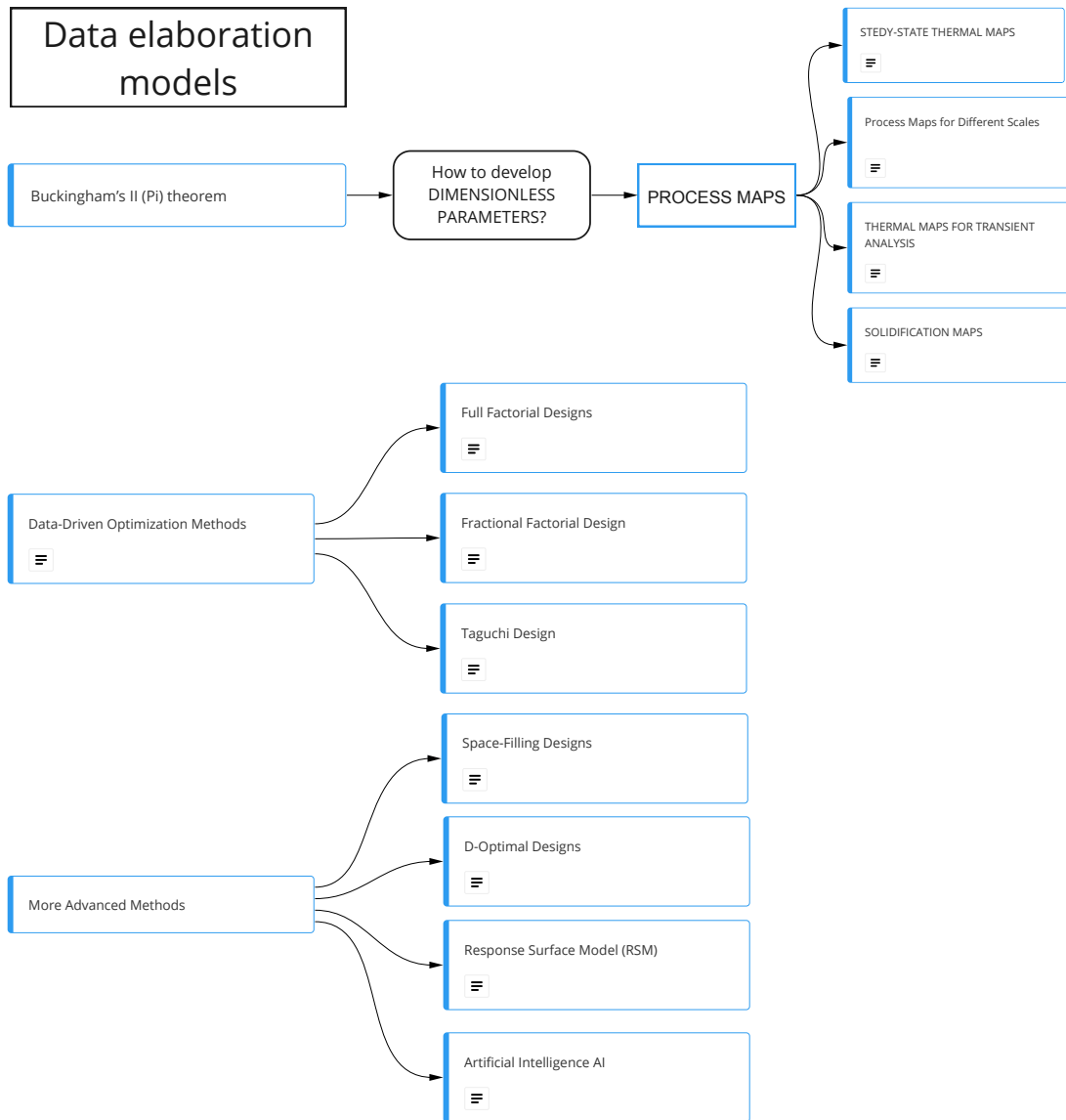


Figure 7: Classification of the Data elaboration models (Adapted from [11]).

## Pi theorem and Process Maps

*Buckingham's theorem*, well known as *Pi theorem*, is based on dimensionless parameters that are developed with the adoption of the process maps. These maps relate different variables, typically by placing numerical or experimental results on the x and y axes, and can be used to understand the impact that they have on the production process. Four maps are here considered and briefly explained:

- *Steady-State thermal maps*:  
useful to predict the melt pool size since it relates 2 or 3 dimensionless parameters (corresponding to a 2 or 3 dimensional map) that can be directly used by engineers or researchers.
- *Process maps for different scales*:  
aim at filling the gap between industrial activities (large-scale products) and laboratory experiments (small-scale products).
- *Thermal maps for transient analysis*:  
link the process variables to the thermal aspects (melt-pool, cooling rate, etc..).
- *Solidification maps*:  
link the process variables to the solidification of the microstructure (grain size, morphology, etc..) [20].

Process maps can be really useful but they also have two main drawbacks:

- They are only established for bulk pieces and thin walls
- They do not consider that the properties of the material could change with temperature and can then be used only inside certain temperature ranges.

## Data Driven Optimization Methods

Data driven methods are associated with the data derived from experiments and then with the choice of a model to be applied to that data. One of the main advantage of these methods is that they are not totally dependent on a specific process and so can be applied also to other processes. Three methods are mentioned here:

- *Full Factorial Design*:  
the basic idea is to analyze the influence of all the combinations of the parameters on the final results. It involves a huge amount of data, that could become unmanageable.
- *Fractional Factorial Design*:  
analyses a portion of all the possible combinations.

- *Taguchi Design*:  
uses orthogonal arrays to analyze the possible combinations of factors.

Full factorial design involve a huge amount of data that could become unmanageable, this is why the fractional factorial design might be preferred, even if certain interactions between the parameters could be ignored. Taguchi design further reduces the number of design points so that the number of tests to perform is also reduced. These models and the ones reported in the next paragraph can be also categorized under the so called *Design of Experiments (DOE)*, while those reported in the previous paragraph are considered *physisc's based models*.

### **More Advanced Methods**

Under this group the following models, that could be also seen as data driven methods, are included:

- *Space-Filling Designs*:  
adopted if many factors have to be analyzed when there are deterministic or near-deterministic systems.
- *D-Optimanl Designs*:  
uses matrices that are usually non-orthogonal and can be convenient when full factorials or fractional factorials cannot be applied.
- *Response Surface Model (RSM)*:  
made of a set of statistical and mathematical techniques.
- *Artificial Intelligence*:  
includes various networks and algorithm that need to be trained and so a big amount of data, that means a big number of experiments, must be available.

### **Process models**

The two models (Fig. 8) can be adopted [18].

An example of numerical model is the Lattice Boltzman method that can also model parameters that have a random effect such as powder bed, even if it is a very demanding method.

### **Commercial process control solutions**

A list of software solutions (Fig. 9) with some characteristics, that can be useful for the designer, is provided [21].

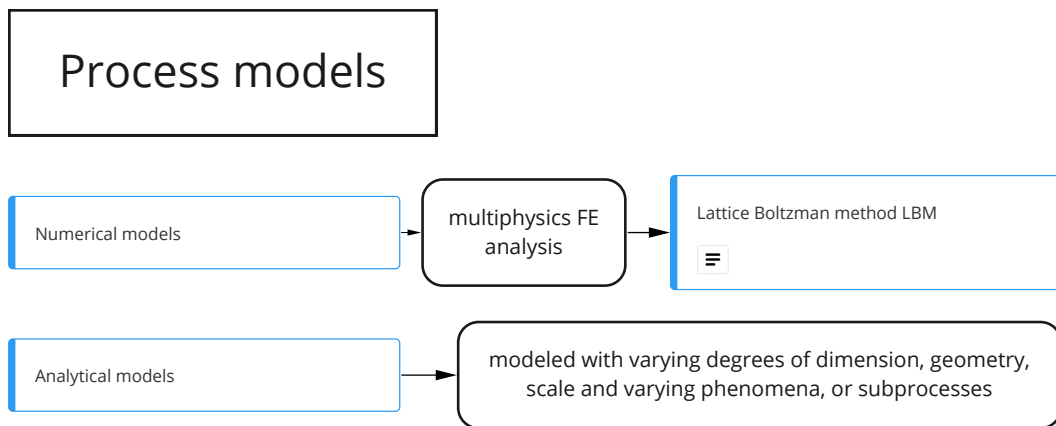


Figure 8: Classification of the Process models (Adapted from [18]).

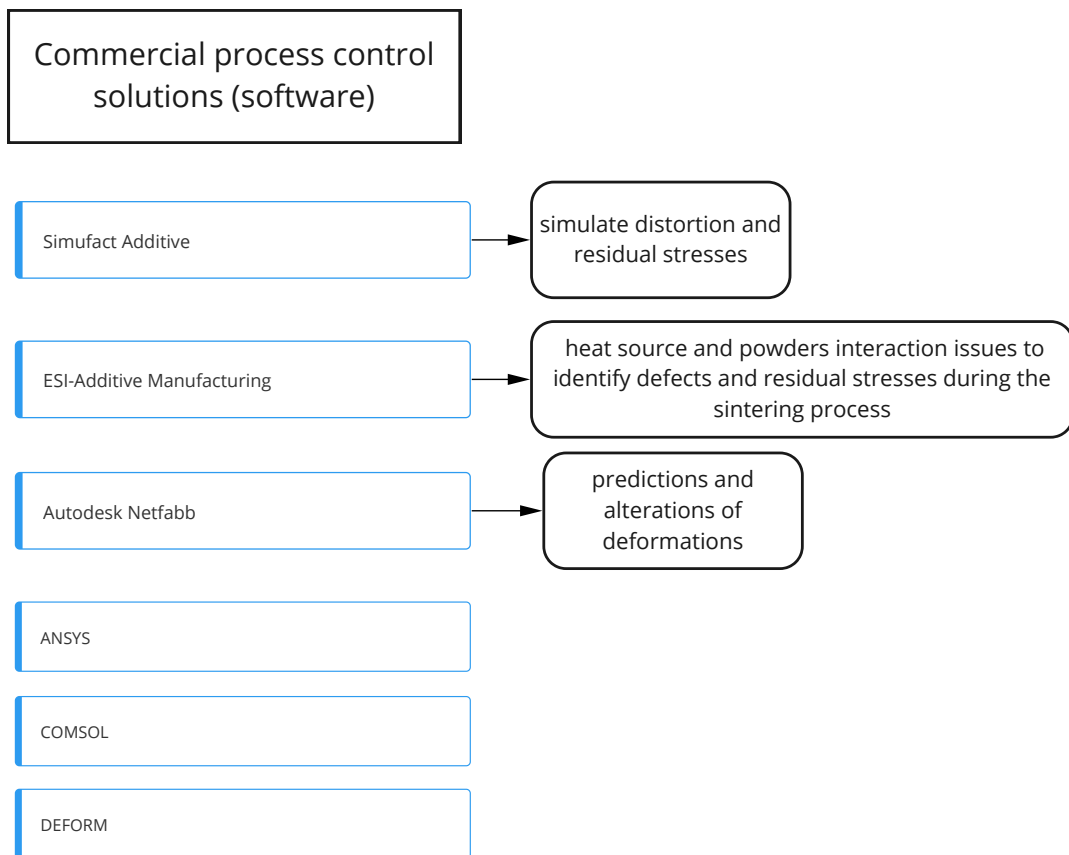


Figure 9: Classification of the Commercial software solutions.

## Process parameters

Many publications refer to the process parameters and to their effect on the quality of the final part. Finding the best compromise between the many factors that the engineer can tune is surely one the most active field of research, and the fact that the majority of the studies do not reveal all the parameters involved in the process makes it even harder to explore.

In the present work the process parameters have been divided in two groups:

- *Process parameters* (Fig. 10):  
selected by the designer before the physical production of the part.
- *In-process parameters* (Fig. 11):  
aspects that depend on the selection of the process parameters and are useful also to monitor the process. These parameters possess a thermal capacity and this is why they should be carefully studied. Moreover, they can be found in the inner part of the melting process and this is how they are presented here.

The process parameters are often related through the energy density ( $E$ ) that can be expressed in a 3-dimensional form or, considering that the powder layer thickness is very small, in a 2-dimensional form [21].

The relation in 3-dimensional form is expressed by:

$$E(3D) = \frac{P}{V * d * t}$$

while in 2-dimensional form:

$$E(2D) = \frac{P}{V * \delta}$$

Where  $P$  is the laser power,  $V$  the scanning speed,  $d$  the hatch spacing,  $t$  the layer thickness and  $\delta$  si the diameter of laser beam/spot size.

## Process parameters

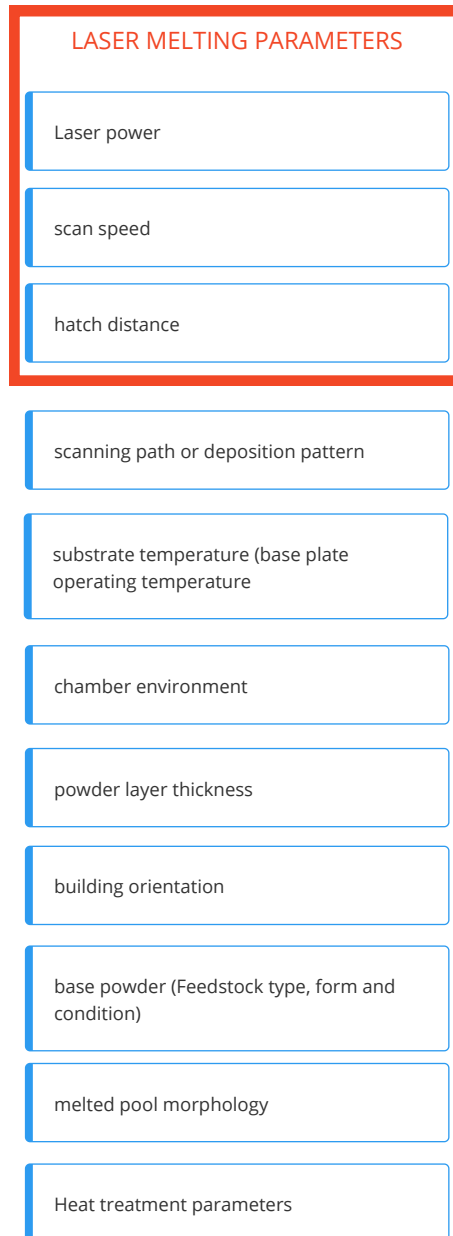


Figure 10: Process parameters.

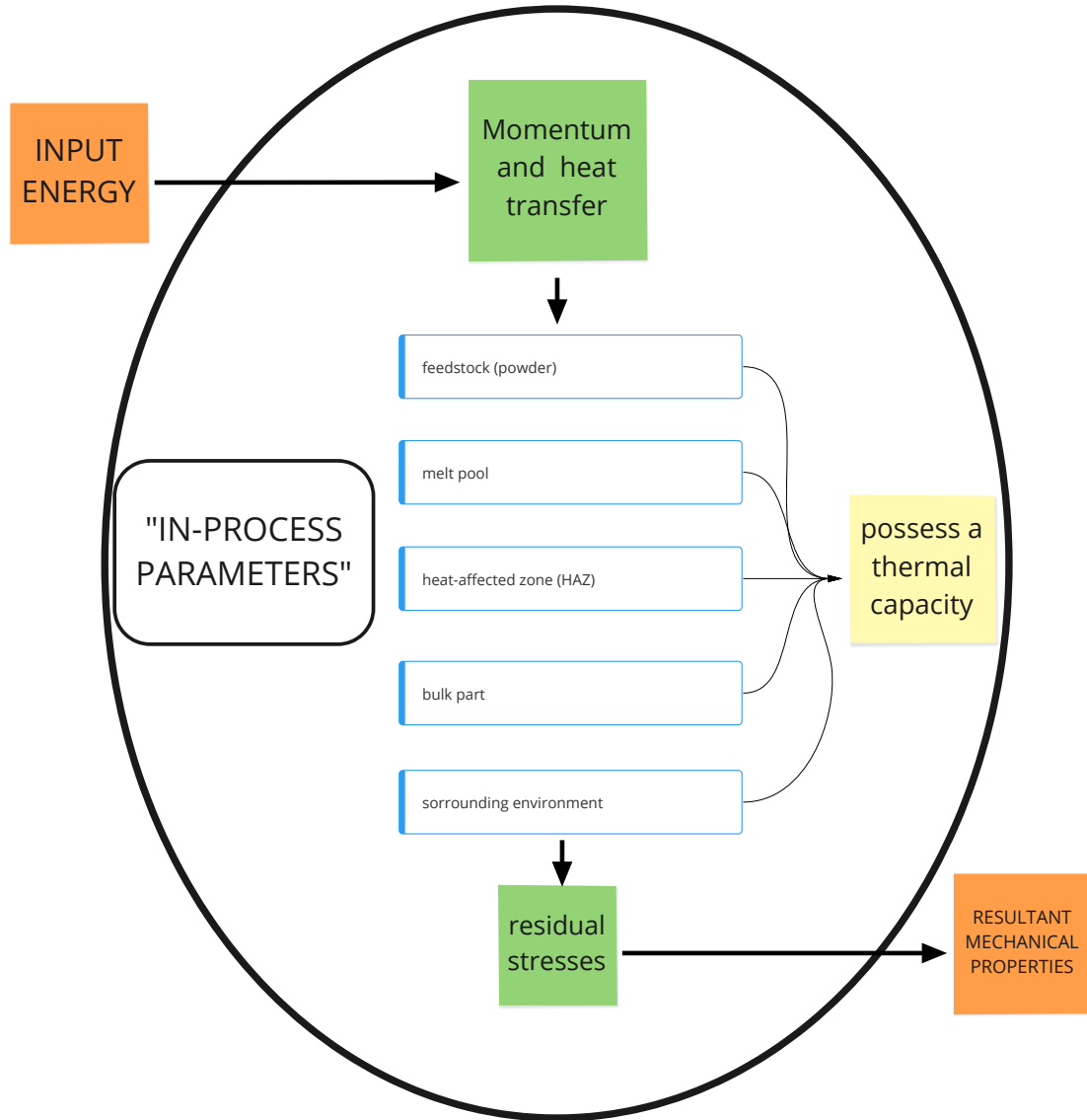


Figure 11: In-process parameters.

After seeing which are the design parameters useful to tune the material properties it can be useful to mention an example of how this parameters can be further subdivided. This classification (Fig. 12) could be useful to perform a better design of the experiments and so reduce the number of trials and errors simply by grouping together certain parameters that are similar or by knowing which parameters can be adjusted and which parameters are constant [18].

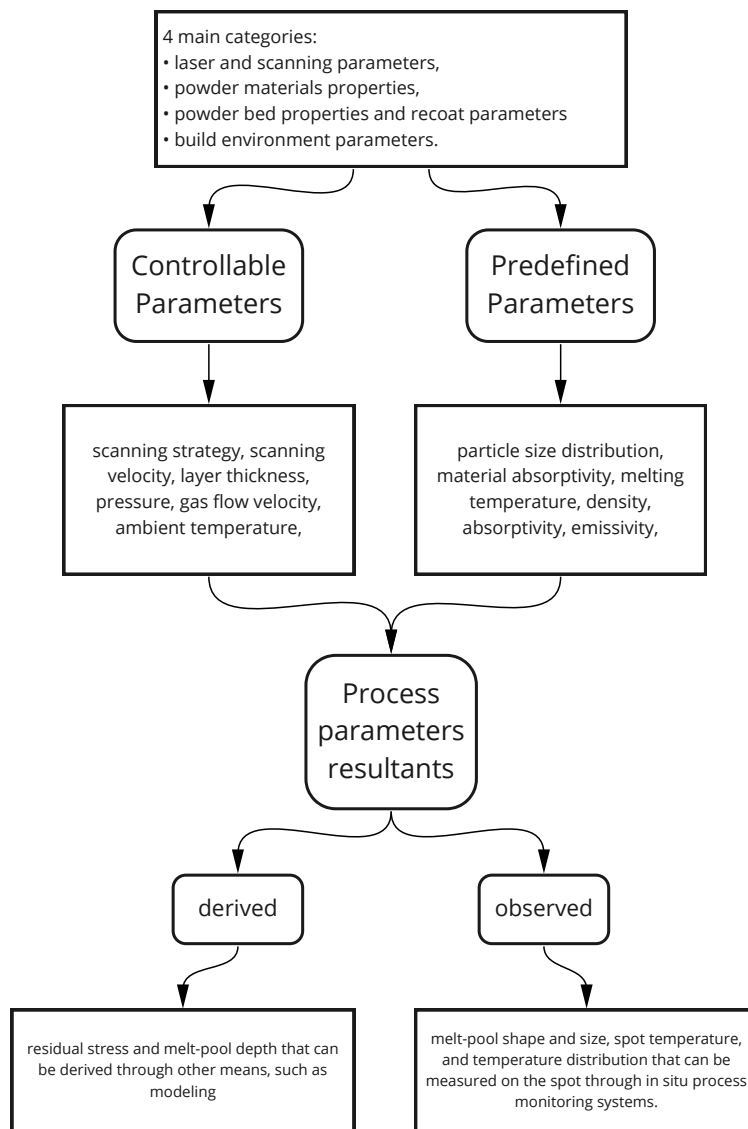


Figure 12: Sub-classification of process parameters.

## Scanning strategy

There are some aspects of AM production process that only belong to this novel technique, selecting the right scanning strategy is one them. Dealing with a laser or an electron beam as source of energy means also taking into consideration features that in traditional manufacturing are not present at all.

The purpose of this short paragraph is to show that, even if the deposited energy is probably one of the predominant and most studied parameter, the designer should be careful when assuming that certain variables are negligible [1] [21]. The effect of different scanning strategies will be described later, here few examples of different scanning paths (or strategies) are showed (Fig. 13).

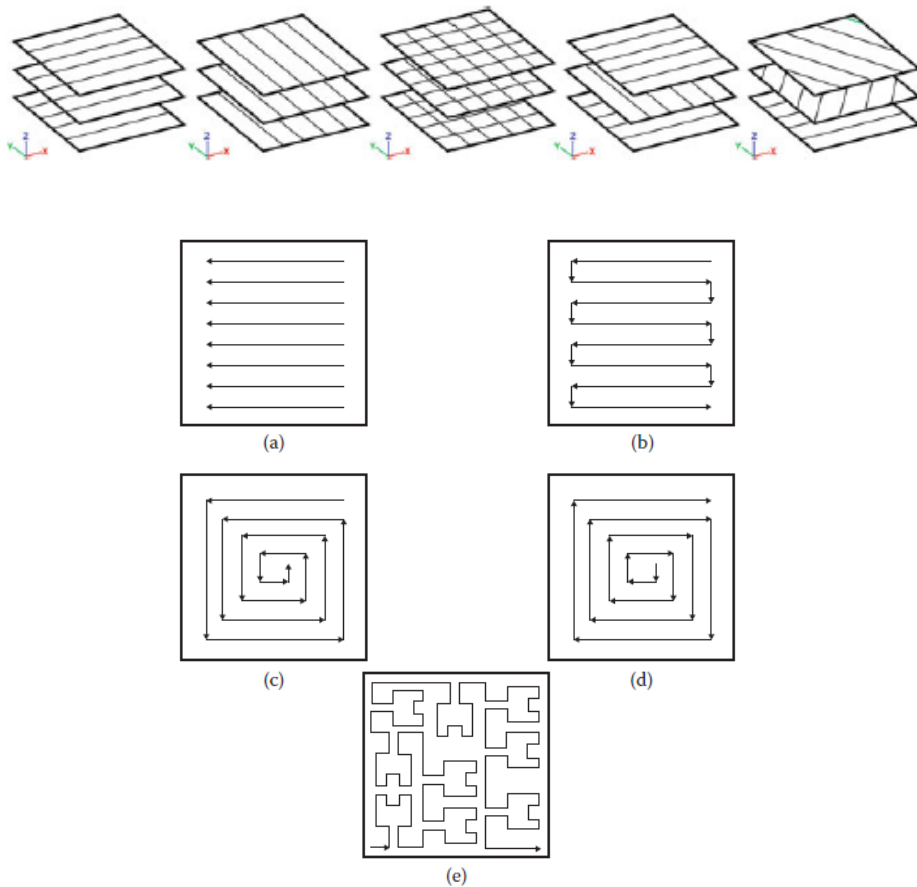


Figure 13: Examples of common scanning strategies. At bottom: (a) raster, (b) bidirectional, (c) offset-in, (d) offset-out, (e) fractal postmanufacturing processing.

## Defects

In general, the designer sees a defect always as a negative characteristic that must be avoided, or at least minimized, to have the best possible outcome.

Referring to AM a list of defect and two main categories of defects have been identified (Fig. 14):

- *as-manufactured defects*
- *as-designed defects*

*As-manufactured defects* are those that come out from the manufacturing process and are unwanted, their elimination or reduction leads to a better final result. On the other side the so called *as-designed defects* should be approached differently and their presence can be favorable. Porosity is an example: in traditional manufacturing is definitely to be avoided but in AM can be controlled to produce, for example, a sponge-like metal material [22] or to fabricate a part that, having the same external volume of the corresponding bulk piece and with satisfying mechanical properties, can be lighter.

## Materials

A short list of the most common materials, based on the researches carried out, has been compiled. Then, this series reflects what are the most studied metal alloys and does not pretend to be exhaustive (Fig. 15).

## Properties

Similarly to the previous *Materials* section a list of properties is here presented (Fig. 16). The majority of the properties are still the same of traditional manufacturing. In AM the porosity (or relative density) takes on greater importance because, as previously said, can be tuned to cope with individual requirements.

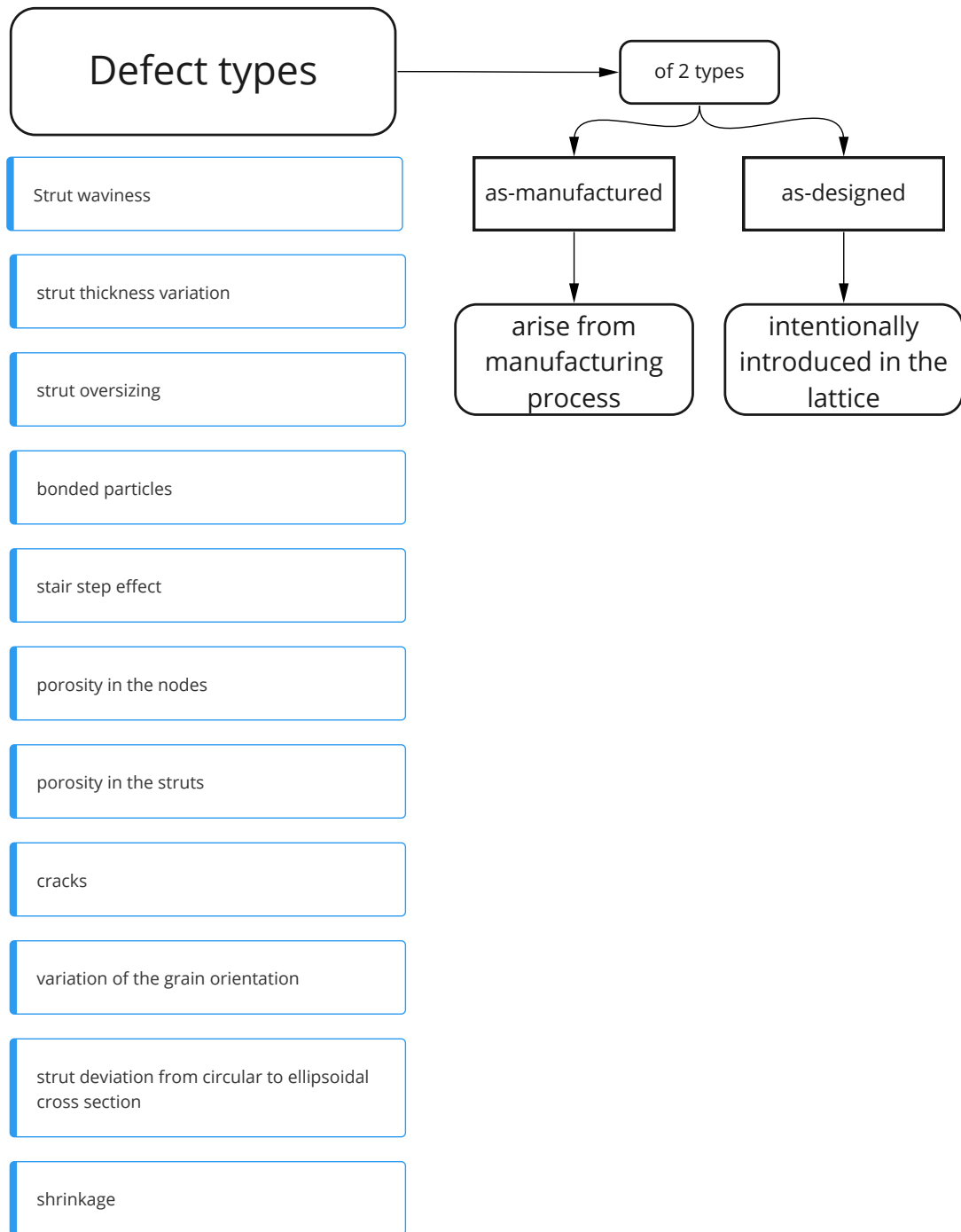


Figure 14: Defects list and classification.

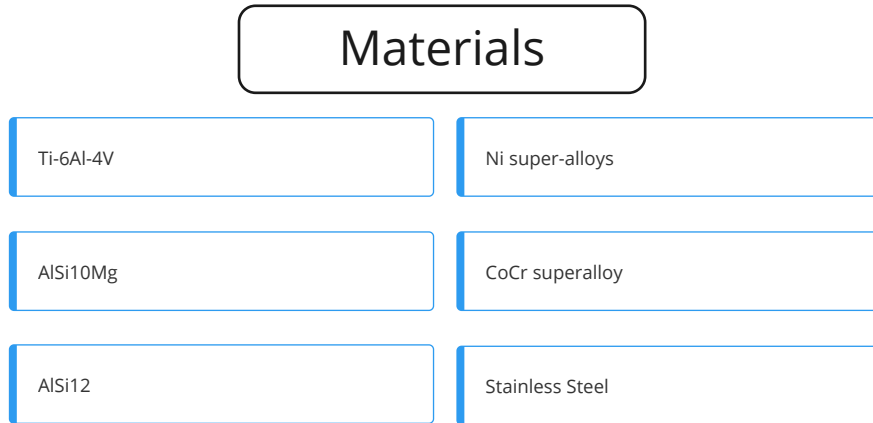


Figure 15: Metal alloys most commonly studied.



Figure 16: Properties most commonly studied.

## Inspection techniques

Quality assurance is one big challenge in AM. The main societies (ASTM and ISO) are working to provide complete standards that cover the full manufacturing process, from the analysis of the powder material to the measurement of the performances. A huge number of parameters have an influence on the final product and ensure the repeatability and the quality of the piece is a key point to enable a wider adoption of AM. To this aim the designers may need to rethink the entire qualification process to find methods that better guarantee the production of high-quality parts [18].

A list of the main inspection techniques with their characteristics has been elaborated and it is here reported (Fig. 17; Fig. 18). These methods can be classified in two categories:

- *OFF-LINE analysis*:  
performed on the part at the end of the production phase.
- *ON-LINE analysis*:  
executed during the production process. It can be interpreted as a live-time monitoring.

Looking at Fig. 17 one will find that the majority of the OFF-LINE methods are already widely adopted and for this reason will not be further described here. On the other side, it can be worth giving a brief explanation about *Electro-magnetic waves control* that is based on the measurement of the electro-magnetic waves emitted by the melt-pool during the process. This technique mainly refers to laser-based process where the melted metal reaches high temperatures and emits electro-magnetic waves mainly belonging to the infra-red spectrum. This information sent by the melt-pool can be analyzed and, based on the waves distribution along the spectrum, it can be understood which are the temperatures of the metal. This information can, in turn, be correlated to the final properties of the material and the presence of residual stresses.

Moreover, adopting ON-LINE analysis the engineer can even stop the process if the data acquired during the monitoring is too far from the expected values. Instead of putting many effort in the detection of defects, as it is done when the OFF-LINE analysis is adopted, such defects can be prevented. In this way time and resources can be saved with a consequent economic advantage, even if the technologies to integrate data coming from the sensors with physical models still have to be fully developed.



Figure 17: Inspection techniques.

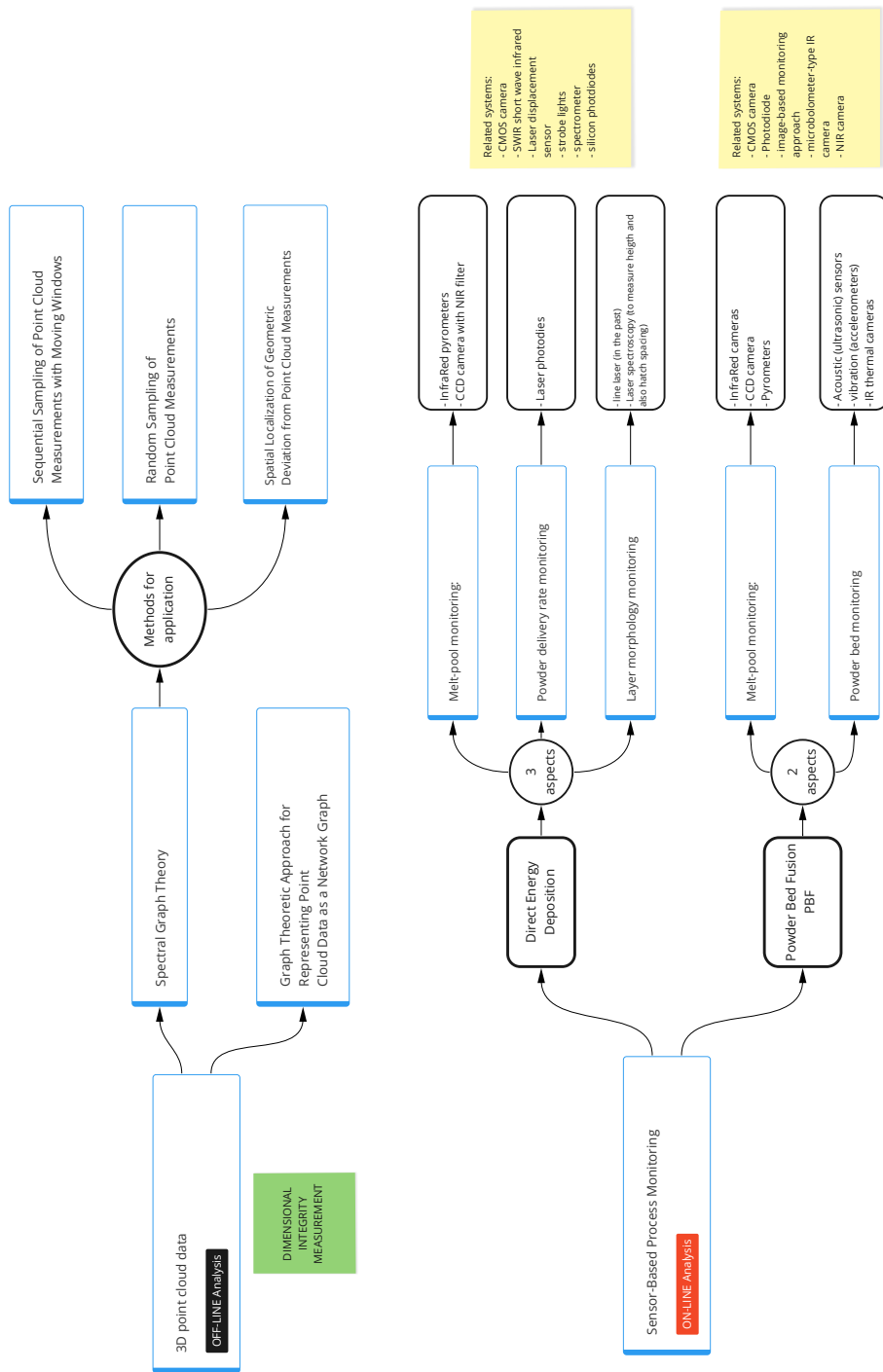


Figure 18: 3D point cloud data and Sensor-Based Process techniques.

## Scanning technologies

One of the biggest advantage of adopting scanning technologies in AM is that they enable the possibility to perform *Reverse Engineering*. An object can then be scanned and replicated, or the engineer can compare the ideal 3D CAD model with the model obtained by scanning the part and be able, for example, to see which geometrical features correspond to the ideal shape and which ones are far from the CAD and then quantify the errors. A list of scanning technologies, subdivided into three categories based on their working principle, is given (Fig. 19).

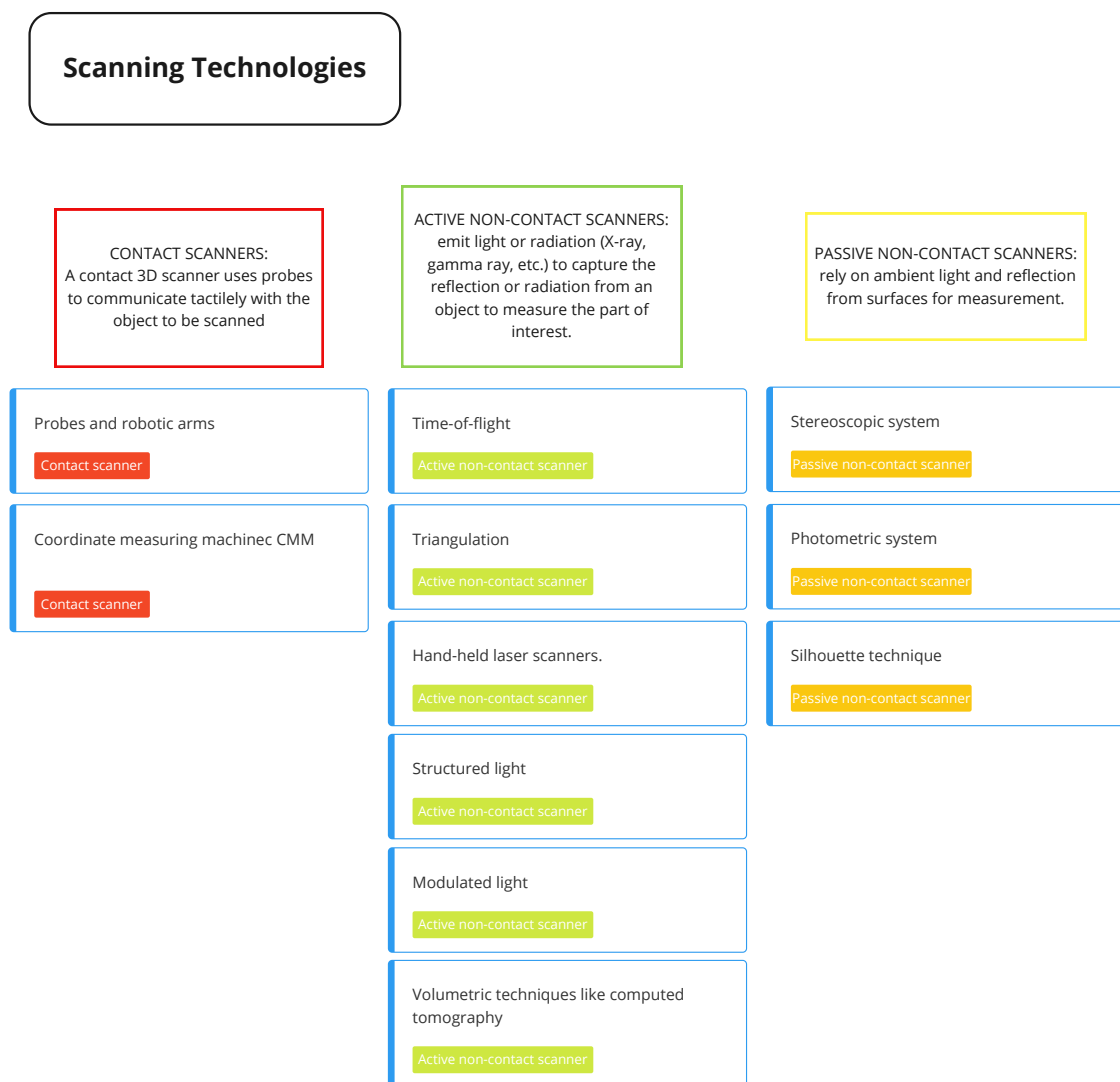


Figure 19: Scanning technologies.

## Standards

AM standards are still in progress, many ASTM and ISO standard have been published even if a complete knowledge is yet to be achieved, and so the standards cannot fully cover the whole production process. In several publications the standards typically adopted for traditional manufacturing are used ([109]) even if standards made ad-hoc for AM would surely suit better. The basic structure of AM standards together with many classification can be found in literature ([18][23]). Here a short list of features with their relative standards is given (Fig. 20).

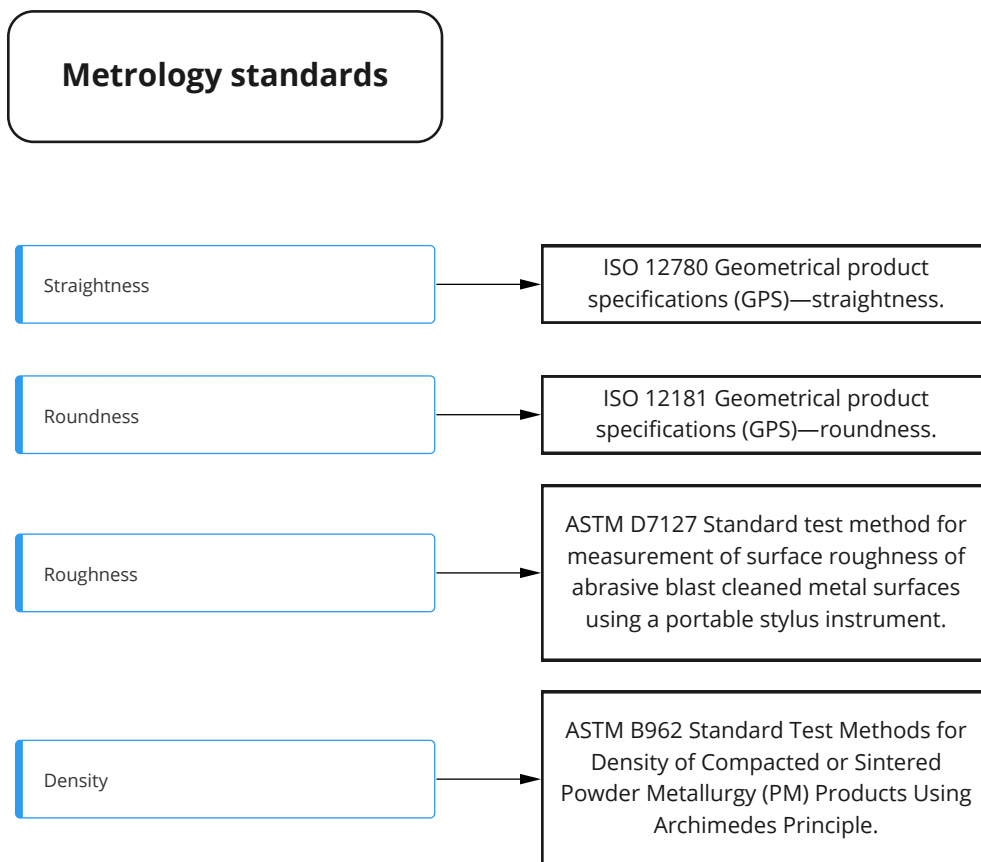


Figure 20: Metrology standards.

## File formats

AM components are designed in a 3D CAD format which is then converted into another format before being printed. The data coming from the 3D CAD file can then be converted in another format depending on the software used. Many of these softwares are produced by the same companies that produce the program to create 3D objects while many others are not shared by the enterprises.

A list of the most common Data formats adopted with main advantages and disadvantages is presented (Fig. 21, Fig. 22). The software are classified in "Traditionally used" and "Under development". *AMF* is developed by the cooperation between ASTM and ISO organizations while *3MF* is the result of a collaboration between Microsoft and its partners. GrabCAD print is not classified under these two categories because it works in a slight different way enabling the AM machine to print directly from the CAD file [18].

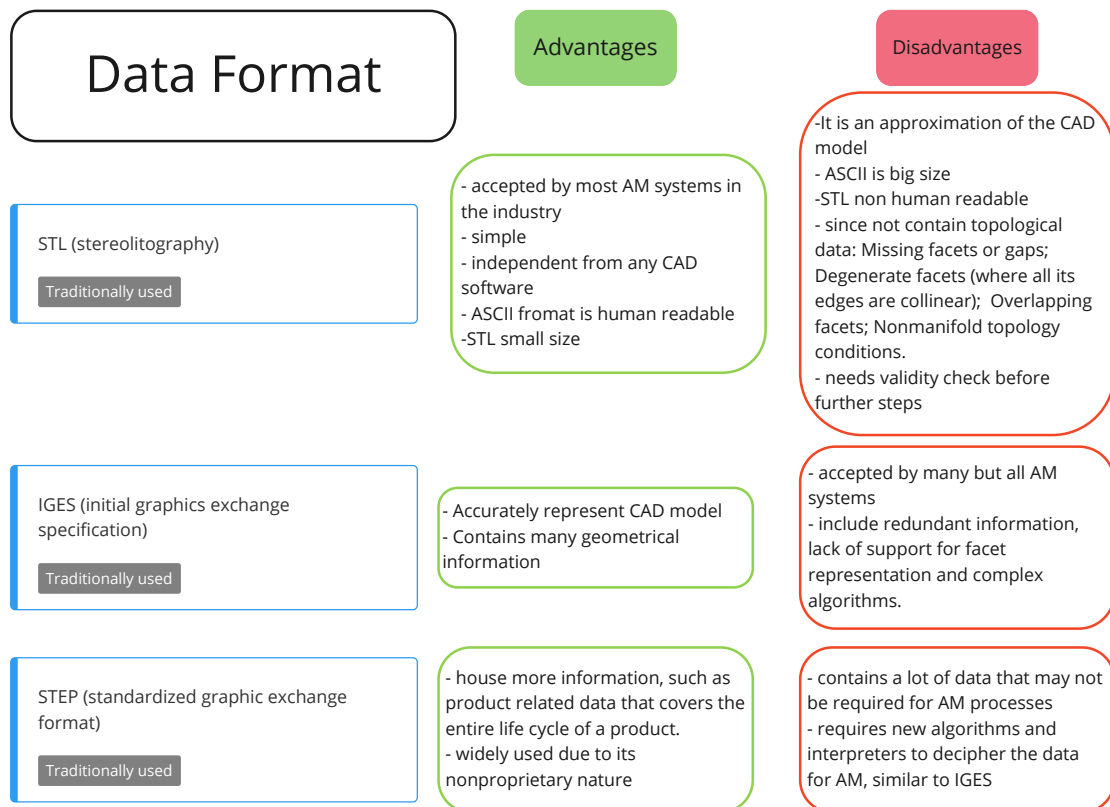


Figure 21: Data formats.

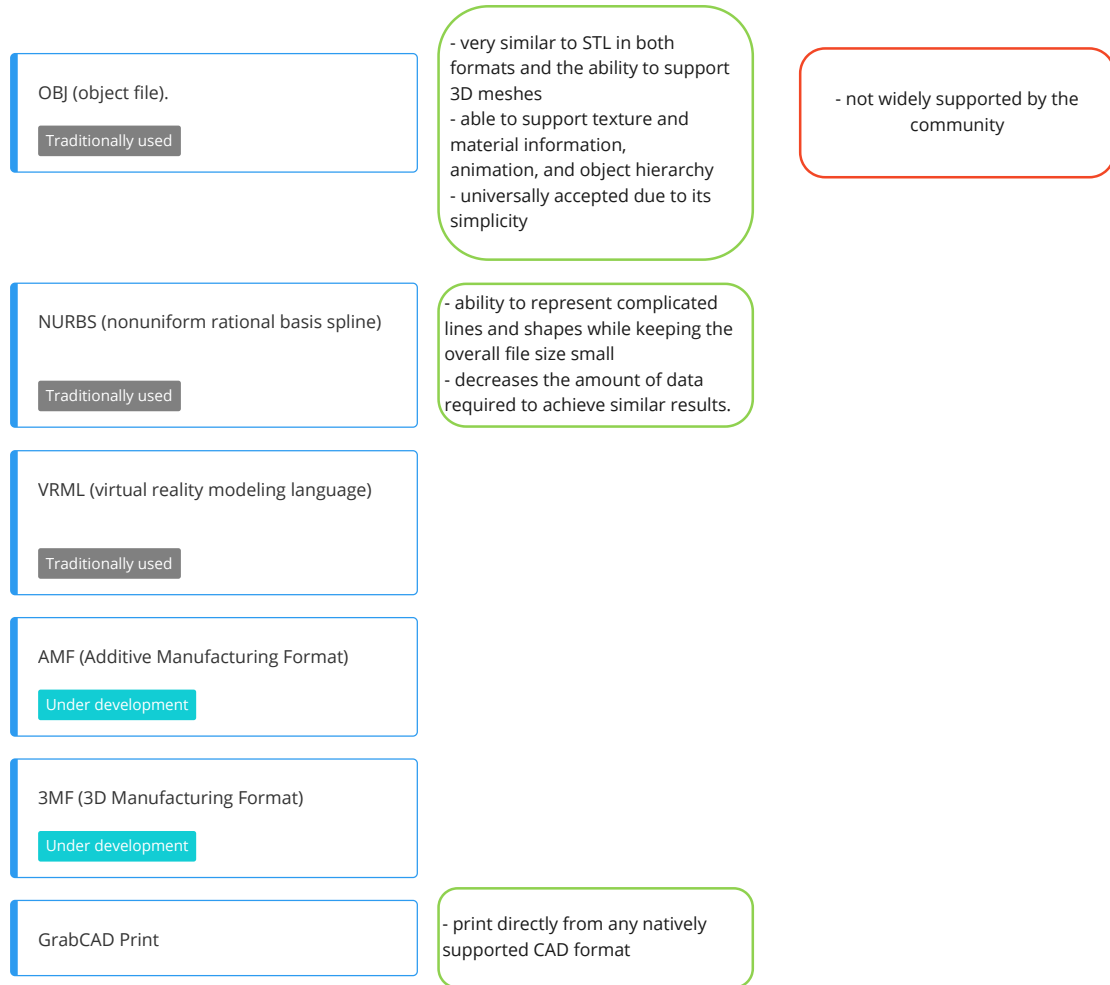


Figure 22: Data formats.

## Classification method

The results of the research have to be properly classified so that they can be elaborated to satisfy the need previously mentioned. The tool chosen to classify each publication found is at the same time very intuitive and effective. It simply consists of tables where two aspects, one in a column and the other one in a row, can be compared and the relation between them can be analyzed.

Considering the huge number of publications related to AM the choice of adopting tables has two main advantages:

- allows to immediately identify which areas are the most studied;
- allows to easily focus on few characteristics at a time and highlights their relationships.

Three tables have been created among which the most important is related to "Design parameters-properties" relationships and will be deepened later in this work (Fig. 25). The other two tables refer to "Data elaboration models/approaches - Material" (Fig. 24) and "Production technique - Cell type" (Fig. 23) are useful to see the focus of the majority of the publications found but, due to limited time, will not be further examined.

All the tables have been built based on the different categories previously found that are, in some case, reduced to adapt to the results of the research. By zooming in enlarging the images one will notice that each publication correspond to a small green, or red if the article does not provide much useful data, square that is a sticker where the citation is written.

The tables are very detailed and it is difficult to read what is written on them without enlarging the image. On the other side, to correlate the different elements, it is important to have the elements composing the first row and first column on the same image, so the author preferred to not divide the tables in many parts and leave them under their original form. The images provided are in very high resolution and this allows an easier exploration of their content.

Production technique - Cell type				
	truss structures (octet, BCC, FCC, etc...)	Strut (in general)	"Bulk" piece	
Selective Laser Melting (or SLS)				
Electron Beam Melting (EBM)				
Direct Metal Deposition DMD Direct Laser Deposition DLD				
From numerical models				

Figure 23: Production technique - Cell type.





## Pathway definition

The aim of this thesis was to satisfy the need previously specified by fulfilling the requirement. The research and classifications showed along this chapter have been conducted to understand the characteristics of the AM production process, by identifying the various features classified in the lists reported above. Then, the focus has been put on the parameters-properties relations that have to be inspected as prescribed by the requirement.

After the research made it has been concluded that trying to foresee the behavior of a component only focusing on the relations between parameters and properties would be too limiting. The number of variables characterizing the AM design and manufacturing phases is so high that the approach to the problem must be widened.

Hence, the various steps must be taken into account from the very first design concept until the final post-process treatment or the final test. Considering that the choices made by the engineer during the various phases are interconnected he should be aware of the various advantages and disadvantages when he decides to follow a path instead of another.

For instance, it can be supposed that the designer have a list of customer requirements to satisfy, so he decide that to have lightness and strength one alloy is what he needs. The piece is then produced and heat treated. After the thermal treatment a modification occurs inside the material due to the formation of precipitates that compromises the correct functioning. This cannot be accepted but the piece must be heat-treated, otherwise it would not have the mechanical properties requested. What to do then?

This simple example is obviously far from a real case but it is useful to understand the importance of knowing how the whole AM system works.

The scope of this thesis is then to provide the designer a suitable tool to make him aware of all the possible options that he has at disposal: starting from the choice and analysis of the raw powder, moving to the topology optimization approaches and then to the selection of the proper process parameters.

Greater attention will be devoted to process parameters-properties relations, already mentioned in the table in Fig. 25, that is one of the most active field of research. In the final part the life-cycle, economic and sustainability perspectives of AM will be explored. The decisional process that will be described is schematically reported in Fig. 26, where the section regarding the manufacturing phase (lower part of the figure) will be investigated by deepening the parameters-properties table (Fig. 25). Each argument will be explored in the following sections assuming that the customer requirements have already been elaborated and are crystal clear, so that the engineer can start to look for the best compromise to satisfy such requirements.

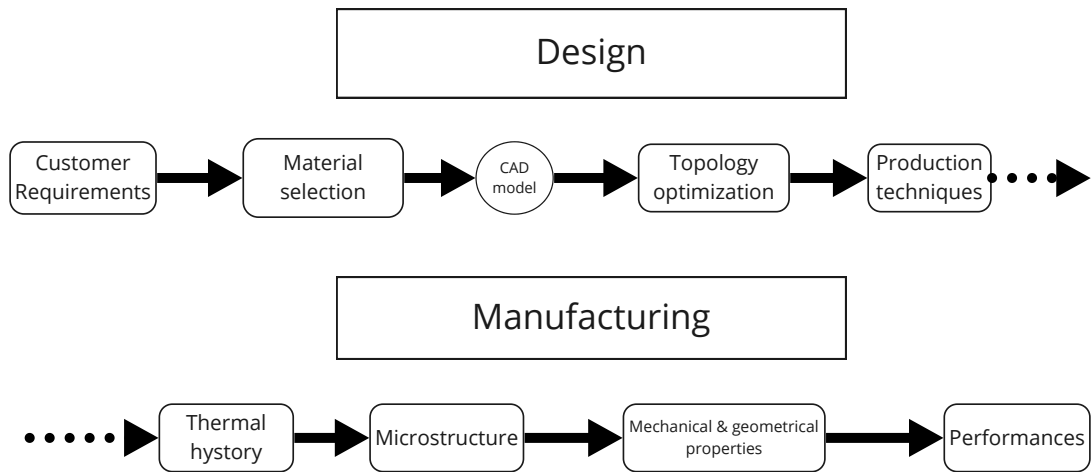


Figure 26: AM manufacturing steps.

**Part I**  
**Design**



---

Many aspects are encompassed inside the term *Design* and, when referring to AM, it becomes *Design for Additive Manufacturing* (DfAM).

DfAM does not consist in drawing an existing component to produce it using AM technologies but it aims at exploiting all the potentials that this disruptive technology can offer. The Design process should be thought not only to reduce the weight of a part or to obtain inner geometries otherwise impossible to create. The engineers should be aware of all the advantages, and also limitations, that AM can give and consequently find a trade-off between all the available options [1]. The current part describes the design phases that in this work includes: *Material selection* and approaches to *Topology optimization*. The designer will find in the following sections various options among which the compromise that suits better the case under analysis has to be found.



# Step 1: Material selection

There are many ways to print a 3-D part and a variety of materials can be used: from polymers to metals or composites. The focus of this work is on metal powders used for powder-bed fusion processes (Laser Beam Melting (LBM) and Electron Beam Melting (EBM)) that are between the most adopted production techniques and are also widely used in the aerospace sector.

The analysis that will follow is schematically reported in Fig. 27. The main part is dedicated to metal powders and their analysis as well as to more recent research topics: the additives that can be mixed with the powders, the compositionally graded materials and the hybrid materials.

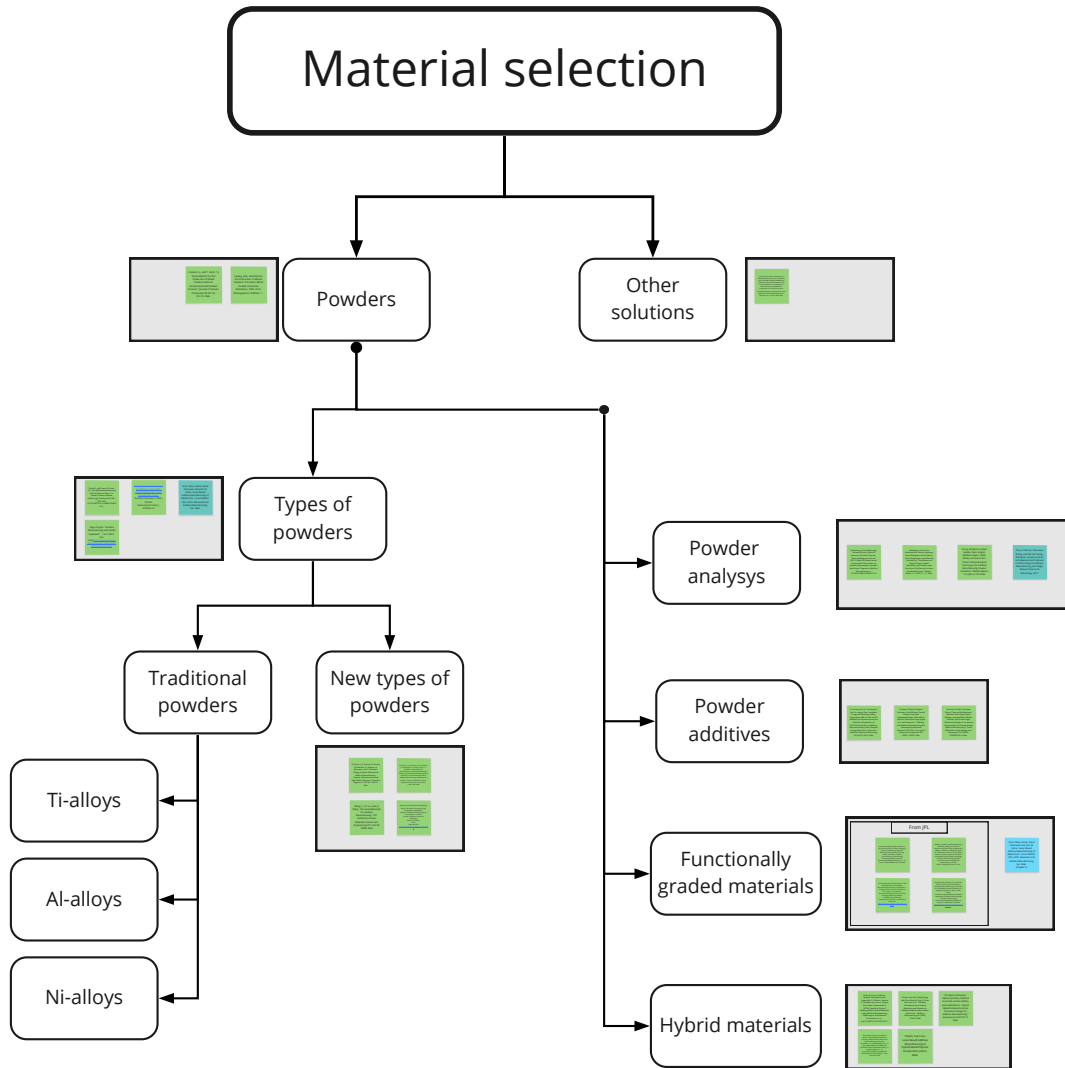


Figure 27: Materials selection.

## Powders

As shown from Fig. 28 metal powders are one of the most used materials in AM. Conventionally the production of metal powders is made by Gas Atomization [25] even if other methods exist, like the one described by Canakci et al. in [26].

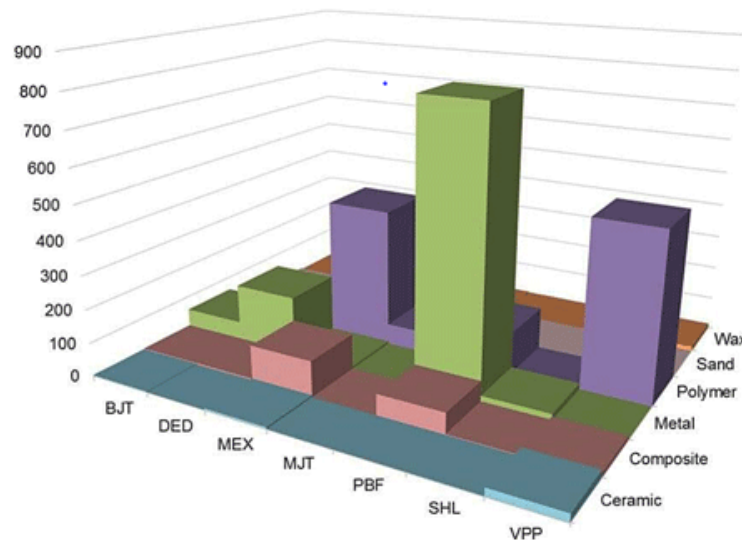


Figure 28: Number of material products for the main AM production techniques (2020) [24].

## Types of powders

In the present a description of some materials is available. The distinction between *Traditional powders* and *New type of powders* rely on the fact that, even if research is still in course on both sides, the first are better known while the latter are newer and their behavior has still to be understood. As a direct consequence the choice of adopting *Traditional powders* is more precautionary and keep the designer on the safe side while working with a recently invented powder would obviously increase the level of risk.

### Traditional powders

Even if a full understanding of the materials used in AM and their behavior during the production process is yet to be reached, the alloys in this section are between the most known and used by the producers (Fig. 29).

### Titanium alloys

Titanium alloys are relatively new materials because they started to be used around the 1950. Titanium is very attractive because it has a high strength/weight ratio, a

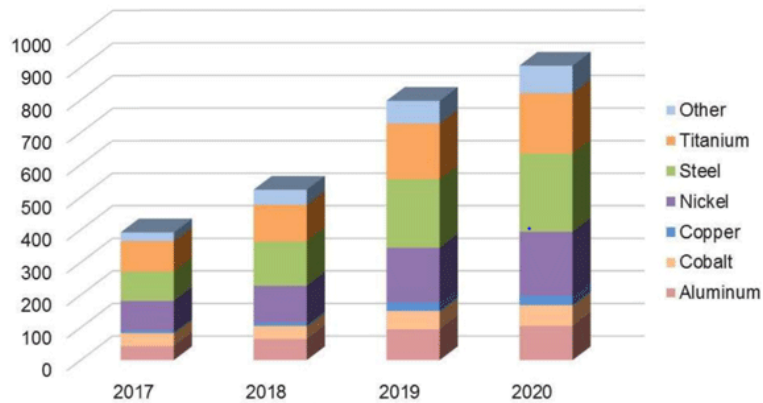


Figure 29: Metal products available for each year [24].

very good corrosion resistance (provided by the oxide layer that naturally forms on its surface) and its properties remain unchanged until elevated temperatures (around 550 °C).

Titanium is in practice never used in its pure form but it can be useful to observe its properties compared with those of iron and aluminum so to have a reference point (Table 1).

Table 1: Titanium, Aluminum and Iron properties.

Properties	Titanium	Aluminum	Iron
Density [kg/m <sup>3</sup> ]	4540	2700	7860
Modulus of elasticity [GPa]	120	69	200
Melting point [°C]	1668	660,32	1535
Thermal conductivity coefficient [W/mK]	6-16	210	80,2
Thermal dilatation coefficient [µm/m°C]	9-11	24	11-12

The main disadvantage of these alloys is the high cost that involves both the raw materials and the production costs. The price of a titanium ingot can be 90 times higher than that of a steel ingot. Moreover, due to its singular properties (low ductile yield and high strength), the machining of titanium with conventional techniques can be very challenging due to the high spring-back effect, for which strong rigid setups are needed that can, in turn, create high pressures and temperatures at which undesired chemical reactions can occur. To avoid the heating of the surface the cutting speeds have to be kept low and this makes the process last longer increasing costs [27]. The increase in production cost (Fig. 30) can be limited by adopting AM technologies especially if a small batch or customized parts have to be produced.

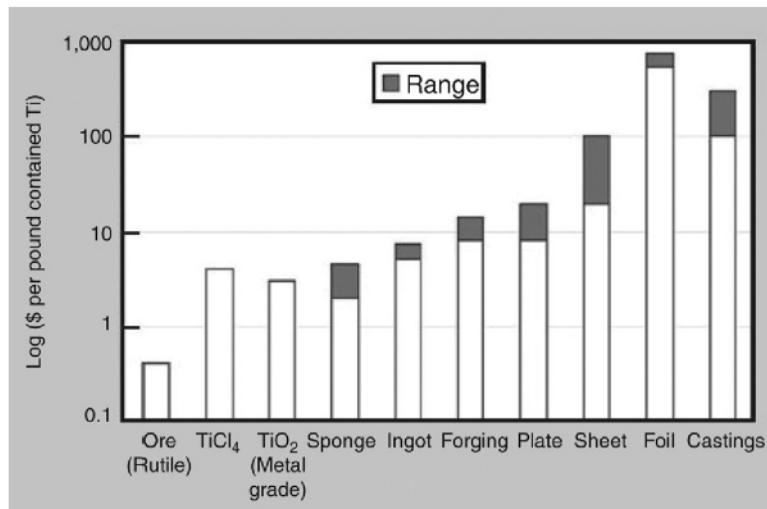


Figure 30: Cost of Ti at different production phases [32].

The other reason why one could decide to use titanium alloys produced by AM methods is the higher properties that the final component holds. Indeed, comparing various production techniques it is evident how the adoption of AM production methods can bring positive outcomes also when referring to mechanical properties (Fig. 31). In conclusion, even if not much information about the processability of powders can be provided, costs and mechanical properties can be alone valid reasons to choose to use titanium alloys.

### Aluminum alloys

The main reason that push the adoption of aluminum alloys is the strength over weight ratio and the high corrosion resistance (properties in Table 1). However, processing Al-alloys is difficult due to the following reasons:

- low density;
- poor flowability;
- high thermal conductivity;
- high reflectivity;
- high susceptibility to oxidation;
- susceptibility to hot cracking;
- susceptibility to hydrogen porosity formation.

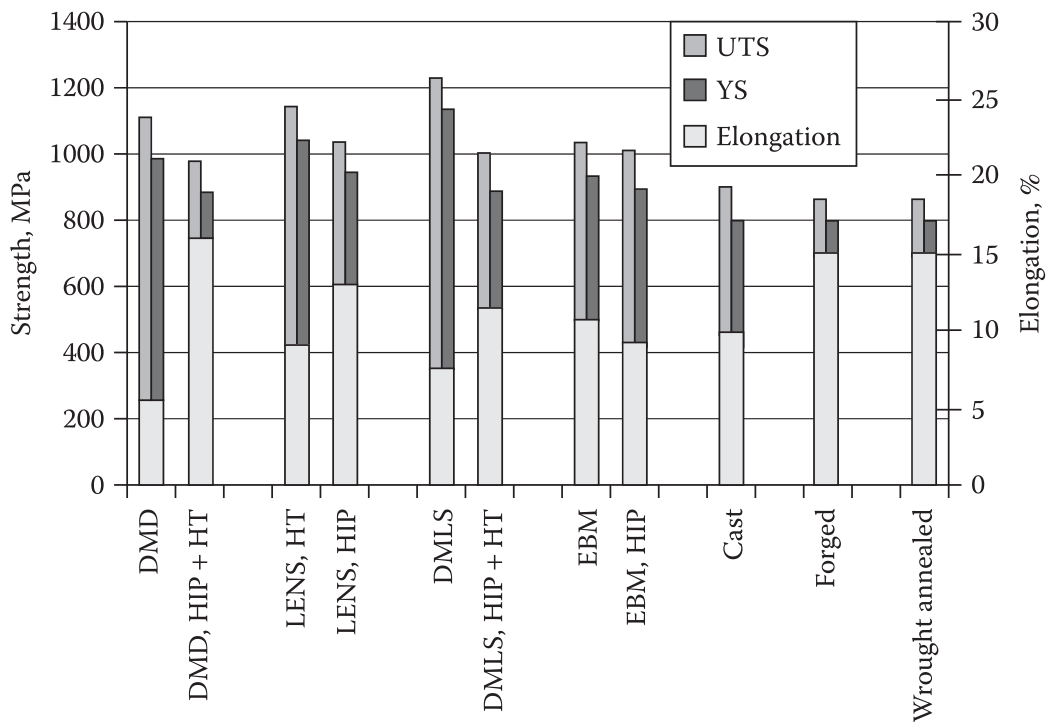


Figure 31: Ti-6Al-4V UTS, YS and elongation for different production techniques [21].

For these reasons a high amount of energy is required, the temperature should be kept under constant monitoring and the working environment has to be well controlled. In addition, different secondary phases can appear depending on the alloy processed and their presence has to be carefully regulated to obtain an optimal microstructure [11] [27].

### Nickel alloys

The term *superalloys* also refers to nickel-iron-base materials while the term *Ni-base superalloys* is attributed to those materials that have the nickel as the only one alloying element [11].

In general Ni-alloys produced via AM techniques can exhibit better mechanical properties. The level of processability varies based on the type of alloy selected. Certain Ni-alloys are easier to produce while the risk of weld cracking is present for other types. Possible solutions to increase the processability of such materials can be the utilization of fractal scan strategies, to ensure a good flow of powder and inert atmosphere to avoid contamination of the part by air molecules or to use a surface energy density and pre-heat the powder. The graph in Figure 32, even if referred to weldability, can be a useful "processability map" helpful in the choice of the right alloy to be processed with AM production techniques.

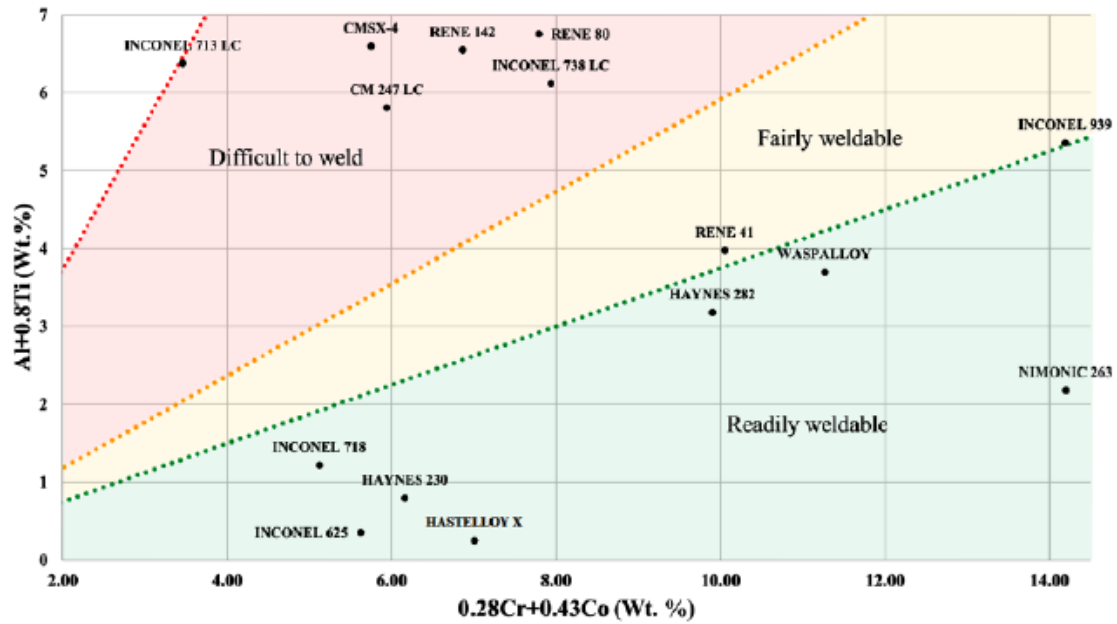


Figure 32: Ni-alloys weldability [33].

### New types of powders

Looking for new types of powders specifically developed or created for AM represents a big challenge. The efforts in this field of research are increasing and, considering the great design freedom that AM methods allow, many aspects still have to be discovered. Günther et al. [34] study the microstructure of CrMnNi processing it for the first with EBM technology. Thanks to the heat-treatments intrinsically present in the EBM production process a very fine microstructure is obtained with no preferred grain orientation, that can hence be considered isotropic. The material obtained has also a low sensitivity to the process-induced defects. Omoniyi et al. [35] develop a new photoactive-based piezocomposite materials by using as matrix the adhesive (NOA 65) combined with particles of Barium Titanate as dielectric filler, allowing to 3D print sensors and actuators. Wang et al. [36] study the use of nano-modified and nano-structured particles to enable the creation of components made of materials, such as ceramics and high strength alloys, otherwise hardly processable. The use of coatings for metal substrate, the adoption of reinforced particulates and other aspects are reviewed by Neng et al. [37].

## Powder analysis

In powder-based fusion processes the characteristics of the powders play a crucial role. The analysis of the powder with proper methods is then essential to obtain a high-quality component and to understand the influence that the powder properties have on the final result. Powders are mainly classified according to:

- Size
- Morphology
- Chemical Composition
- Flow Characteristics
- Density
- Laser Absorption Characteristics (absorptivity)

Methods, standards and examples of the measuring techniques can be found in Table 2 (elaborated from [18]). These characteristics are very important and determine the quality of the final part. For instance, particles of smaller size guarantee a thinner layer and improve surface finish, the shape of the particles can improve flowability. A chemical analysis is needed especially if re-cycled powder is used. Good flowability means good uniformity in the spread powder that, in turn, means a final component with lower porosity. Density is also an index of the quality of the raw material. Knowing the absorptivity of the powder, set between 0 and 1, one can understand the amount of energy that will be necessary, that can also vary depending on the characteristics of the source of energy.

The number of publications in literature that aims at discovering and analyzing the relations between the powder feedstock characteristics and the properties of the final component is not very big and, in addition, the majority of the articles is quite recent. Haferkamp et al. [29] show that the apparent density is higher than the density of a single layer of powder, the density of a single layer increases if finer powders are used and find out the existence of a limit for the particle size distribution under which the spreadability is hindered. In another publication from the same author [30] it is demonstrated that the flowability is improved if the particles are more spherical allowing higher layer density. On the opposite higher porosity is present for lower flowability of the powder deriving from low circularity of the particles even if, above a level of circularity of 0.8 this relation is no more valid and there is no influence on the density of the part. Young et al. [31] proposes novel techniques to characterize the powder feedstock, highlighting the fact that by adopting traditional techniques certain properties, such as compressibility and compactibility, of the powder would not be identified and two lots of powder could be wrongly classified as equivalent.

Table 2: Powder properties, measuring methods and standards.

Powder Property	Measuring method/analysis	Standard / examples
Size	microscopy	direct measure
	sieving	ASTM B214-07
	gravitational sedimentation	ASTM B761-06
	light scattering	ASTM B822-10
Morphology and shape	qualitative	ASTM B243-11
	quantitative	formulas from literature
Chemical Composition	microanalysis	Energy dispersive X-ray spectroscopy
	surface analysis	atomic emission spectroscopy
		X-ray photoelectron spectroscopy
		secondary ion mass spectrometry
bulk analysis	X-ray diffraction	
	X-ray fluorescence	
	inert gas fusion	
	atomic absorption spectroscopy	
		inductively coupled plasma optical emission spectroscopy
Flowability	Hall flowmeter funnel	ASTM B213-11
	Carney funnel	ASTM B964-09
Densities	apparent density	ASTM B212-09; ASTM B703-10
	tap density	ASTM B527-06
	skeletal density	ASTM B923-10
Absorptivity	computer calculations	ray tracing method
	experimental techniques	

## Powder additives

Adding elements to the powder feedstock seems to be very useful to ease the production process of certain materials or to obtain a component with enhanced properties [37]. Another example is provided by Yunlong et al. [38] that analyses the effect of the addition of Zr and Mo to Nb-Ti-Si based alloys obtaining an increase in the fracture toughness of about 30% and a significant decrease in hardness. The addition of nanoparticles additives (TiC) is experimented by Oropeza et al. [39] that use them to process the nanoparticle-enhanced aluminum 7075, obtaining an alloy easier to produce and free of cracks. Canziani et al. [40] proposes the use of supra-particles made of polystyrene/silica composite to be used with the base powders in powder bed fusion processes. These tailored particles with high flowability and well defined composition and morphology positively influence the powder flowability and so a higher-quality powder bed can be obtained.

## Functionally graded materials

Functionally graded materials (FGMs) are materials composed of two or more phases. The difference with respect to composite materials rely on the fact that the materials composition gradually varies from a region to another, which means that the distinction between different phases is not so net like in the case of composite materials. FGMs can provide many advantages, for example gradually varying the composition of a component from its core part to the outer surface can be beneficial for the corrosion and wear resistance, concentrating and enanching the certain properties of a component in those regions where they are needed.

Among the various options two systems, related to AM, are here reported:

- *Blown Powder AM Systems:*  
include direct laser deposition (DLD) and laser engineered net shaping (LENS) and involve the use of nozzles to deposit different materials in the desired quantities allowing to realize a gradually varying composition of the material.
- *Powder-Bed AM Systems:*  
include the selective laser melting systems. In this case the variation in composition can be realized only along the building direction, it is more difficult to vary the composition because the powder is supplied by a pre-filled tank but, being the thickness of each layer very reduced, the gradual variation in composition can be obtained with good accuracy.

One of the most important requirement can be identified as the "flexibility of the feedstock", meaning that the success of the manufacturing process strongly depends on how easily the composition of the feedstock can be tuned. However, to exploit the full potential of these materials the designer should not exclusively focus on the production

phase but also on the design, recognizing, for example, the need of a 3D CAD model made of FGMs instead of discrete materials and the importance of selecting the proper analytical model to foresee the properties of the component [11].

Interesting research about FGMs has been done by members of the *Jet Propulsion Laboratory* (USA) and collaborators [41]. The evolution of  $\sigma$  phase has been analyzed in different alloys [42]. The blown powder DED system was successfully implemented to produce compositionally graded cylinders made of FeCo-2V and 316L stainless steel (magnetic dissimilar alloys), and molecular dynamics simulations were correlating the tensile strength with the composition of the component [43]. DED production method was again used to join dissimilar metals (SS316 and C300 Maraging steel) and tensile strength equal to the stainless steel was measured together with a decrease in elongation [44].

FGMs are still under development and not very used in industries but a full understanding of their properties would for sure boost their expansion and decrease the need for welding or joining together different materials.

## Hybrid materials

This section could seem somehow similar to the previous two related to *Powder additives* and *Functionally graded materials*. However, the term *Hybrid materials* can be related to the previous two sections but can also refer to other solutions in which multiple materials are used, that also includes the so called multiple materials additive manufacturing (MMAM). A similar expression *hybrid manufacturing* is given to that category of production process that combines already assessed manufacturing method, like CNC, with novel AM techniques, here not considered.

The number of publications related to hybrid materials is increasing and concerns various aspects, few examples that could be useful for the engineer to overcome some design limitations are reported. The feasibility of making a metallic structure in Inconel-718 and Co-Cr, where the two materials are set in distinct regions of the components, is analyzed in [45]. Chueh et al. [46] printed a component made of metal and composite through a multiple material laser powder bed fusion system that uses an ultrasonic vibration-assisted powder delivery system and also providing a more extended analysis of MMAM [48]. De Pasquale and Sibona [47] investigate the increase in energy absorption capability of a material composed of a metal lattice structure combined with polymers, observing an impressive increment in the strain energy of up to 75%. A numerical tool to analyze the composite/metal structure and able to automatically select the design that holds the best structural performance is introduced by Di Caprio et al. [49].

## **Other solutions**

Solutions different from those that can be encompassed in one of the previous sections are very difficult to find, however, for the sake of completeness and for eventual future extension of the present work this section has been added. An interesting research has been conducted by Varela et al. [50] that used a non-spherical precursor, cheaper than the powder commonly used, to produce a component in Ti-6Al-4V that resulted to have properties comparable to the one manufactured using the spherical powder.

# Step 2: approaching topology optimization

According to the path previously defined the main aspects of topology optimization will be here described. A number of examples will then be proposed according to the general classification adopted of macro and micro topology optimization. A schematic of the content can be seen in Fig. 33.

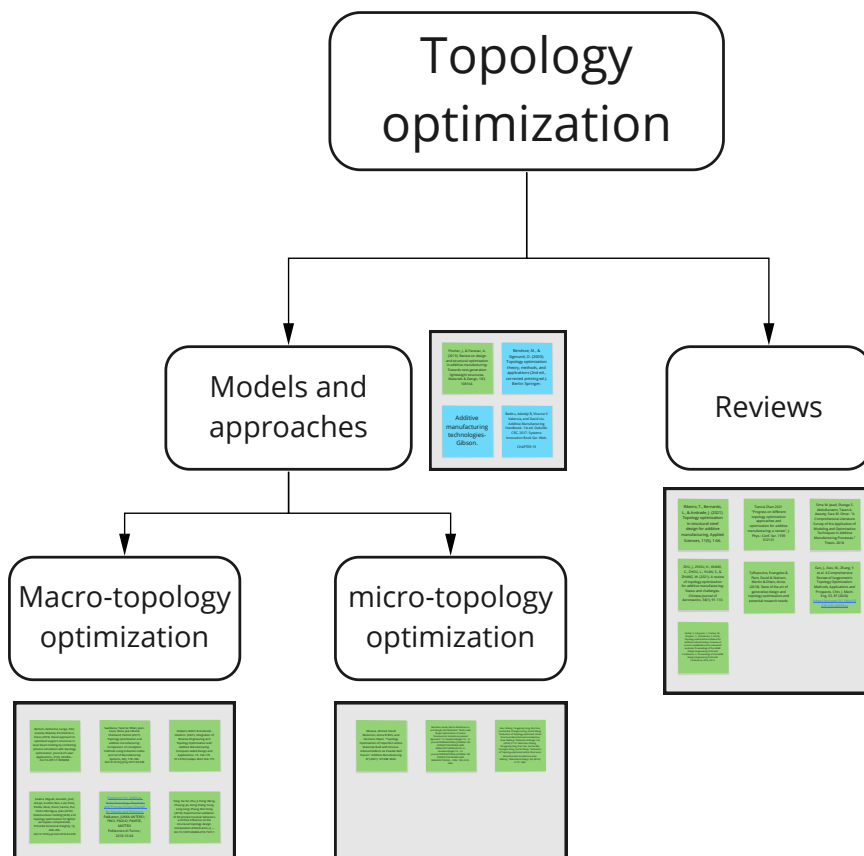


Figure 33: Topology optimization approaches.

## Topology optimization and how it works

Additive manufacturing technologies allow a design freedom that has never been available before. Objects with very complex geometries can be made and many different options are available at each design step. Then, a question that for sure the engineer will have to answer while designing an object is:

*Where to put the material to get the best achievable result?*

The answer is: Topology Optimization (TO). Indeed, TO consist on "*finding the ideal material distribution given certain objectives and load cases*" [1]. Ideally any shape can be realized but in practice there are different types of constraints that can be due, for example, to limitations on the manufacturability as well as to interactions of the component under analysis with the structure. Once that these limitations and the load cases (boundary conditions) are clear the *design space* can be defined and topology optimization can be performed.

TO is not the only method that can be adopted, size optimization and shape optimization are, together with TO, the most common approaches. The general objective of the optimization methods is to change certain design variables to improve the design of the object and can be done in different ways. Size optimization search for the best values of certain given dimensions while shape optimization adjust the shape of the surfaces to improve the outcome. Size, shape and topology optimization hold an increasing degree of complexity and all of them are commonly adopted along the same optimization procedure. Usually the first to be applied is TO and after, in the order, shape and size are used to further sharpen the design (Fig. 34) [2].

The problem of topology optimization can be seen, in a simple mathematical form, as a function  $f(x)$  that has to be minimized or maximized, where the  $x$  of the function are the variables that coincide with the design points. In real applications TO problems are obviously more complex and can require assumptions and decisions based on the judgment of the designer. The logical path followed to find a solution, that is not always present or not always unique, is an iterative procedure performed by a software and is described with an algorithm. Depending on the idea at the base of the optimization strategy there exist a considerable number of algorithms (two basic examples have been reported in Fig. 35).

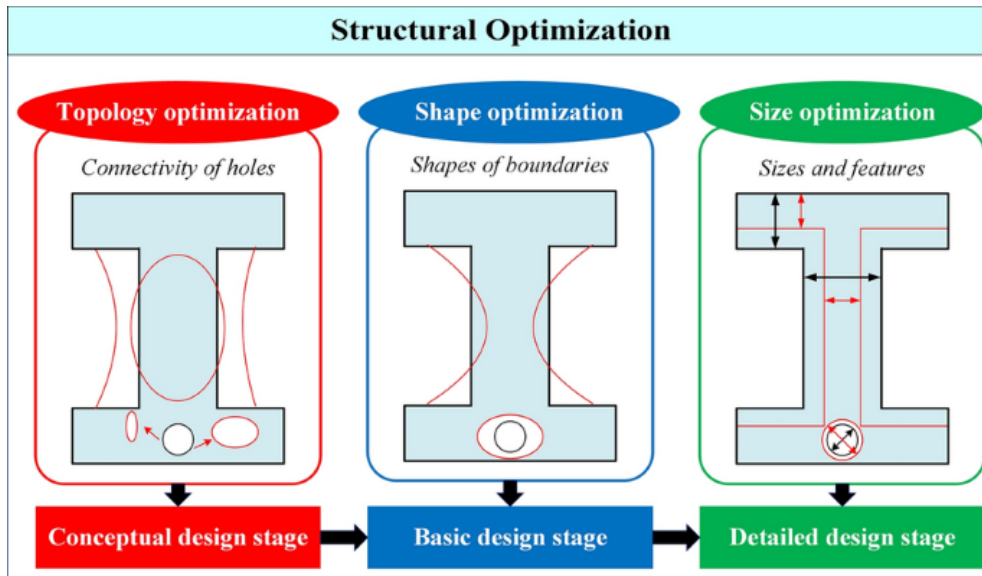


Figure 34: Topology, shape and size optimization [51].

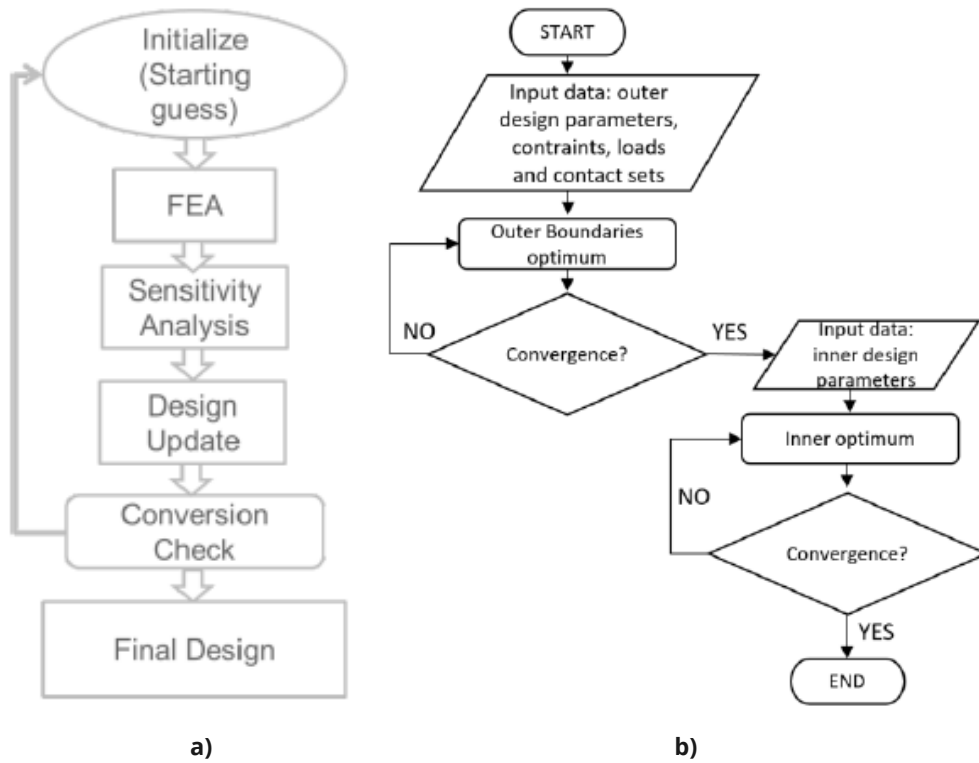


Figure 35: a) TO basic algorithm [23]; b) 2-level TO algorithm [52].

## Topology optimization approaches

The TO problem, that could be extremely simplified as a "material distribution problem", can be faced in different ways. In the present work all the approaches has been classified under two main categories:

- **"macro-topology" optimization:**

includes all the approaches that perform optimization at a macroscopic level, considering the whole shape and geometry of the component;

- **"micro-topology" optimization:**

includes all the approaches that perform optimization at a microscopic level, focusing on the optimization of the structure at the lattice level.

Typically, to perform an optimization at macroscopic level the object of interest is meshed in a set of voxels that assume the value of 0 or 1 corresponding to the value of the density. In other words they can represent a void or a "full-material" volume. Intermediate values are unwanted because they can be a problem during the production phase. This is why these approaches are also called *Volume-Based Density Methods*. Optimizations at microscopic level are also very common and aims at finding the best number, position and geometry of struts and nodes. Micro-topology optimization approaches, also called *Truss-Based Methods*, focus on much smaller volumes (e.g., unit cell) and aims at finding the best lattice configuration [2].

Considering the many possibilities that the designer have it can be possible that different topology optimization methods are needed for different components. The two sets of examples provided in the following paragraph, together with the most common approaches ([2][21][53]) and with reviews already published (general reviews: [51][52][54][55][56][57], software review: [58]), can then be useful to tailor the proper method case by case. It also should be said that the piece cannot be produced straightforward after the optimization, a simulation of the building phase is needed to avoid ruptures and undesired defects during the manufacturing phase [1].

## Macro-topology optimization

Table 3 contains publications referred to macroscopic characteristics such as mechanical properties of the components, geometry and shape of the part, relative density and support structures. These can be useful when an optimization of the outer geometry of the component needs to be performed to improve its full shape.

Table 3: Macroscopic topological optimization approaches.

Key words	Description	Bib. ref.
Support structures, SIMP method, cantilever beam.	Procedure consists of 2 steps. First a simulation of the production process is performed and the loads and residual stresses are identified for the worst case scenario. This data is then used to perform topology optimization and find the best geometry for the support structures. Validation is made analyzing the case of a cantilever beam.	[59]
Level of penalization, industrial codes.	The validity of three approaches is proved (stress-constrained, continuous compliance and discrete compliance optimization problems). Specimens are then produced via SLM techniques to find the best method and to measure the level of penalization. Stress-constrained optimization resulted to provide the best result.	[60]
Reverse Engineering, level set based TO, 3D inspection.	The positive outcomes coming from the integration of reverse engineering, topology optimization and additive manufacturing is demonstrated with the designing and manufacturing of a simple mechanical component. The object has been first scanned, then re-designed, produced and tested. A considerable mass reduction has been obtained.	[61]
Aircraft bracket, aluminium and Ti6Al4V.	The design, optimization, production and testing of an aircraft bracket are explored. Different loading cases are analyzed and FEA has been adopted. Changing material, from aluminium to titanium alloy and performing TO a 28% weight reduction has been achieved.	[62]

*Continues in the following page*

*Continues from the previous page*

Key words	Description	Bib. ref.
SIMP method, LSM method, 3-point bending test.	Two case studies are presented. In the first case a comparison between the SIMP and the LSM algorithms is conducted for both 2D and 3D case. In the second case the shape of a specimen for the 3-point bending test is optimized and then fabricated and tested.	[23]
Building direction, anisotropy, microstructure and macro mechanical performances.	Stereolithography and selective laser melting techniques are used to produce resin and titanium materials. Tests are performed to understand how the mechanical properties are influenced by the building direction and to analyze anisotropies of stiffness and strength. The design is optimized considering two aspects separately: printing direction and isotropy. Results are then compared.	[63]

*Begins in the previous page*

## Micro-topology optimization

Characteristics of the lattice, struts defects and features related to the elementary unit cell are described in the publications of Table 4. A "small-scale approach" can be adopted in cases where the proper type of unit cell has to be defined and its influence on relative density or on the mechanical properties of the component needs to be clarified.

Table 4: Microscopic topological optimization approaches.

Key words	Description	Bib. ref.
Process-induced defects, cell orientation, tetrahedron-based and octet-truss unit cells.	Geometric defects are embedded in non-perfect models. Behavior and properties of the unit cell are analyzed and then topology optimization is performed. Method of Moving Asymptotes is used to compute the design variables. The analysis is then applied to fixed-beam and L-shaped beam for verification.	[64]

*Continues in the following page*

*Continues from the previous page*

Key words	Description	Bib. ref.
Multi-scale strategy, NURBS curves, octahedral lattice structure, FE-based homogenization, automatic dynamic penalization (ADP) method.	The optimization of a representative volume element (RVE) is performed considering geometrical, manufacturing, thermodynamic and structural constraint. Geometry of the RVE is generated recurring to the B-spline and NURBS curves then FE-based homogenization has been performed. Both local and global parameters have been used to generate the FE model of the lattice structure. The numerical optimization procedure resulted in equivalent mechanical properties and a weight saving up to 39%.	[65]
FCC, VC and ECC structures, porosity, Gibson-Ashby model.	Face Center Cube (FCC), Vertex Cube (VC) and Edge Center Cube (ECC) lattice structures are manufactured via SLM method with different porosity levels. Both standard and optimized structures are then tested under different loading conditions and Gibson-Ashby maps are developed. In general, optimized specimens have better mechanical properties. FCC and VC have better mechanical properties than ECC that, in contrast, has the highest energy absorption capacity. The influence of yield phenomena becomes negligible at levels of porosity lower than 70%.	[66]

---

*Begins in the previous page*



**Part II**

**Manufacturing**



The physical production of the component is here analyzed. Following the process that actually takes place, the production techniques will be briefly explored. Then, attention will be put on the thermal history of the component which means that the behavior of the melt pool will be deepened. After the solidification of the material its properties are investigated. The cornerstones of the manufacturing process, most of which will be analyzed in the following, are schematically summarized in Figure 36.

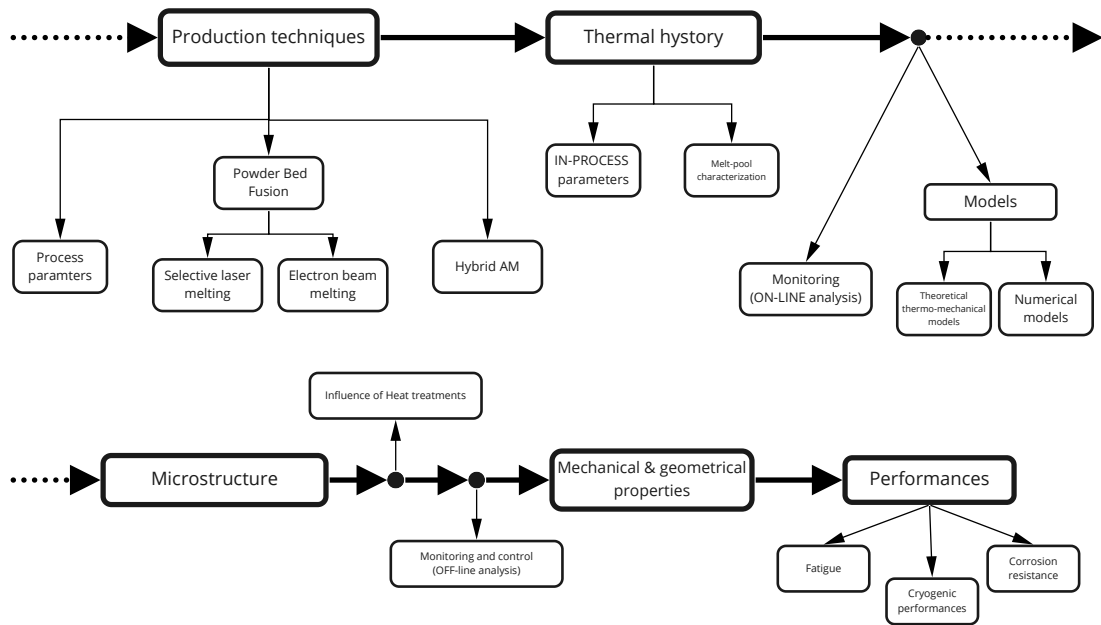


Figure 36: Manufacturing phases.



## Step 3: Tuning parameters

The parameters that will be investigated here have been presented in the introduction of this work. Tuning the parameters to see their effects on the produced component and to find the optimal set of parameters is probably the most active field of research related to AM. If an enterprise is able to perfectly control the outcomes it can obviously have an absolute advantage over the competitors, and this is one of the reasons why many resources are invested in this field and many companies do not publicly share the results of their research. However, a considerable amount of interesting publications can be found in literature and general trends can be delineated. This is what will be done along this step by comparing one, or few, design parameters at the time with the properties from Fig. 25, re-written and adapted in Fig. 37. Inside the group of design parameters one will also find “defects”, even if the defects are obviously not considered as a design parameters. It has been included in the design parameters for convenience, to easily analyze the effects of defects on materials properties.

Due to time constraints the analysis will be mainly focused on three alloys: nickel, titanium and aluminium, and on two production techniques: selective laser melting and electron beam melting, both included in the powder bed fusion production methods.

Understanding the design parameters - properties relation is of fundamental importance. By properly tuning the parameters the engineer will create a piece that is as close as possible to the ideal CAD model. Understanding this third step will not provide a perfectly precise set of parameters, because the production of a single component involves so many variables, just to mention a few: the type of machine used, the quality of the powder, that can change even for the same alloy type, and the melt pool morphology, that in practice it would be impossible to provide a “ready-to-use” set of parameters. Instead, taking step three the designer will save time and efforts, he will understand what could be the ranges inside which the parameters has to be searched, he can have a benchmark and then be aware of the direction that the production process is taking, he can estimate from the initial stages of the design what are the properties of the final component and, if something goes wrong, identify the probable causes.

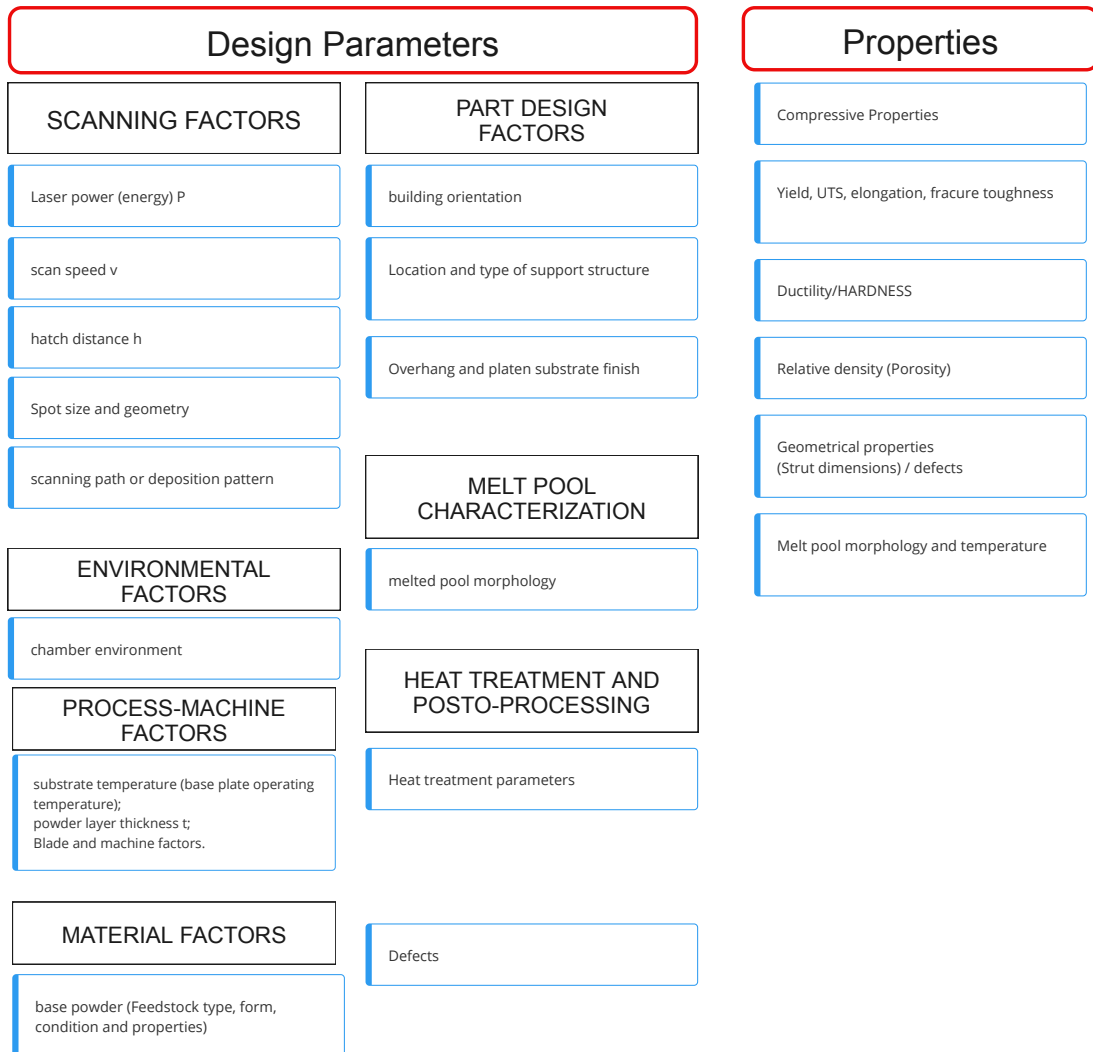


Figure 37: List of design parameters and properties.

## Production techniques

There are various methods to additively manufacture a component, a scheme of the most adopted techniques in the building industry is reported in Fig. 38. The choice of the proper manufacturing method can rely both on the experience of the engineers and on systematic methods (e.g., [69]).

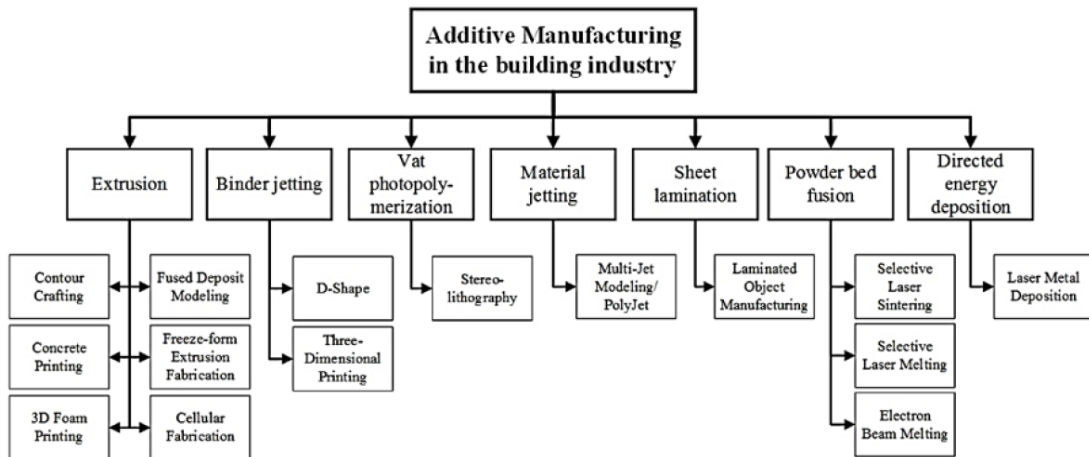


Figure 38: AM techniques and methods [68].

Among the many possibilities, only selective laser melting (SLM) and electron beam melting (EBM) will be analyzed herein. Both SLM and EBM methods are powder bed fusion (PBF) production techniques that, as can be deduced from Figure 28, is one of the most used for manufacturing metals and it is expected to grow even more in the future (Fig. 39).

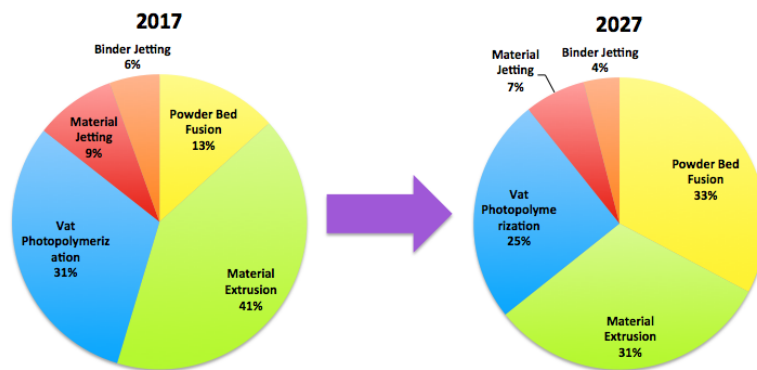


Figure 39: Evolution of polymer 3D printing hardware revenues from use in professional environments: 2017 vs. 2027.

Explanations of the basic functioning of SLM and EBM methods is not presented here but can be easily found in literature [11, 2, 1].

## Materials microstructure

Before investigating how the microstructure changes in relation to the process parameters, it is also useful to mention its main features. Different compositions of the alloys obviously mean different microstructures that present diverse characteristics. General information about titanium, aluminum and nickel alloys will be provided in the following sections and can be used as a reference point.

### Titanium alloys microstructure

Titanium shows a hexagonal lattice structure (HEX) for temperatures below 882.5° C ( $\beta$  phase) and a body centered cubic (BCC) structure for temperatures above 882.5° C ( $\alpha$  phase), this is why it is defined as a transition element. The transition temperature (882.5 °C) can be modified by adding  $\beta$ -stabilizer elements (Fe, Mo, V, Cr, Ni, Cu, W, Co, Nb, Ta) or  $\alpha$ -stabilizer elements (Al, C, O, N, B). So, based on these elements and on the microstructure exhibited, titanium alloys can be classified as:  $\alpha$  alloys and near- $\alpha$  alloys that are characterized by low tensile strength at room temperature and by high corrosion resistance;  $\beta$  alloys and metastable  $\beta$  alloys that have a lower resistance to plastic deformation, high ductility, high anisotropy, low elastic modulus and high corrosion resistance;  $\alpha+\beta$  alloys characterized by higher values of the strength due to the bi-phasic structure [27].

One of the most used titanium alloys is the Ti-6Al-4V (phase diagram in Fig. 40) that is also extensively studied in many publications related to AM and present in the standards (ASTM F2924-14 and ASTM F3001-14).

Typically its microstructure produced by Selective Laser Melting technique shows columnar prior  $\beta$  grains together with acicular  $\alpha'$  even if many are the factors that influence it. For example, it has been observed that controlling the input energy a very fine lamellar ( $\alpha+\beta$ ) structure can be obtained. Usually the component has residual stresses due to the high thermal gradient experienced during the SLM process and it cannot be used as it is, then post-processing is needed. During the heat treatment below the  $\beta$  transus, if the dwell duration is increased then the evolution of globularized  $\alpha$  grains increases while, if it is above the  $\beta$  transus, larger  $\alpha$  colonies are observed [11].

The presence of the  $\alpha+\beta$  phase has a great positive influence on the properties of the components and on the process parameters. The post-process heat treatments parameters can be adjusted to increase the amount of this phase on the produced part. Lower importance, but still not negligible, is attributed to other variables such as the oxygen content, that can influence the hardness and the strength of the alloys [27].

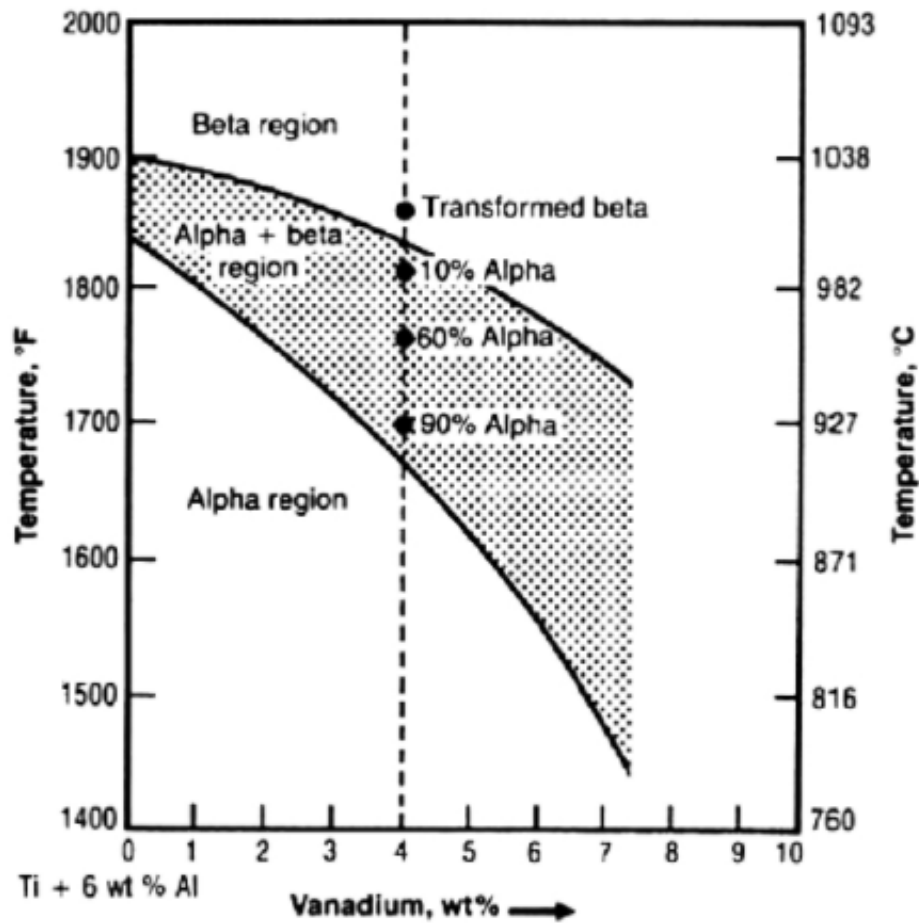


Figure 40: Ti-6Al-4V phase diagram [28].

## Nickel alloys microstructure

The so called Ni-based alloys are in practice Ni-Cr alloys characterized by a face centered cubic matrix that contains carbides inter-metallic precipitates. These precipitates guarantee notable mechanical properties to the alloy that can also operate at elevated temperatures. The addition of other metals (Al, Ti, Ni, Ta) contributes to the creation of the  $\gamma'$  phase while Mo, W and Cr improve the strength. A list of the alloys frequently used in PBF is reported in Figure 41. Among the many alloy types analyzed the most common in literature are [70]:

- *INCONEL*® 625:  
is a Ni-Cr-Mo alloys characterized by very good corrosion resistance.
- *INCONEL*® 718 and *HAYNES*® 230:  
Ni-Cr-Fe-Mo-Cu alloys. *INCONEL*® 718 has a very good strength in a wide range

of temperatures and an high resistance to oxidation. HAYNES® 230 has an excellent strength at high temperatures.

- *HASTELLOY® X*: solid-solution strengthened nickel alloy that exhibits exceptional oxidation resistance and very high strength until 1200 °C.

Alloy	Cr	Co	Mo	W	Al	Ti	Ta	Fe	Nb	Re	Hf	Zr	Ni
CM 247 LC	8.0	9.3	0.5	9.5	5.6	0.7	3.2	-	-	-	1.4	-	Bal.
CMSX-4	6.5	9.6	0.6	6.4	5.6	1.0	6.5	-	-	3.0	0.1	-	Bal.
HASTELLOY X	22.0	1.5	9.0	0.6	0.25	-	-	18.5	-	-	-	-	Bal.
HAYNES 230	22.0	-	2.0	14.0	0.3	-	-	-	-	-	-	-	Bal.
HAYNES 282	20.0	10.0	8.5	-	1.5	2.1	-	0.7	-	-	-	-	Bal.
INCONEL 625	21.5	-	9.0	-	0.2	0.2	-	2.5	3.6	-	-	-	Bal.
INCONEL 713LC	12.0	-	4.5	-	5.9	0.6	-	-	2.0	-	-	0.1	Bal.
INCONEL 718	19.0	-	3.0	-	0.5	0.9	-	18.5	5.1	-	-	-	Bal.
INCONEL 738LC	16.0	8.5	1.75	2.6	3.4	3.4	1.75	-	0.9	-	-	-	Bal.
INCONEL 939	22.4	19.0	-	2.0	1.9	3.7	-	-	1.0	-	-	0.1	Bal.
NIMONIC 263	20.0	20.0	5.9	-	0.5	2.1	-	-	-	-	-	-	Bal.
RENE 41	19.0	11.0	1.0	-	1.5	3.1	-	-	-	-	-	-	Bal.
RENE 80	14.0	9.0	4.0	6.0	3.0	4.7	-	-	-	-	0.8	-	Bal.
RENE 142	6.8	12.0	1.5	4.9	6.15	-	6.35	-	-	2.8	1.5	-	Bal.
WASPALLOY	19.5	13.5	4.5	-	1.3	3.0	-	-	-	-	-	-	Bal.

Figure 41: Ni-alloys for PBF [33].

## Aluminum alloys microstructure

Microstructure of aluminium alloys strongly depends on the alloy composition. In general they are characterized by  $\alpha$ -Al matrix where different types of secondary phase can be found such as: precipitation hardening phases, constituent particles (primary precipitates), divorced eutectic phases and dispersoids (secondary precipitates) [11]. Al-Si and Al-Si-Mg alloys are subjected to particular interest by the researchers. AlSi10Mg is particularly suitable for AM production process, its composition is near the eutectic (Fig. 42) and the range of solidification temperature is short. The presence of silicon improves the flowability of the melted metal that can easily wet the solid sub-strate, and also increases the absorptivity of the powder, while magnesium forms precipitates ( $Mg_2Si$ ) that strengthen the material [71].

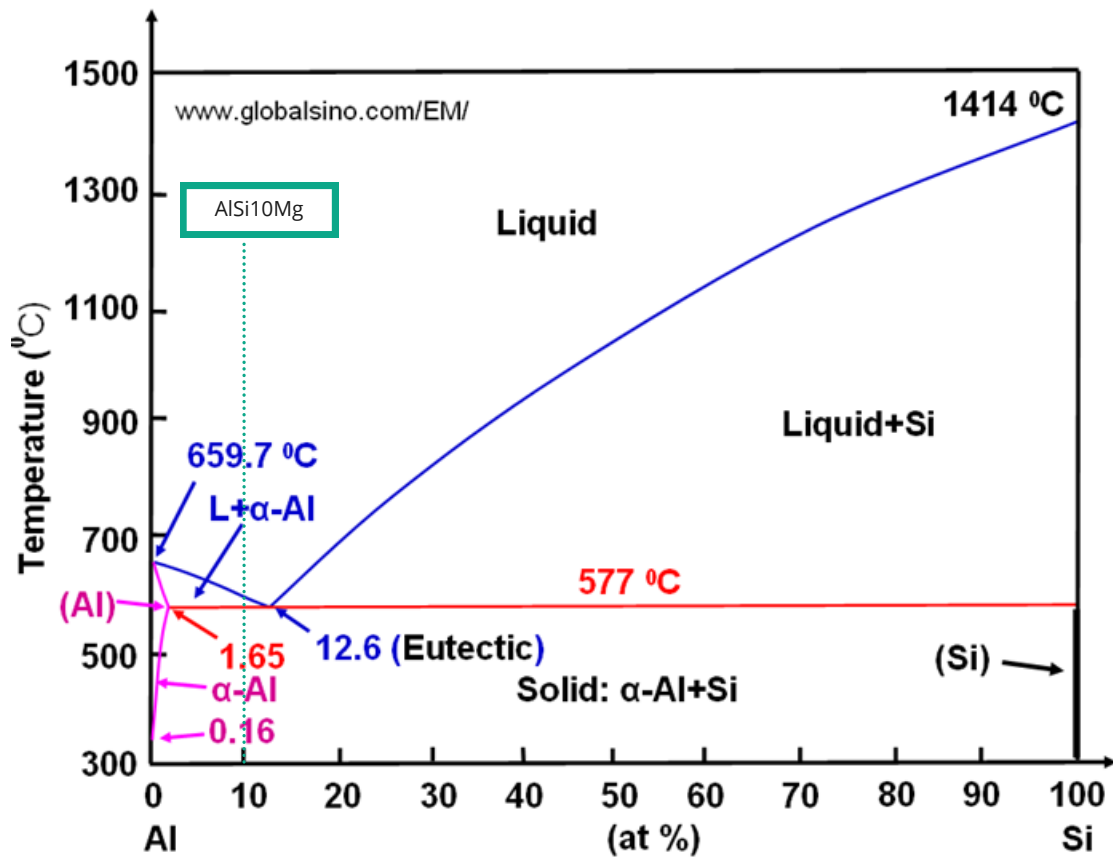


Figure 42: Al-Si phase diagram [72].

## Parameters-Properties analysis

The analysis of the relations that correlate the design parameters to the properties and the characteristics of final components is developed by the greatest part of the publications present in the literature. However, the approach commonly adopted consists in selecting a specific number of design parameters and correlate them with certain properties or characteristics of the produced part. Examples can include the analysis of the relation between laser scanning speed and porosity, between laser power and surface roughness or between laser energy and compressive strength. Despite of the fact that the outcomes of such studies can be very interesting, their validity, and more precisely their applicability and repeatability, are limited to very specific cases and it can be very difficult to replicate the exact conditions that would then produce the same results. In addition, by focusing on the influence of a limited number of parameters other factors are obviously neglected even if their negligibility is, very often, not demonstrated. Considering the great attention that the researchers give them it seems that the parameters that play a major role in the production process are those strictly correlated with the energy beam: beam power, scan speed, hatch distance and scanning strategy. Even if the effects of other factors are not so pronounced and it could be assumed that they have a negligible influence, the number of variables that, in this way, would be considered as unimportant is so high that it becomes hard to believe that they are all irrelevant, or that their combined effect has no influence on the final result.

The aim of the following sections is to analyze the relations linking the design parameters, starting from the characteristics of the raw powder, to the properties of the produced components, including geometric features, defects and mechanical behavior. A quantitative and precise description would require a huge amount of time and resources, however broad considerations can be made and general guidelines will be provided.

The detailed analysis of the big table correlating design parameters and properties (Fig. 25) presented in the introduction has been done. In general each publication refers to more than on aspects and hence occupy more than one cell of the table. So, the first passage was to modify the table to make each article appear only once in the table, the cell where it has been placed is to be considered as the argument on which the article is more focused. A further classification related to the alloys analyzed have been done according to the legend shown in Figure 43.



Figure 43: Legend of the colors used in Figure 44.

Despite of the classification made it has to be said that the greatest part of the

publications regarding Al-alloys and Ti-alloys refer to a reduced number of alloys that are AlSi10Mg, AlSi12Mg and Ti6Al4V. The Ni-alloys are quite varied even if is great attention given to the Ni-base superalloys. The materials labeled as *Others* are in general stainless steels and articles where virtual experiments are performed. Then, the analysis of the new big table obtained (Fig. 44) has been done by sub-dividing it in a number of smaller tables that are presented in the following sections.

		Design Parameters - Properties						
		Correlated by the Energy density/function	Compressive Properties	Vital, UT, elongation, failure toughness	Density/AMHONES	Porosity	Geometrical properties (form, dimensional defects)	Metallurgical morphology and temperature
SCANNING FACTORS	Laser power (energy/P)							
	scan speed							
	hatch retrace							
ENVIRONMENTAL FACTORS	Spot size and geometry							
	Scanning path/or deposition pattern							
	chamber environment							
PROCESS/MACHINE FACTORS	substrate temperature (base plate, powder layer thickness, C, fluid and nozzles flow)							
	base powder (feedback, gas, form, condition and properties)							
MATERIAL FACTORS	building orientation							
	Lattice structure type							
	Location and type of support structure							
MELT POOL CHARACTERIZATION	Overhang and pattern size as finish							
	metallurgical morphology							
HEAT TREATMENT AND POSTO-PROCESSING	Heat treatment parameters							
	DEFECTS							

Figure 44: Design-Properties table allows classification.



- *Basic flowability energy*: amount of work done while moving the blade within the powder bulk in a downward motion.
- *Specific energy*: amount of energy to move the blade within the powder bulk in an upward motion in an unconfined (i.e., low stress) environment as there is no constraint on top of the powder bulk.
- *Tapped density*: the bulk density of the powder when it is consolidated.
- *Compressibility*: shows the change in volume as a function of applied normal stress.
- *Cohesion*: amount of shear stress needed to flow the powder while the applied normal stress is zero.
- *Pressure drop*: indicates how easily the gas can permeate the powder while is under applied compression (3 kPa) and the gas flows from below the powder bulk.
- *Aeration energy*: indicates how easily the powder fluidizes when it is subjected to gas flow.

The properties listed above are intercorrelated, it is thus advisable to observe them all to have a clear picture and to inspect the same characteristic from different points of view. The specific energy is an index of the flowability but, being measured with the blade moving upwards it expresses the flowability in a low-stress environment, while the capability of the powder to fluidizes when crossed by a gas flow is defined by the aeration energy.

The dimension of the powders is one of the most studied characteristic. Analyzing two different batches composed of fine and coarse powder it has been observed that the oxygen contents is slightly higher for the fine powder. The basic flowability energy and the capability to compact under the re-coating arm was, in turn, slightly higher for the coarse powder (3.3% vs. 2.5%), pointing out that a coarser powder may behave better during the re-coating phase.

Nevertheless, these differences are so small that the two batches can be considered comparable as it can be observed in Table 5, where the order of magnitude of such parameters can also be captured (values are referred to Ti6Al4V alloy).

The dimensional distribution of the powder particles is expressed by the PSD that usually has a bell curve shape. In general this curve can be wider or sharper (Fig. 46 a ). The shape of the curve gives information about the behavior of the powder providing both the dimension and the distribution of the particles.

The dimension of finer powders is obviously smaller, that translates into an higher surface-to-volume ratio resulting in more frictions and so in lower flowability and higher “stickability”. The empty spaces between the particles are reduced and so it is the capability of a gas to permeate the powder. On the contrary a coarser powder is expected to have a higher flowability.

A wider PSD implies the presence of a batch where there are considerable amounts of

Table 5: Powder properties for Ti6Al4V fine and coarse powders (from [95]).

Powder properties	Fine powder	Coarse powder
Powder size distribution ( $\mu\text{m}$ )	15-45	15-53
Basic Flowability Energy (mJ)	$280 \pm 3.6$	$282.0 \pm 2.5$
Specific Energy (mJ/g)	$1.6 \pm 0.2$	$1.8 \pm 0.1$
Conditioned Bulk Density (g/ml)	$2.6 \pm 0.2$	$2.8 \pm 0.0$
Tapped Density (g/ml)	$2.8 \pm 0.0$	$2.9 \pm 0.0$
Compressibility (%)	$2.6 \pm 0.5$	$3.3 \pm 0.1$
Cohesion (kPa)	$0.10 \pm 0.00$	$0.10 \pm 0.02$
Pressure Drop (mbar)	$9.5 \pm 0.6$	$7.1 \pm 0.2$
Aeration Energy (mJ)	$5.3 \pm 0.9$	$5.0 \pm 0.3$

particles of different sizes. When mixed the finer particles tend to adhere between each other resulting in separated agglomerates of fine and coarse powder, this phenomenon can also be observed in case of sharper PSDs but it is less evident (Fig. 46 b) ). Empty spaces appears around these agglomerates improving the compressibility and the permeability of the powder. A higher permeability results in a lower pressure drop.

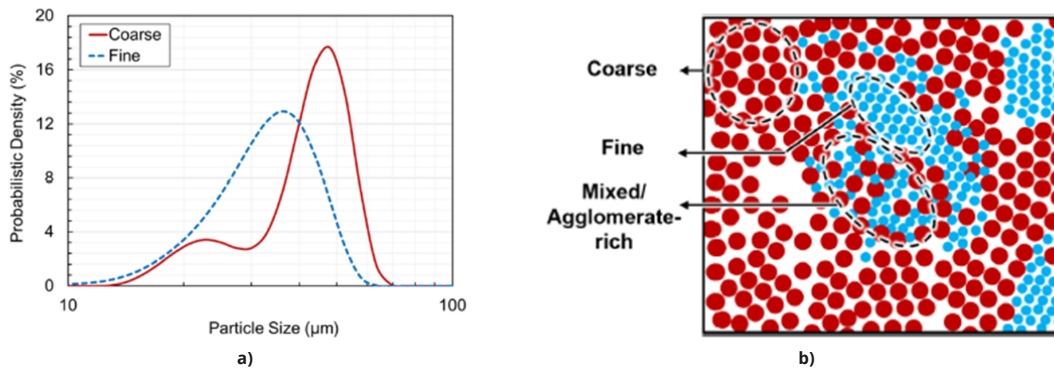


Figure 46: a) PSDs for fine and coarse powders, b) agglomerates of fine and coarse powder [95].

Data about the PSDs can be found in Table 6 where the limited data published is reported in two commonly used forms:

- Providing the size range and the mean value in micron.
- Using the statistic method D10, D50 and D90 that indicates that the 10, 50 and 90% of the analyzed particles fall below the corresponding value in micron.

Table 6: Powder sizes for different materials.

Material	Alloy type	Size range ( $\mu\text{m}$ )	mean ( $\mu\text{m}$ )	D10 ( $\mu\text{m}$ )	D50 ( $\mu\text{m}$ )	D90 ( $\mu\text{m}$ )	Bib. ref.
Aluminium	TiB <sub>2</sub> /AISI10Mg	55-18	33	-	-	-	[73]
	AISI10Mg	55-10	-	-	-	-	[76]
	AISI10Mg	45-15	-	-	-	-	[91]
	AISI10Mg	50-25	-	-	-	-	[96]
Al6061; AISi10Mg	AISI10Mg	120-12	-	-	-	-	[13]
	AISI10Mg	45-15	-	25	35	55	[99]
	AISI10Mg	35-1	-	-	-	-	[104]
Titanium	Ti6Al4V	-	-	7,6	28,6	41,9	[74]
	Ti6Al4V (SLM)	45-15	-	-	-	-	[80]
	Ti6Al4V (EBM)	106-45	-	26	38	51	[83]
	Ti6Al4V	50-25	-	51	72	109	[83]
	Ti6Al4V	69-35	-	-	-	-	[89]
	Ti6Al4V	45-15	-	-	-	-	[87]
Nickel	Inconel 625	45-15	-	25	32	42	[99]
	Inconel 718	45-10	-	33	40	49	[99]
	Alloy 718	45-10	-	-	-	-	[94]
Others	Inconel 939	45-15	-	16,8	26,1	40,7	[105]
	SS 316L	45-15	-	-	-	-	[77]

Together with the powder size distribution and the other properties listed above also a more detailed analysis can be done to inspect the chemical properties by using, for example, an ion beam-scanning electron microscopy to observe the sphericity of the particles and the presence of satellites particles (Fig. 47 a) where the arrows indicates the satellite particles and the circles the particles with non spherical shape). The inner part of the particles can be analyzed observing the cross sections (Fig. 47 c). Few entrapped gas pores can be detected and usually are the result of the gas atomization process used for the powder production. A scanning electron microscopy can be useful to see the powder microstructure (Fig. 47 c). In this particular case the IN939 Ni-base superalloy was inspected resulting in few satellites, a good sphericity, a reduced presence of gas pores (order of magnitude of 20  $\mu\text{m}$ ) with a total porosity around 0.4%. The presence of dendrites (1-2  $\mu\text{m}$  width) enriched in Ti, W and Nb while Ni, Cr and Co has also been found in the inter-dendritic regions [105].

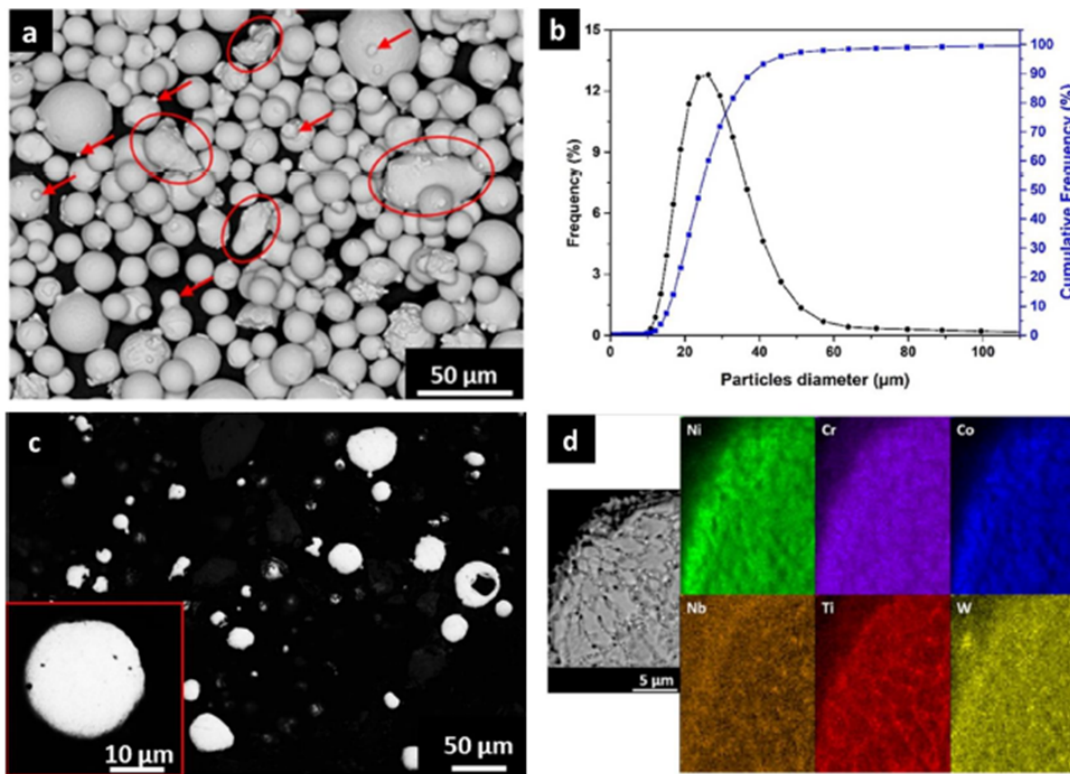


Figure 47: Powder analysis revealing: a) powder satellites (arrows) and powder sphericity (circles), b) PSD, c) inner gas pores, d) SEM images [105].

Relations between materials factors and properties of the final component are not very much explored, however certain aspects can be observed and will be described in the following.

### Material factors on mechanical properties

Productions techniques such as selective laser melting and electron beam melting allow to easily add extra components to the base alloys commonly used. It is the case of the SLMed Al-Mg-Sc-Zr alloy that exhibited interesting mechanical properties together with a brittle crack. After aging at 325 °C for 4 hours the material showed a yield strength (YS) of 510 MPa, an ultimate tensile strength (UTS) of 531 MPa and an  $\epsilon_f$  around 15%. The intrinsic toughening has been attributed to the precipitates that formed at the boundary of the melt pool while the  $\alpha$ -Al matrix contributed to the extrinsic toughening. The post heat-treatment improved the homogeneity of the properties even if discontinuous yielding was still present [100][121]. Pre-alloyed TiB<sub>2</sub>/AlSi10Mg is another example of the combination between aluminum alloy and other components produced via SLM. An improvement in tensile strength and elongation has been obtained both along the vertical (139% and 208%) and horizontal (19% and 13%) directions if compared to AlSi10Mg [73]. The two batches of powder (Ti6Al4V) analyzed in the previous section didn't exhibit considerable changes in the mechanical properties, the  $\epsilon_f$  was a bit higher in the coarse powder but the YS and UTS were very close. Hence, considering the small number of publications related to the influence of the PSD on the mechanical properties of the components no general conclusions can be made because the slight effects observed cannot be linked directly to the different PSDs but could be due to other reasons [95].

### Material factors on ductility and hardness

Due to the fact that the Ti6Al4V coarse powder produces components with smaller defects an increase in ductility has been observed [95].

Another study proposed the addition of variable quantities of Mo and Zr in a Nb-alloy produced via laser direct energy deposited (L-DED). This resulted in variations of the microstructure and in different values of the hardness, both before and after heat treatment at 1400 °C for three hours (Fig. 48) [38].

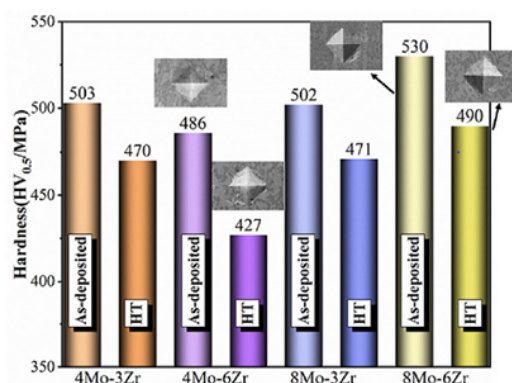


Figure 48: Hardness of the Nb-alloy with addition of Mo and Zr before and after HT [38].

Inconel 690 alloy (FCC) cladding 316L SS (FCC) is manufactured trying to obtain a material with better mechanical properties and improved corrosion resistance. The sub-grain boundaries of Inconel 690 are adopted for coherent twin boundaries so that the precipitation of carbides can be avoided and the corrosion resistance can be enhanced. In addition, the Inconel cladding showed superior mechanical properties compared to the SS 616L substrate, in particular an increase of 33% and 23% has been observed in hardness and yield strength, respectively, together with 21% elongation that decreased of 7% after aging at 685 °C for 50 hours. Thanks to the columnar and highly textured grain boundaries the free energies at the interface are reduced so that, at high temperatures, the precipitations at the grain boundaries are reduced and the capability of the component to operate is improved [129].

### Material factors on geometry and defects

As previously mentioned the coarse powder has a lower surface-to-volume ratio that results in a lower energy absorption capacity and then in higher cooling rates. This, together with the higher number of empty spaces created by a non-uniform distribution, produces a higher number of defects. On the contrary, specimens produced using a finer powder contain a lower number of defects even if they can be greater in size. The ranges of volumetric defects size for the fine and coarse powder are 171-130  $\mu\text{m}$  and 113-83  $\mu\text{m}$ , respectively. The density is above 99.99% in both cases. The higher energy density required by the coarse powder to reach full melting seems to be also the reason why the specimen produced with coarse powders have a higher surface roughness. Indeed, partially melted particles have been observed in all the specimens but they are higher in number when the coarse powder is used. The analysis of the number of defects as a function of the location on the build plate (east or west) also revealed that parts produced with fine powders are more "location-independent" (Fig. 49) [95].

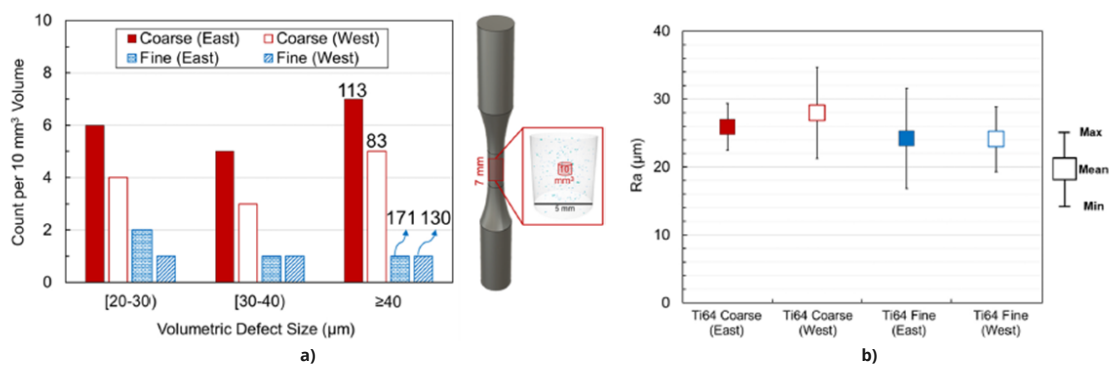


Figure 49: a) defects size and density and b) surface roughness for fine and coarse powders and different building locations. [95].

The powder production method seems to have a certain influence on the quality of

the powder. Comparing plasma-atomized (PA) and gas-atomized (GA) Alloy 718, the latter shows a more irregular morphology. Satellites particles are present in both the powders. After recycling agglomerates of powder particles has been found. The pores content was higher for the GA powder while fine secondary phase was present in PA powder [15].

### **Material factors - Guidelines**

Considerations on the influence of the material factors on the characteristics of the final component can be made and can be used as a reference for further activities.

- Powders with a narrower PSD (lower span) have a higher flowability.
- Powders with a wider PSD occupy better the space available resulting in higher powder bed density (PBD).
- When powders with a wider PSD are mixed tend to form separated agglomerates of fine and coarse particles.
- Real PBD is typically lower than theoretical PBD.
- Measured powder layer density (PLD) of a single layer differs from measuring many layers at once.
- PLD seems to decrease for decreasing layer height.
- Higher PLD is obtained with finer powders.
- Powder cohesion, wall effect and percolation effect are more relevant during the layer deposition phase.
- A more uniform PBD can be reached with a lower aeration energy.
- Coarse powders have higher flowability and higher capability to compact under the re-coating arm that makes them behave better during the re-coating phase.
- No considerable differences in mechanical properties has been observed between specimens produced with fine and coarse powders.
- Coarse powders have a lower energy absorption capability (due to lower surface-to-volume ratios) and an inferior packing state (more empty spaces) resulting in a higher number of defects.
- Fine powders have a lower number of defects of bigger dimensions that may be connected to the splashing during production.
- For fine powders, the location on the building platform has no influence on the presence of defects (not true for coarse powders).

- Specimens from fine powders show higher ductility attributed to the lower number of defects.
- Fine powders shows a higher degree of roundness even if the difference is negligible.
- Pieces produced using coarser powders have higher surface roughness due to the higher number of partially melted particles.
- Plasma-atomized (PA) powders have a more regular morphology than gas-atomized (GA) powders.
- Recycled batches contain agglomerates of powder.
- After-recycling: GA powders have higher porosity content than PA powders where, in contrast, a secondary phase has been observed.

## Part design factors

In the present section the part design factors considered are mainly the building orientation and the lattice cell size and shape. Their influence on mechanical properties, geometry and defects will be explored.

## Part design factors on mechanical properties

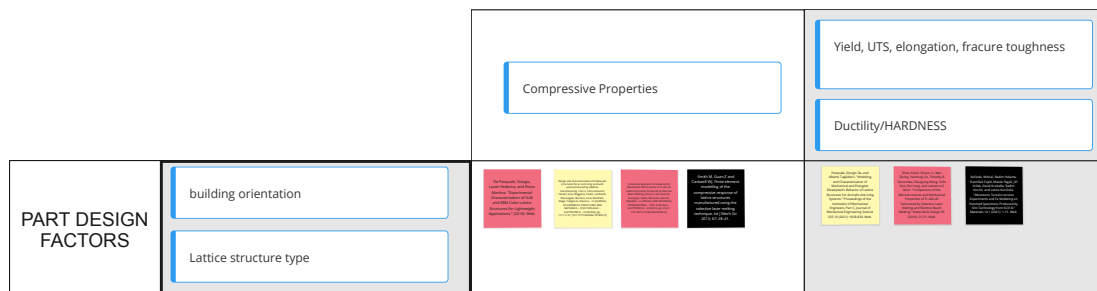


Figure 50: Part design factors on mechanical properties.

In Figure 50 the building orientation and the lattice structure type are shown as a function of the main mechanical properties. In the following the relations between these elements will be investigated. It has been chosen to not explore one mechanical properties at the time because it would result inconvenient, considering that each publications usually analyses the influence of one factor on more properties at once and, more important, taking into account that the designer has to select the proper factors being aware of the consequences of such choice on many aspects to accomplish the final requirements.

### Building orientation on mechanical properties

Considering the basic functioning of the powder bed fusion technologies the orientation of a piece on the building plate (building orientation) plays a crucial role. The manufacturing phase is performed layer by layer and the high temperature gradients taking place influence differently the microstructure of the same component depending on its orientation resulting in different mechanical properties.

In the present section the effects of building orientation on bulk parts will be analyzed while the inspection of lattice structures will be done later.

Specimens are mainly analyzed along the horizontal and the vertical building direction, and the exhibited properties varies depending on the alloy used.

Considering 316L stainless steel specimens produced via SLM, the yield stress is higher for the horizontally built ones than for those built vertically, the difference is approximately 75 MPa. This has been observed both in case of machined and "as-printed"

state. The ductility of machined specimens is approximately 1/3 lower [77]. A similar trend has been observed for the aluminium alloy TiB<sub>2</sub>/AlSi10Mg where the UTS, YS and elongation decrease moving from horizontally ( $536.9 \pm 14.4$  MPa,  $332.3 \pm 6.7$  MPa, and  $16.5 \pm 1.7$  %) to vertically ( $517.3 \pm 9.1$  MPa,  $277.9 \pm 6.9$  MPa, and  $15.4 \pm 1.6$  %) built specimens [73].

Ti6Al4V alloy microstructure is characterized by a prior  $\beta$  columnar grains parallel to the building direction. So, in case of horizontally printed specimens these grain are perpendicular to the loading direction and it is supposed that the stresses concentrate near the grain boundary at the  $\alpha/\beta$  interface where some defects are present, resulting in lower ductility. Manufacturing the specimens along the vertical direction the prior  $\beta$  columnar grains are aligned with the direction of the tensile stress applied encouraging more pronounced necking phenomena that result in higher reductions of the cross sectional area and higher ductility.

These differences in the microstructure lead to have slightly lower strength and ductility for the horizontally built specimens, and this is true both for SLM and EBM and for specimens of different sizes (Fig. 51). It can also be noted that the specimens produced via EBM hold a bit lower strength and higher ductility that those produced via SLM. In addition looking at SLMed samples, the strength increases and the elongation decreases when the size of the part decreases. These variations of the mechanical properties are more evident for smaller components (size < 4 mm) and for EBM, while the effect is almost negligible for SLM[83]. These trends of the mechanical properties strongly depends on the microstructure.

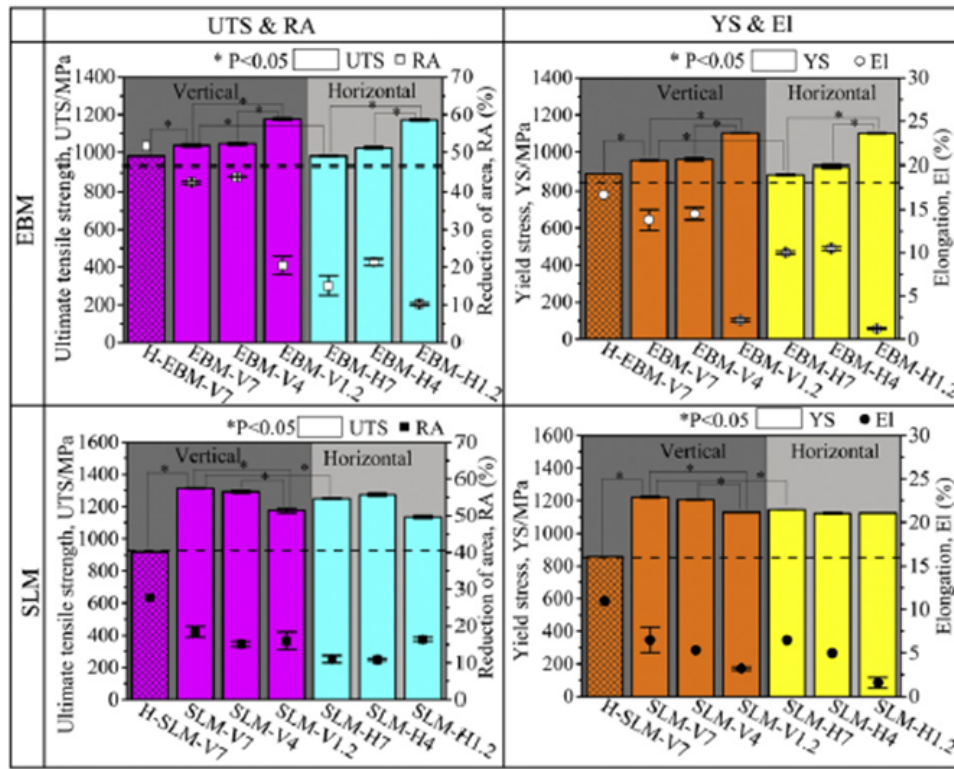
### **Lattice type on mechanical properties**

Among the various elements characterizing the elementary cell of the lattice structures the size and shape of the elementary cells are those of major concern. The two following paragraphs aim at clarifying the relations between these features, the mechanical properties and the failure mechanisms.

Various attempts to understand the lattice behavior are done via finite element modeling (FEM) but some critical issues have been encountered. The number of parameters characterizing one elementary cell is very high considering that, just to mention a few, the thickness of each strut element have to be measured as well as the geometrical dimensions at each node to have a decent description of the lattice shape. This allows to estimate the mechanical properties only of a limited number of unit cells. A reverse engineering approach and proper statistical methods may be a solution to some critical issues but the experimental characterization remains still fundamental [88].

### **Lattice cell features on mechanical properties**

Shape and size are the two main design parameters influencing the mechanical properties of the component. The basic idea followed by the majority of the researchers



\* The elongations of samples with diameter in 1.2 mm are estimated from stress-strain curves.

Figure 51: Tensile properties of Ti6Al4V for SLMed and EBMed specimens, for different sizes and orientations (dashed rectangles refer to wrought alloys) [83].

is to observe separately the effect of these two factors: varying the shape keeping the size fixed and viceversa.

Nonetheless, in the present paragraph it has been decided to shortly focus on the cell shape and size and then, considering that for our purpose the two properties are strictly correlated, to move to broader considerations.

The most common types of cells are classified accordingly to the presence of vertical elements. The body-centered-cubic (BCC) cell has no vertical struts that, instead, can be found in the FCCZ, FBCCZ, FBCCXYZ. Under compressive loads the presence of vertical struts notably improves the mechanical properties. The variation of Young's modulus and  $\sigma_{max}$  in SLMed AlSi10Mg components made by cells of the same size is evident from Table 7.

It has been observed that the BCC exhibits a bending-dominated behavior while other typologies (FCCZ, FBCCZ and FBCCXYZ) follow a stretch-dominated behavior. The latter have vertical struts aligned with the direction of the load. The FBCCXYZ for Ti6Al4V and the FBCCZ for AlSi12Mg (Fig. 52) show the highest moduli [98].

The effect of different unit cells made of Ti6Al4V has also been studied in case of dode thin, G-structure and rombi dodecahedron for a cell size of 4 mm. The trend of

Table 7: Young's moduli and  $\sigma_{\max}$  for BCC to BCCZ cell types in AlSi10Mg (elaborated from [81]).

Cell size (mm)	Strut size (mm)	Young's Modulus (MPa)		$\sigma_{\max}$ (MPa)	
		BCC	BCCZ	BCC	BCCZ
4	1	271	1139	10	29
4	1.2	745	1721	23	54
5	1	65	720	4	15
5	1.2	299	1146	10	29

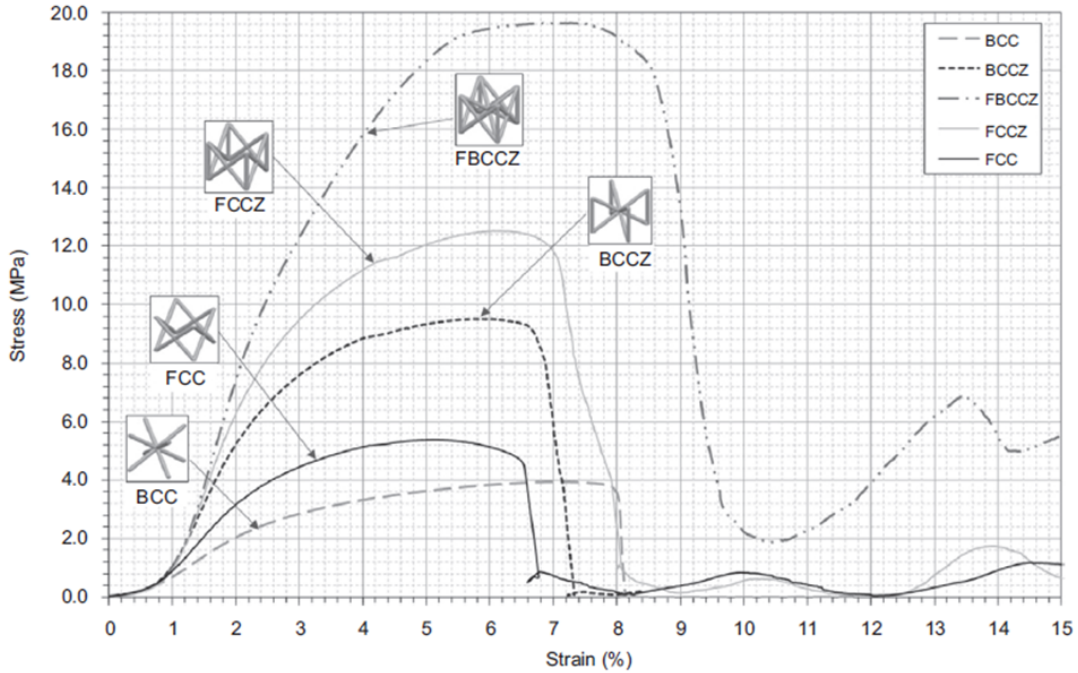


Figure 52: Stress-strain curves for different unit cell types (AlSi12Mg, uniaxial compression tests) [98].

mechanical properties observed was not the same for different sizes of the cells (7 and 10 mm), it is then evident that the analysis seen until now should be combined with that related to the cell size [85].

In Table 7 it can be noted that higher properties belong to the structures characterized by greater struts thickness (1,2 mm). An even more interesting result can be depicted observing that the properties reported in the first and fourth rows are somehow comparable, this means that similar properties can be obtained with a smaller unit cell and thinner struts. However, the densities of the two unit cells considered are very close suggesting that lattice density is also a relevant parameter. Thicker struts (in this case 1,2 mm) allow to have a greater cross section and a higher capability of bearing loads,

while smaller cell sizes (4 mm) lead to higher density that means higher mechanical properties[81].

Exceptions to this trend can be found considering the fact that the same specific modulus has been measured for the same cell type of different size (2 and 3 mm), in this case a lighter component exhibit similar stiffness[98].

In addition, mechanical properties of EBMed Ti6Al4V lattice structures decrease for increasing cell size. Instead, the increase in mechanical properties appear strongly dependent on the increase in relative density of the unit cell [85], and an increase in the unit cell size can worsen the load bearing capacity [123].

Attention must be paid to local plasticity phenomena that can occur under compressive loading resulting in Young's moduli lower than those commonly observed (1 or 2% strain) underestimating the stiffness of the parts. This does not occur for bulk pieces.

The previous observations have been made considering compression tests, moving to a tensile curve some differences have been noted between EBM and SLM production techniques. Usually EBM is considered to be faster than SLM that, in turn, is more precise in modeling small features. In the case of Ti6Al4V cubic lattice structures the building direction does not have a considerable effect on the mechanical properties rather than the production technique that has a crucial role. This may be attributed to the higher precision of SLM method considering that the thicknesses are, in this particular case, quite small (0.4-0.6 mm). The average Young's moduli for the SLMed specimens are  $64.390 \pm 2.53$  MPa (horizontal) and  $63.411 \pm 3.792$  MPa (vertical), while for EBMed ones are  $38.349 \pm 9.164$  MPa (horizontal) and  $36.431 \pm 2.811$  MPa (vertical) [80]. Lattice structures seems to be promising also for the production of impact absorbers. Performing an impact test on BCC and BCCZ unit cells (cell size: 4 and 5 mm, strut thickness: 1 and 1.2 mm) resulted in increasing energy absorption capacity for increasing density of the unit cell [82].

### **Lattice cell characteristics on fracture mechanism**

Starting from a simple cubic lattice structure made of Ti6Al4V three failures modes have been identified. In the first mode the collapse of an entire layer due to buckling at the strut intersections has been observed, the second mode is characterized by the presence of shear forces that caused the brittle fracture of horizontal struts while the third mode is a combination of the previous two. In both mode one and mode two there is the collapse of one plane over another (densification) along  $90^\circ$  and  $45^\circ$  planes with respect to the vertical direction, respectively (Fig. 53). The first failure mode occurred for SLM and EBM and involves simultaneously an entire layer, in the other two modes, that are only related to EBM, single cells collapse in random locations probably due to defects or imperfections [80].

Considering different types of cell it is evident that the effect of vertical structural element is important as it was also for mechanical properties. For BCC and FCC, that do not have vertical struts, a large deformation has been observed prior to failure (both

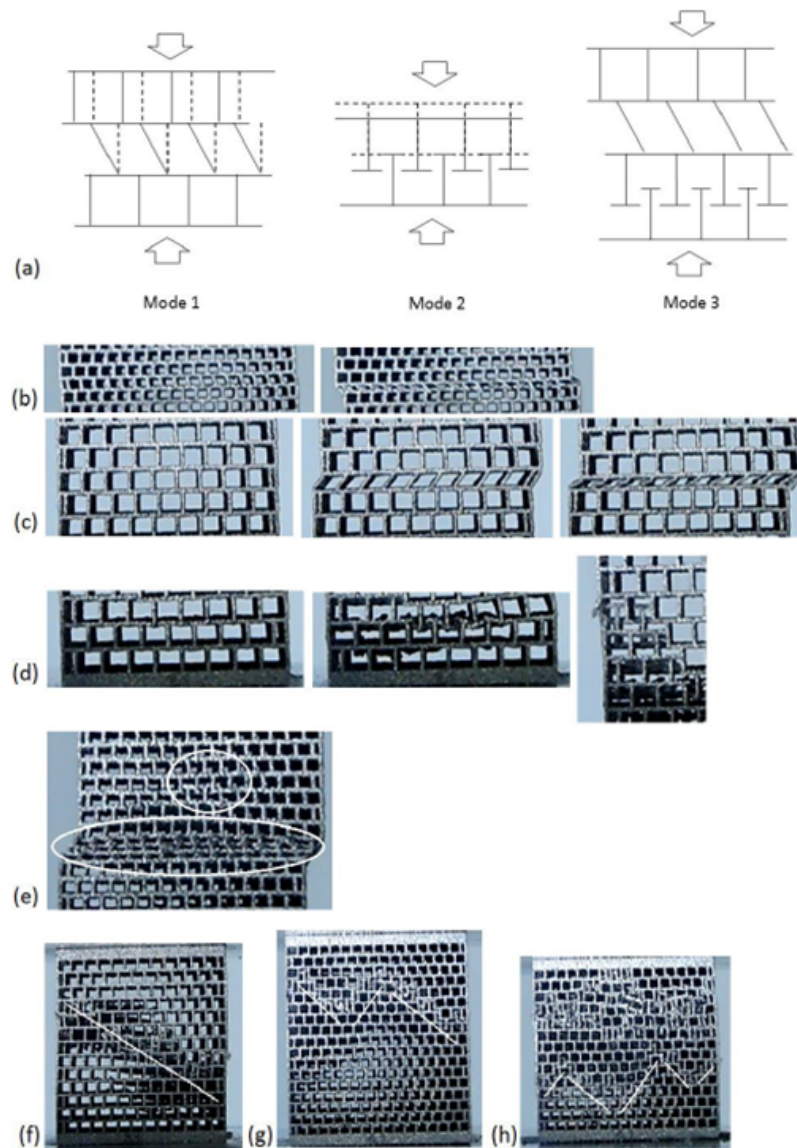


Figure 53: (a) cubic Ti6Al4V lattice structures failures modes, mode 1 SLM (b) and EBM (c), mode 2 EBM (d), mode 3 EBM (e), 45° brittle lattice failure for EBM (f) (g) (h) [80].

for AlSi12Mg and Ti6Al4V) while the horizontal crushing of a layer occurred for stiffer lattice structure with vertical struts [98].

The collapse of a plane along the 45° direction with respect to the vertical axis can also occur for both BCC and BCCZ (Fig. 54). In this case AlSi10Mg SLMed specimens have been tested and the collapse of the structure has been attributed to the deformation of the horizontal plane for the BCC, and to the buckling of the vertical struts for the BCCZ. It has to be noted that after collapsing the separation of the component in two parts did

not occur only for the BCCZ specimens [81].

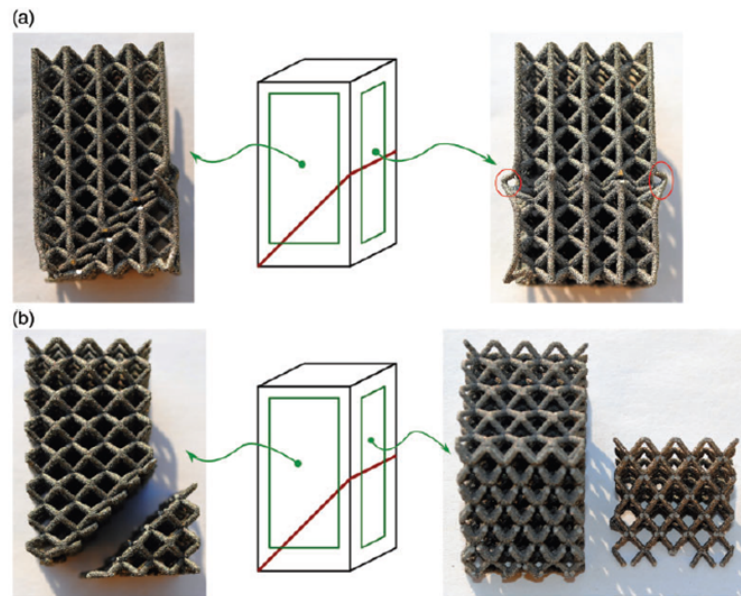


Figure 54: Collapse of lattice specimens (SLMed in AlSi10Mg) for BCCZ (a) and BCC (b) [81].

In general, the failure process identified by mode 1 (always present for SLM and sometimes for EBM) can be compared to that of metal foams and trabecular structures where, after reaching the maximum load, one plane collapses over another one and a new equilibrium point is reached. Then this process repeats and the component undergoes what is called densification. In practice the failure of the component is not catastrophic. This failure mode is attributed to the dissipation of energy over a large area as opposite to the other types of failure that are caused by local defects [81] [80]. The first failure mode is the most interesting considering that the collapse of the component can be pre-designed resulting in a controlled process that is crucial, for example, for impact absorbers or for structure that are required to be compliant. Differences can also be present in case of machined or and as-printed components. Compression tests conducted on SLMed 316L stainless steel specimens revealed that brittle fracture prevailed for the machined samples while ductile fracture occurred for the as-printed ones [77].

## Part design factors on mechanical properties - Guidelines

### Bulk components

- Vertically built specimens exhibit slightly lower mechanical properties than horizontal ones for stainless steels and Al-alloys.

- Vertically built specimens exhibit slightly higher mechanical properties than horizontal ones for Ti6Al4V alloys (due to prior- $\beta$  columnar grain characterizing the microstructure)

### **Lattice structures**

- The parameters that have greater effects both on mechanical properties and failure mode are:
  - cell type (together with the presence/absence of vertical struts)
  - cell relative density (given by cell size and strut diameters)
- For a fixed cell type the relative density is the most influencing parameter.
- In general the performances (mechanical strength, Young's modulus, absorbed energy) improve for higher density levels.
- Presence of vertical struts plays a crucial role.
- Failure modes can be designed. Intentionally compliant structures can be realized by manufacturing cells without vertical struts.
- Lattice structures failure modes seems to be independent from the alloy used.
- Ductile fracture and brittle fracture behavior prevail for "as-printed" and machined specimens, respectively.

## Part design factors on geometry and defects

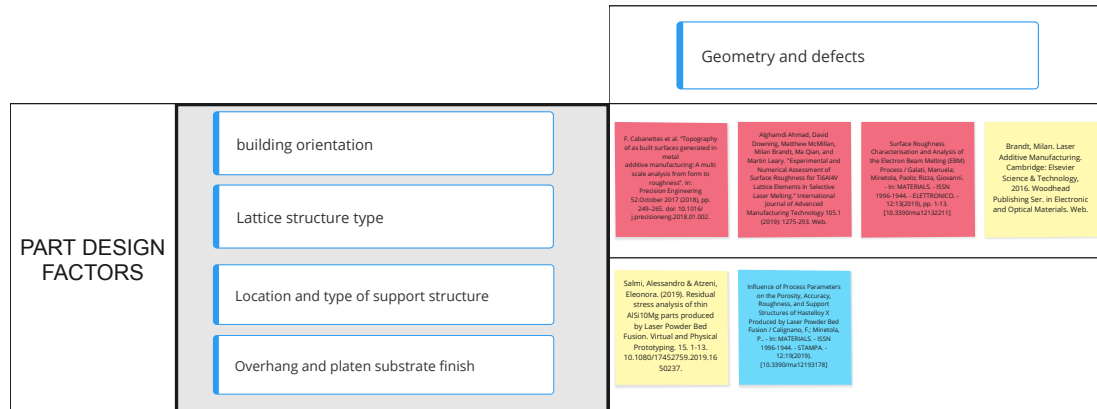


Figure 55: Part design factors on porosity, geometry and defects.

Part design factors have an important effect on the geometry and the defects that the produced component will have. Porosity as a function of the building orientation and the type of unit cell is marginally investigated, this is the reason why, despite of the initial intentions, greater attention will be put on the influence of the building orientation on the surface and part quality and on the lattice characteristics.

First of all it can be interesting to understand if the removal operations performed at the end of the manufacturing phase have consequences on the quality of the component. Wire EDM cutting is commonly used to remove the part from the build plate and it has been observed that it has a negligible influence on the surface flatness, both considering the downskin and the upskin surfaces [74]. In Figure 56 also the effect of heat treatments on surface flatness is reported and it is greater than the effects due to wire EDM cutting. It has also been observed that the heat treatments improve the flatness of downskin surfaces and that they do not have a considerable effect on upskin surfaces [89]. However, the effects of heat treatments on properties will be investigated later in this work and will not be deepened here.

In the following sections the effects of part design factors will be investigated before on bulk specimens and then on lattice structures.

### Building orientation on manufacturability and surface characteristics

Building orientation is the most studied part design factor. Analyzing the effects of the building orientation on specimens produced without supports it has been found that the manufacturability can be assured for build angles (angle between the build plate and the downskin surface) equal or greater than 50°. Lower angles can be manufactured but the designer should be aware that there is an high risk for

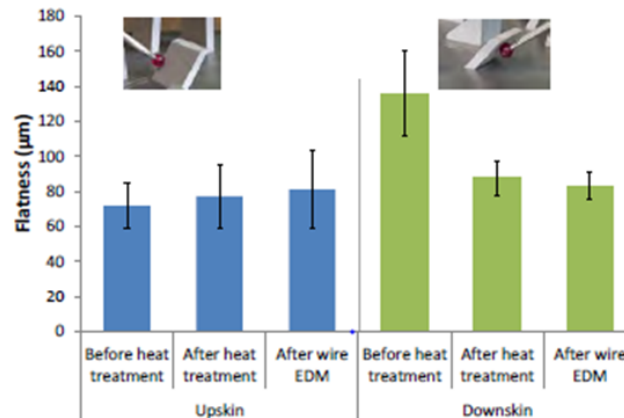


Figure 56: Effects of EDM wire cutting and heat treatment on upskin and downskin surface flatness (SLMed Ti6Al4V) [74].

the part to collapse. Another aspect seldom considered is the angle between the part and the coating blade. In this particular case where SLMed Ti6Al4V specimens with simple shapes are produced, this angle has been fixed at 45° to reduce the interactions between the parts and the powder. However, general considerations cannot be made and individual choices has to be taken case by case.

Once that the manufacturing phase is concluded a first external observation at the micrometer scale can reveal the presence of weld tracks. These are clearly visible on horizontal surfaces and their presence and distribution depend on the scan strategy adopted. Increasing the build angle the staircase effect appears and the welded tracks gradually disappear until reaching an inclination angle of 40° where they are no more visible being hidden by the partially melted particles attached to the surface. As a consequence, for angles above 40° the surface isotropy increases to almost 100%, meaning that the surface is more uniform. This is quite obvious considering that the anisotropy factors are the weld tracks themselves that disappear.

The flatness of the upskin and downskin surfaces is also a function of the building orientation. Flatness of horizontal surfaces (10° to 40°) is very poor if compared to vertical surfaces (above 70°). Printing a specimen with a build angle between 50° and 70° and without supports can show a curved shape with the downskin and upskin surfaces exhibiting different level of flatness (Fig. 57) [74].

### Building orientation on surface roughness

The analysis of the surface roughness of 3D printed parts can be complex due to the many factors influencing the final results. As a consequence many parameters can be used to describe in detail the characteristics of the surface, analyzing both two and three dimensional aspects. Due to limited time, in this context only two commonly adopted

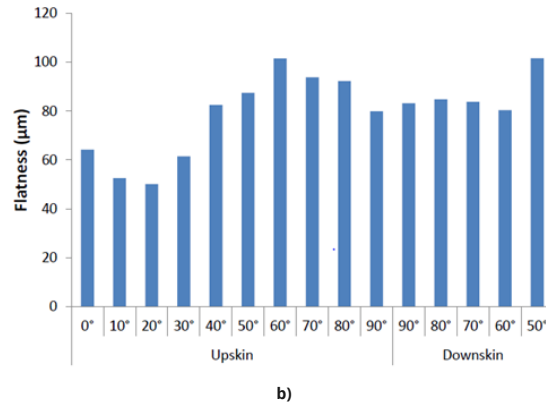


Figure 57: Effects of building orientation on the upskin and the downskin surface flatness [74].

parameters will be investigated:  $R_a$  and  $R_{sm}$ .

$R_a$  is defined by ASME B46.1 as the “arithmetic average of the absolute values of the profile height deviations from the mean line, recorded within the evaluation length”.

$R_{sm}$  can be identified referring to the staircase (Fig. 58) effect and it is defined as:

$$R_{sm} = \frac{d}{\sin(\alpha)}$$

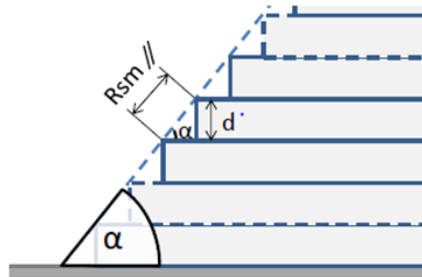


Figure 58:  $R_{sm}$  and the staircase effect [74].

$R_a$  is usually lower for the upskin surfaces that have a higher surface quality than the the downward surfaces. For EBMed specimens made of Ti6Al4V it has been found an average  $R_a$  around 6 µm and 17 µm for the upward and downward surfaces, respectively. The different results are attributed to different phenomena occurring during the manufacturing phase. The upper surface quality is affected by the staircase effect while the particles adhesion worsens the lower surface finish. So, moving from horizontal to vertical orientations the trend of  $R_a$  is different, for upward surfaces there is a linear relation between the build angle and  $R_a$ , while for downward surfaces the surface roughness has a minimum around 70°. In the latter case the sloping angle does not go below 50° due to manufacturing constraints previously explained, and the trend is independent from the

orientation of the part (Fig. 59). This is reasonable considering that the staircase effect depends upon the build angle while the particles adhesion, involving the lower surfaces, is related to the heating phenomena occurring during melting. This makes the  $R_a$  for the downward surfaces independent from the building orientation [90].

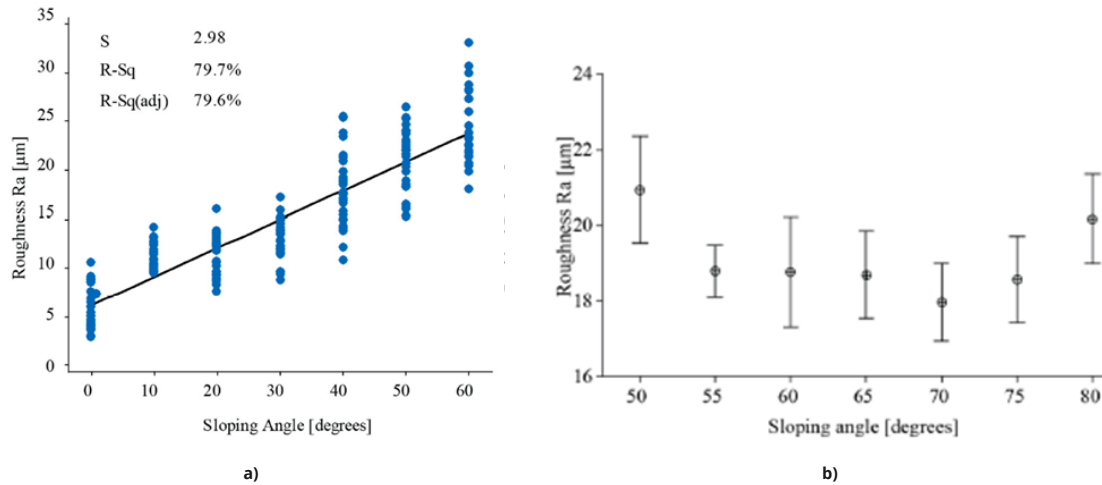


Figure 59: Sloping angle effect on  $R_a$  for upward a) and downward b) surfaces [90].

$R_{sm}$  has been analyzed for SLMed Ti6Al4V specimens. In general the  $R_{sm}$  decreases for increasing build angle for profiles both parallel and perpendicular to the welding tracks. The real trend is somehow in contrast with the expected one (Fig. 60) and the possible explanations are related to the attached particles that could interfere with the measurements of  $R_{sm}$ , and to the differences in the melt pool behavior between the core and the external part of the components. In this case a back-and-forth scanning strategy has been adopted and this has to be specified when referring to the  $R_{sm}$  because, if the profiles where the  $R_{sm}$  is measured are perpendicular to the weld tracks: it coincides with the hatch spacing when  $R_{sm}$  is measured on the top surface, and with twice the hatch spacing when it is measured on the side surface. Instead, if the selected profiles are parallel to the weld tracks the  $R_{sm}$  can directly measure the magnitude of the staircase effect. In Figure 61 it is evident the effect of the back-and-forth scan strategy. The influence of other types of scanning strategy on  $R_{sm}$  should be individually inspected.

Differences have been identified also comparing SLM and EBM techniques. SLM is performed at lower temperatures, lower scanning speeds and lower energies compared to EBM where a higher temperature is kept during the whole manufacturing process. Then, in EBM the heat diffuses much easier and the amount of partially melted particle, that usually are also bigger in size, is higher. The EBM has the advantage to be faster than the SLM that, in turn, guarantees a higher surface quality [83].

It is now clear that the staircase (or stair stepping) effect and the particles adhesion are

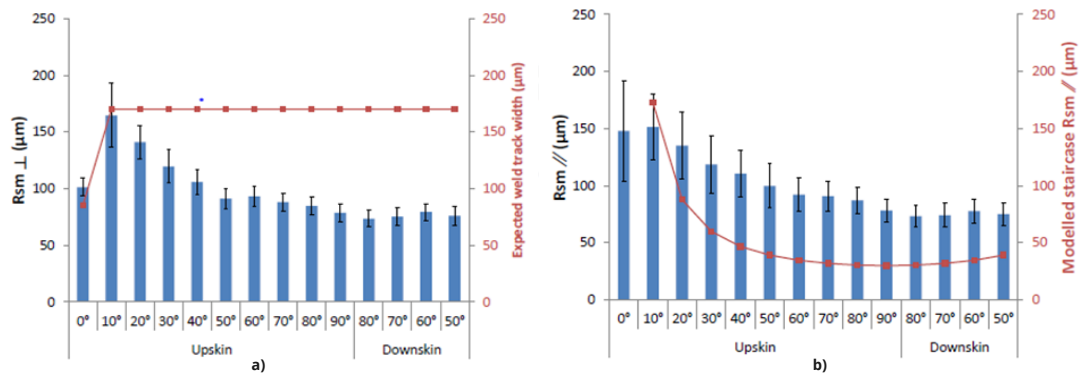


Figure 60: Effect of build angle on  $R_{sm}$  for profiles perpendicular a) and parallel b) to the weld tracks [74].

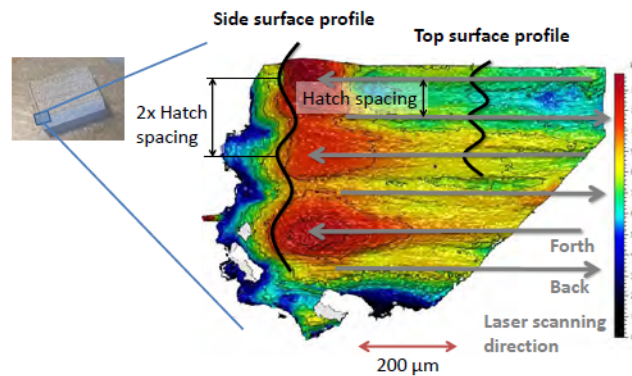


Figure 61: Effect of back and forth scanning strategy on  $R_{sm}$  [74].

the two main phenomena degrading the surface quality. The building orientation should be carefully considered while designing the part, and the laser scanning parameters can be varied during the manufacturing phase to overcome the problem of over-melting that causes the powder particles adhesion. Thus, for instance, changing the scanning strategy or the scanning parameters to modify the melting area while manufacturing the part can result in a non-uniform heat distribution, resulting in a better downward surface finish [90].

### Support structures on manufacturability and defects

The presence of support structure is sometimes strictly necessary or strongly recommended especially for those components characterized by complex shapes. To reduce the fabrication time and the amount of powder needed and to ease their removal, the supports are usually designed with high levels of porosity. As a consequence, powder

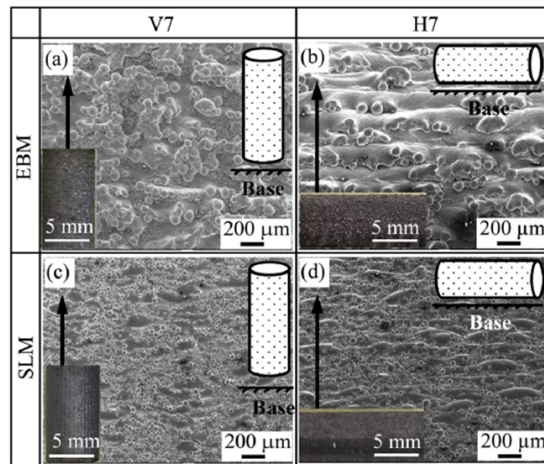


Figure 62: EBM vs. SLM surface finish [83].

particles are entrapped between the supports and the component, and the initial layers are built on a mixture of solid metal and powder particles. The consequences has been observed while manufacturing Hastelloy X specimens via SLM where the production process had to be interrupted because balling phenomena occurred, causing the deformation and then, after the contact between the specimens and the re-coating blade, the delamination. The component has been successfully fabricated with the following parameters parameters: 80 W laser power, 400 mm/s scan speed for the supports and 170 W laser power, 1000 mm/s scan speed and 0.08 mm hatch distance for the part. An alternative solution can be to increase the density of the supports, so to have a higher and more uniform heat flow from the part to the supports. By doing so the fabrication time increases and it is more difficult to remove the support, this is why this option is not desirable [92].

In addition to the fact that the presence of supports is mandatory under certain circumstances, the key element that link them to the produced part is the heat transfer between the two. The capability of a component to diffuse heat determines the presence and the magnitude of temperature gradients inside the component itself, resulting in temperature differences between the core and the external part and causing sub-surface stresses. The fact that the supports can have a considerable effect on the heat that the part is able to diffuse makes them one of the most important factors in influencing the sub-surface stresses. Experiments on AISi10Mg specimens produced via L-PBF revealed that the supports improved the heat transfer during the manufacturing phase reducing the stress state. In general, the measured sub-surface stresses are tensile and are always below 40% of the YS. Moreover, it can be said that closed geometries hinder the stress release resulting in higher sub-surface stresses. Vertical specimens are characterized by tensile stresses near the surface that change to compressive ones moving deeper, and curved walls have higher sub-surface stresses than flat walls [91].

**Part design factors on lattice geometry and defects**

Due to their small size the manufacturing of the struts exhibit manufacturing constraints that limit the design freedom of the lattice structures. Typically horizontal struts have many geometric defects, are over-sized, have many partially melted particles attached, and their length has to be limited also when they are supported at both ends to avoid manufacturing complications. Thus, it is recommendable to not have building inclination of the struts lower than 30° [89].

Other limitations, still related to SLMed specimens, are represented in Figure 63. To keep a precautionary approach it can be suggested to avoid strut diameters lower than 0.3-0.4 mm and 0.5 mm for Ti6Al4V and AlSi12Mg, respectively, and strut spans larger than 5 mm regardless of the alloy used.

Material		Ti6Al4V										AlSi12Mg									
Diam. (mm)		0.1	0.2	0.3	0.4	0.5	0.6	0.7	0.8	0.9	1.0	0.1	0.2	0.3	0.4	0.5	0.6	0.7	0.8	0.9	1.0
Angle (degrees)	0	L	L	L	L	L	L	L	L	L	L	L	L	L	L	L	L	L	L	L	L
	10	L	L	M	M	M	M	M	L	L	L	L	L	L	L	L	M	M	M	M	M
	20	L	L	H	H	H	H	H	H	H	H	L	L	L	L	L	M	M	M	M	M
	30	L	M	H	H	H	H	H	H	H	H	L	L	L	M	H	H	H	H	H	H
	40	L	H	H	H	H	H	H	H	H	H	L	L	L	H	H	H	H	H	H	H
	50	L	H	H	H	H	H	H	H	H	H	L	L	L	H	H	H	H	H	H	H
	90	L	H	H	H	H	H	H	H	H	H	L	L	L	H	H	H	H	H	H	H

a)

Material		Ti6Al4V										AlSi12Mg									
Diam. (mm)		0.1	0.2	0.3	0.4	0.5	0.6	0.7	0.8	0.9	1.0	0.1	0.2	0.3	0.4	0.5	0.6	0.7	0.8	0.9	1.0
Span (mm)	1	L	M	H	M	H	H	H	H	H	H	L	L	L	L	H	L	H	H	H	H
	2	L	M	H	H	H	H	H	H	H	H	L	L	L	L	H	H	H	H	H	H
	3	L	M	H	H	H	H	H	H	H	H	L	L	L	L	H	H	H	H	H	H
	4	L	L	M	H	H	H	H	H	H	H	L	L	L	L	H	H	H	H	H	M
	5	L	M	M	M	H	H	H	H	H	H	L	L	L	L	H	M	H	H	H	M
	7.5	L	L	L	L	L	M	L	M	L	L	L	L	L	L	M	M	M	M	H	H
	10	L	L	L	L	L	L	L	L	L	L	L	L	L	L	M	M	M	M	M	M

b)

Figure 63: Ti6Al4V and AlSi12Mg SLMed lattice struts manufacturing constraints. Legend: L = many defects, M = some defects, H = successfully manufactured. a) strut diameter vs. build angle, b) strut diameter vs. span [98].

Observing more in detail the struts it can be inferred that the same issues (particles adhesion and stair stepping) analyzed in the previous parts are responsible for surface

quality as it was for bulk specimens. However, it seems that in this case the building orientation is less influencing the surface roughness (Fig. 64).

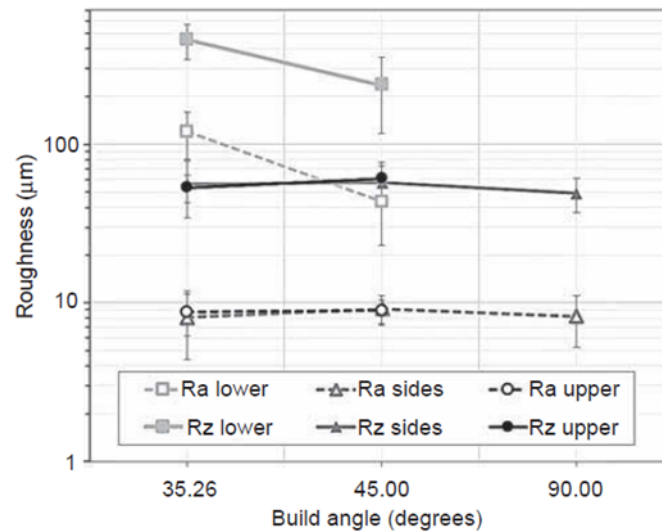


Figure 64: SLMed AlSi12Mg lattice struts build angle on surface roughness [98].

Considering the different types of unit cell an average density increase between 20% and 30% has been observed. The variations from the ideal CAD models are mainly due to geometric defects at the intersection between struts and nodes and partially melted particles attached to the surfaces [98]. This addition of material around the nodes of the structure increases the relative density of the unit cell but does not imply an improve of the strength of the part because the material added is characterized by an high porosity [89].

### Part design factors on geometry and defects - Guidelines

- Wire EDM cutting operations for part removal have a negligible influence on surface flatness.
- The angle between the re-coating blade and the part should be considered to reduce the interaction between the part and the powder.
- Build angles grater than 50° are suggested.
- For build angles from 0° to 40° the weld tracks are visible, above 40° attached partially melted particles prevail.
- For (unsupported parts) build angles from 0° to 40° the surface flatness is poor, from 40° to 70° the part assumes a curved shape, above 70° the surface flatness considerably improves.

- Up-skin and down-skin surfaces generally assume different values of the surface flatness.
- Building location has no influence on the surface roughness of the upward surface.
- Staircase effect and partially melted particles adhesion degrade the surface finish of upward and downward surfaces, respectively.
- $R_a$  is lower (better surface finish) for upward surfaces.
- $R_a$  is linearly dependent on building orientation for upward surfaces.
- $R_a$  is independent on building orientation for downward surfaces.
- $R_{sm}$  decreases for increasing build angle
- EBM is faster than SLM that, in turn, guarantees a higher surface quality.
- Variations of the scanning parameters and the scanning strategy to reduce the melting area can improve the surface finish of downfacing surfaces (for EBM).
- Support structures characterized by high porosity are faster to produce and easier to remove.
- Support structures have the greatest effect on sub-surface stresses.
- For Lattice struts: inclinations above  $30^\circ$ , diameters above 0,5 mm and spans lower than 5 mm are suggested.
- Strut length may influence the strut surface roughness.
- Strut surface roughness is independent upon the location of the measurement along the strut.
- The actual relative density of the unit cells is 20%-30% higher than the ideal models.
- The material added to the unit cell (increasing relative density) due to imperfections does not imply an improvement of mechanical properties.
- Oversize in the strut geometry may be compensated modifying the CAD model.

## Process-machine and environmental factors on properties

		Mechanical properties	Relative density (Porosity)
ENVIRONMENTAL FACTORS	chamber environment		
PROCESS-MACHINE FACTORS	substrate temperature (base plate operating temperature); powder layer thickness $t$ ; Blade and machine factors.		

Figure 65: Process-machine and environmental factors on properties.

The environmental factors refer to the environment inside the build chamber while the substrate temperature, the blade and machine characteristics, the powder layer thickness and other powder properties are defined as process-machine factors, and have been analyzed in *Step 1: Material selection*.

The studies focused on the effects of process-machines and environmental factors on properties are very few (Fig. fig:ProcessFactorsProperties).

The effects of process-machine factors on porosity are focused on the influence that the powder properties have on the porosity of the final component. Considering SS 316L and AlSi10Mg alloys produced by PBF, it has been found no dependency of porosity upon the particle circularity, the Hausner ratio and the powder layer density. Nonetheless, these results are in contrast with others present in literature and cannot be considered of general validity [30].

Moving to the environmental factors a slight effect of the protective environment on the mechanical properties has been observed. Laser direct energy deposition has been used to produce AISI 316 SS in two different protective atmospheres:  $N_2$  shielding gas (SG) and  $N_2$ -filled build chamber (BC). The BC solution led to slightly higher YS (12%), UTS and  $\epsilon$  (Fig. 66).

These effects are mainly attribute to the effects of the protective atmosphere on the oxide content of the part. For BC finer oxides has been observed which were also half in amount. Actually, it should be pointed out that a certain amount of oxides is already present inside the raw powder, and that BC is better than SG in preventing their formation but, in both cases, the oxides content was acceptable [93].

Due to the limited number of results the only one suggestion can be provided.

- The protective atmosphere inside the build chamber can have a slight influence on the oxides formation, and then on the properties of the manufactured component.

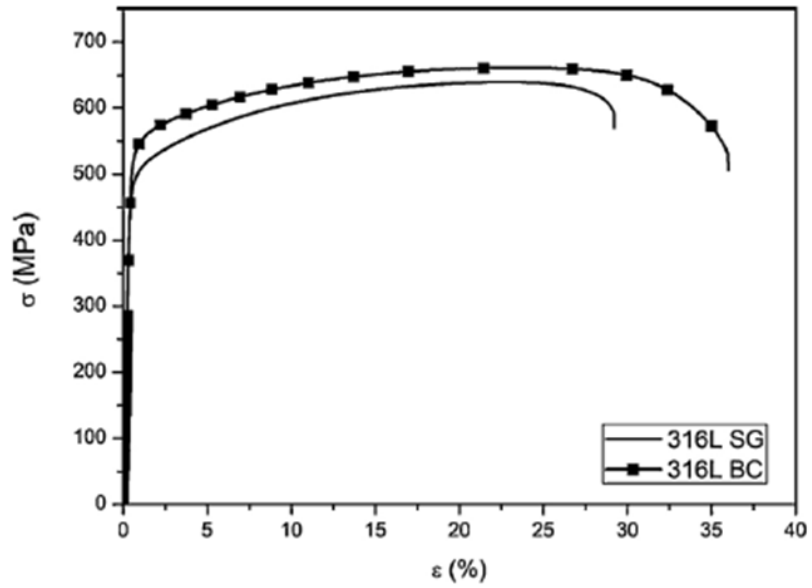


Figure 66: Effect of N<sub>2</sub> shielding gas (SG) and filled build chamber (BG) on stress-strain curve for SS 316L [93].

## **Scanning factors**

In the present section the effects of scanning factors on mechanical properties, ductility and hardness, porosity and geometrical properties, and defects will be analyzed considering individually, when it is possible, aluminum, titanium and nickel alloys.

This section does not pretend to find the perfect numerical values for each one of the design parameters, that would require much more time and resources than those actually available, but to give a picture on what are the trends that the properties follows and to provide process windows to help the engineer in identifying the proper set of design parameters.

## Scanning factors on mechanical properties

		Compressive Properties	Yield, UTS, elongation, fracture toughness
SCANNING FACTORS	Laser power (energy) P scan speed v hatch distance h	 	  
	scanning path or deposition pattern		

Figure 67: Scanning factors on mechanical properties.

## Al-alloys

The dependence of mechanical properties upon laser power, scanning speed, hatch spacing and energy density has been investigated in case of SLMed AlSi10Mg and Al6061 alloys.

The graphs reported in Figure 68 refer to SLMed lattice specimens under compression while those in Figure 69 are referred to SLMed AlSi10Mg bulk specimens [96] [13]. Analyzing them it can be seen that:

- Machined samples have a higher UTS than as-built ones (Fig. 69). Differences are in the range 20-50 MPa. This is probably due to the influence of surface roughness on mechanical properties.
- UTS is more affected than YS by changes in the laser scanning parameters (Fig. 69 a).
- Laser power is the parameter with the greatest influence on both UTS and YS.
- In general, for lattice structures the maximum strength increases for increasing laser power regardless of the other parameters.
- The trend of the stress has a maximum for the lowest scanning speed, then it decreases until a minimum and increases again. This is evident in Figure 68 (lattice) where a wider range of scanning speeds is considered (1000-7000 mm/s) while it is almost constant in Figure 69.
- YS decreases for increasing laser power, while slightly increases for increasing hatch spacing and scan speed (Fig. 69, bulk parts).

- The maximum values of the stress and the strength are:
  - Max. stress = 36.4 MPa (Fig. fig:PowerSpeedOnStressStrain ). Obtained for: 400 W, 1000 mm/s.
  - Max UTS = 396.5 MPa (Fig. fig:PowerSpeedOnStressStrain ). Obtained for: 370 W, 1300 mm/s and 0.19 mm hatch spacing.

Despite of the fact that the two studies considered refer to lattice structures and bulk specimens, it is interesting to notice that the values of the laser scanning parameters giving the max. stress and max. UTS are not so far between each other: 370 and 400 W, 1000 and 1300 mm/s.

Now, focusing on SLMed Al6061 bulk specimens (Fig. 70) further consideration can be deducted.

- Energy density and scan speed have a great effects on both UTS and YS.
- UTS and YS decrease for increasing energy density.
- UTS and YS increase for increasing scan speed.
- High UTS and YS are obtained for higher values of the hatch spacing (0.19 mm).
- Max. UTS of 184 MPa (range: 150-184 MPa) is obtained for 1300 mm/s scan speed, 0.19 mm hatch spacing and  $47.2 \text{ J/mm}^3$  energy density.
- Max. YS of 172 MPa (range: 125-172 MPa) is obtained in the energy range:  $40.5\text{--}47.2 \text{ J/mm}^3$ , when the other parameters are high.

On an overall, Al6061 specimens exhibit lower mechanical properties than AlSi10Mg ones and this is attributed to the presence of Si in the microstructure.

It is evident that a good trade-off among the various laser parameters has to be found for each alloy type. It might be assumed that using lower scanning parameters a finer microstructure and thus higher mechanical properties can be obtained, this is actually not correct, because experiments put in evidence that lower scanning parameters can result in keyhole pores and in lack of fusion defects, while too high scanning parameters produce an excessively coarse microstructure and hydrogen pores.

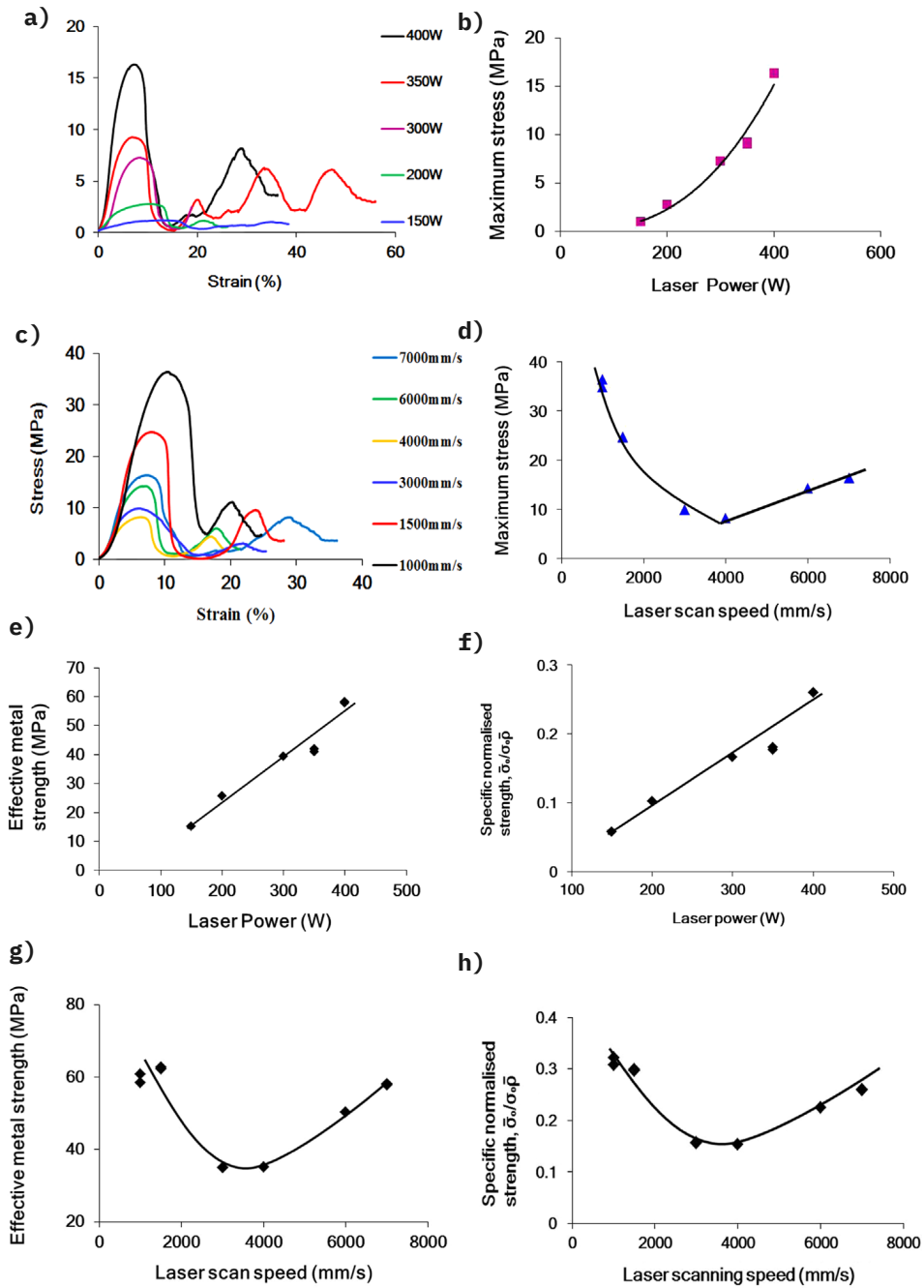


Figure 68: SLMed AlSi10Mg lattice specimens under compression. Stress-strain curves for different (150-400 W) laser powers at fixed (7000 mm/s) scanning speed a) and for different scanning speeds (1000-7000 mm/s) at fixed (400 W) laser power c). Maximum stress vs. laser power at fixed scanning speed (7000 mm/s) b) and maximum stress vs. laser scanning speed at fixed laser power (400 W) c). Effective and specific normalized strength vs. laser power at fixed scanning speed (7000 mm/s) e) and f), and for different scanning speeds (1000-7000 mm/s) at fixed (400 W) laser power g) and h) [96].

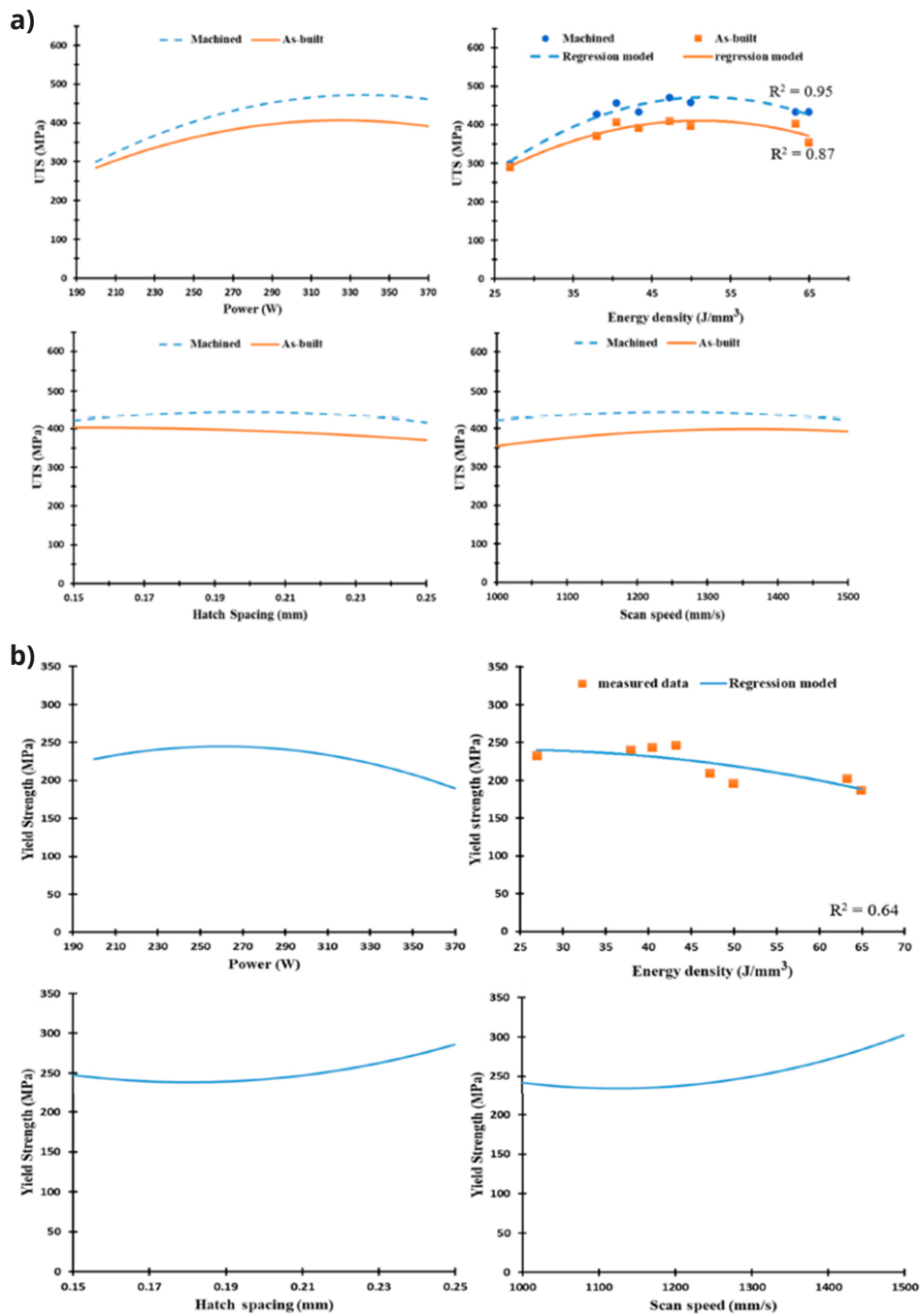


Figure 69: SLMed AlSi10Mg specimens. UTS dependence upon laser power, energy density, hatch spacing and scan speed for as-built and machined specimens a). Yield strength dependence upon laser power, energy density, hatch spacing and scan speed b) [13] .

Step 3: Tuning parameters

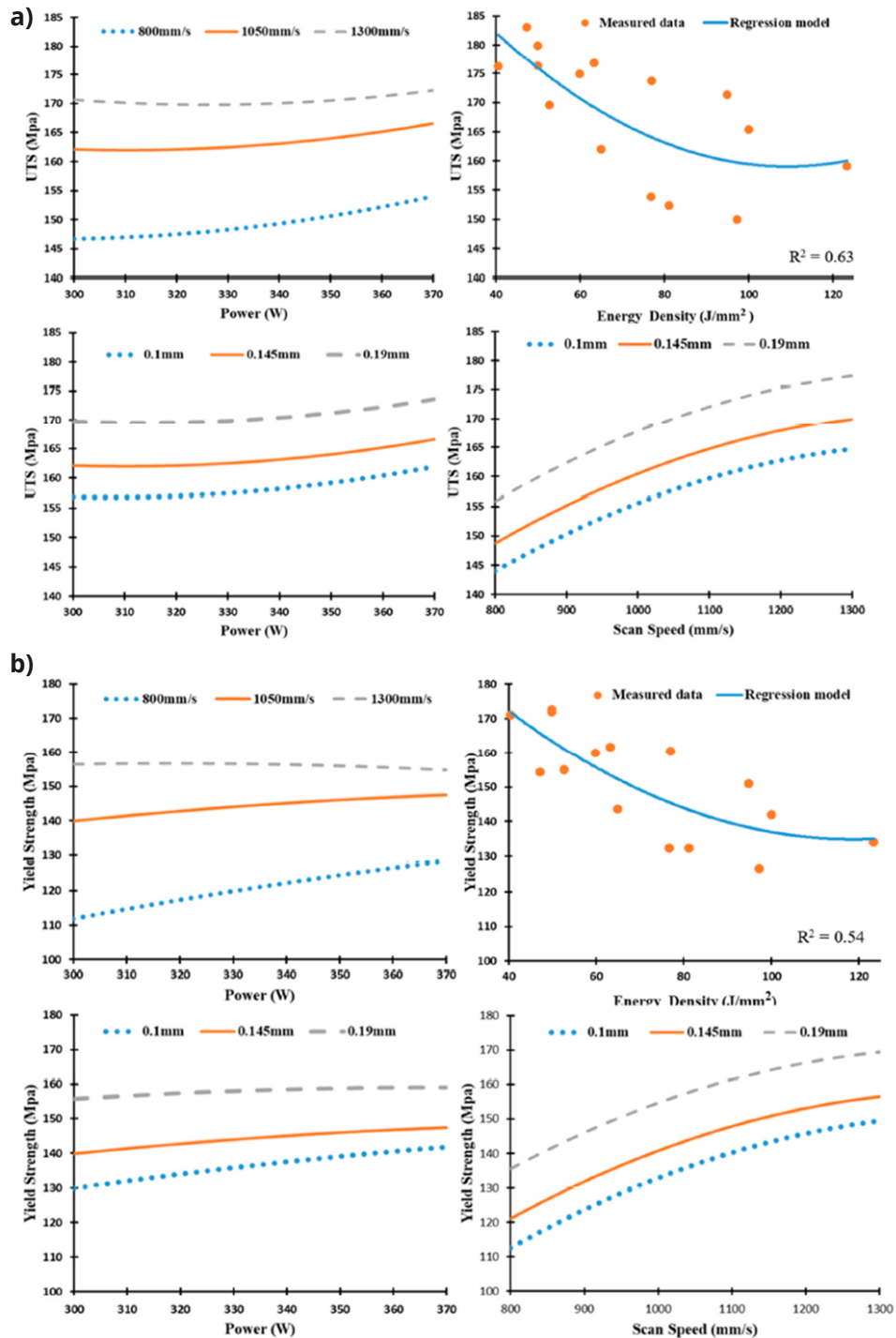


Figure 70: SLMed Al6061 specimens. UTS dependence upon laser power, energy density, hatch spacing and scan speed for as-built and machined specimens a). Yield strength dependence upon laser power, energy density, hatch spacing and scan speed [13].

## Ti-alloys

Ti6Al4V have been manufactured via SLM. Compressive tests have shown that, despite of the initial expectations, the minimum porosity level was reached for an energy density around  $110 \text{ J/mm}^3$  but the highest mechanical properties have been found around  $150 \text{ J/mm}^3$ . In general a decrease in the mechanical properties is observed for increasing porosity (Fig. 71 b), however the results are quite scattered and trying to find the scanning parameters leading to the minimum porosity level does not imply that the maximum mechanical properties will automatically result (Fig. 71 a).

During the experiments the laser power has been kept constant (200 W) and the laser scanning speed (600-1250 mm/s), the hatching distance (30-120  $\mu\text{m}$ ) and the energy density (40-400  $\text{J/mm}^3$ ) have been varied. The mechanical properties obtained were 896-1468 MPa compressive yield strength (CYS) and 1323-1904 MPa ultimate compressive strength (UCS) [97].

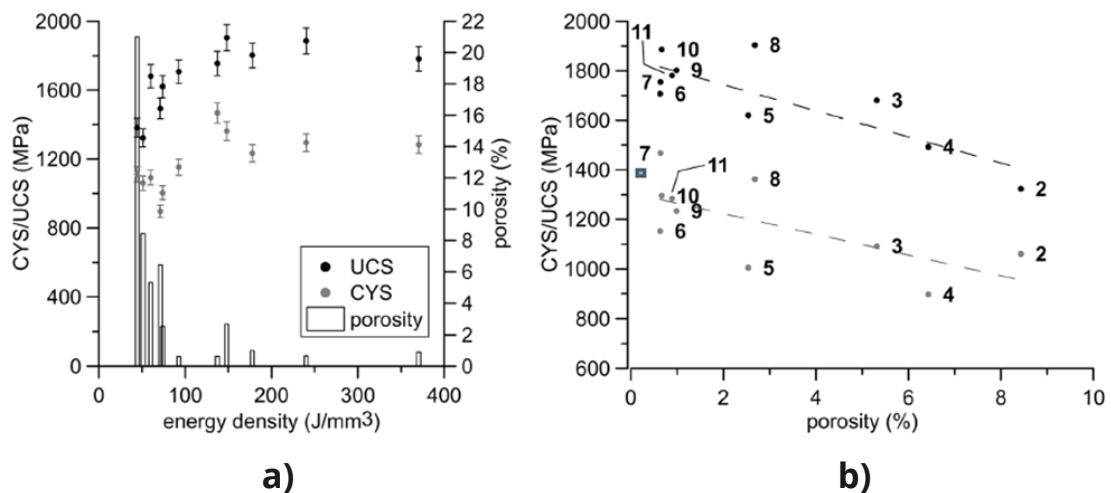


Figure 71: a) energy density vs. compressive yield strength (CYS) and ultimate compressive strength (UCS), b) porosity vs. CYS and UCS [97].

Mechanical properties ranges of Ti6Al4V alloy produced via SLM can also be depicted from Figure 72.

## Ni-alloys

In addition to the other laser parameters that are more often analyzed, it is interesting to observe the effects of scanning strategies on mechanical properties. Different samples have been manufactured in Ni-base superalloy IN738LC by SLM for various ranges of the laser parameters: 150–400 W, 0.05–0.12 mm and 800–3500 mm/s, and adopting three different scanning strategies:

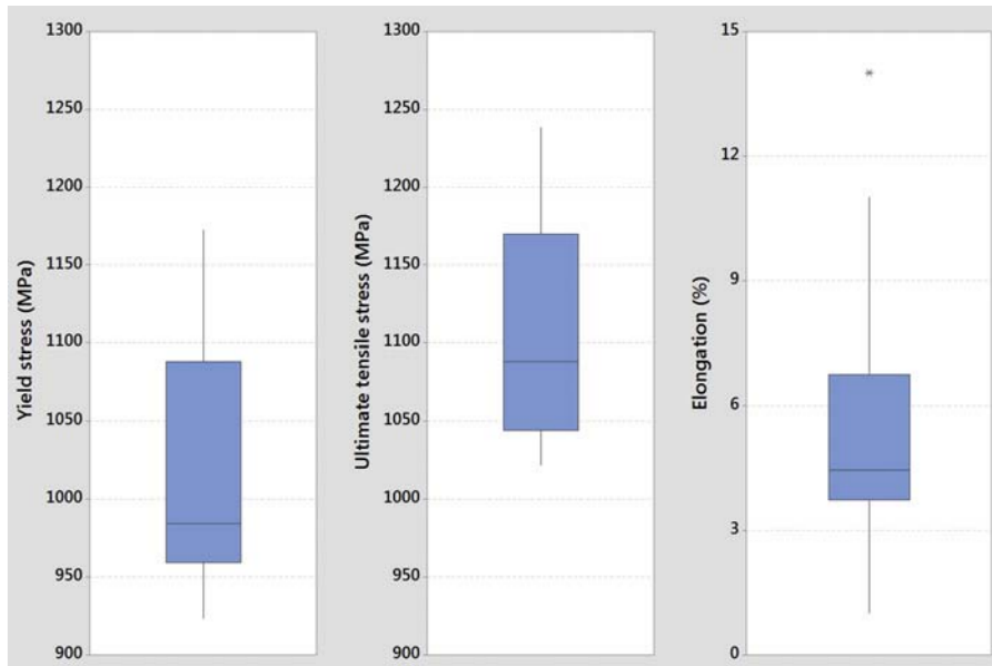


Figure 72: Mechanical properties at room temperature of SLMed Ti6Al4V specimens [16].

- A: 90° rotation (vectors parallel and perpendicular to the reference directions)
- B: 90° rotation (vectors at  $\pm 45^\circ$  to the reference directions)
- C: 67° rotation (around the reference directions)

The samples has been tested before and after heat-treatment, at room temperature and at 850 C°. Despite of the fact that the specimens produced with the scanning strategy B hold the highest anisotropy, they also exhibit the highest YS (228 GPa), followed by those manufactured with the scan strategy C (YS = 204 GPa) and A (YS = 196 GPa). Additionally, another important result derives from the analysis of the YS anisotropy. It has been proved that adopting the proper scanning path there is the possibility to tailor the crystallographic texture, meaning that the anisotropy of the mechanical properties can be designed with high precision (in the order of magnitude of few powder layers) along different directions. In this particular case the texture has been modified to pass from transverse anisotropic YS to transverse isotropic YS [101]. Unexpected events that stop the manufacturing process can also occur and their effects have been analyzed. Luckily process interruptions have negligible consequences on the mechanical properties of AlSi10Mg, Inconel 625 and Inconel 718 printed components [99].

## Scanning factors on mechanical properties - process windows

Table 8: Scanning factors on mechanical properties - process windows.

Material	Alloy type	Laser power (W)	Scan speed (mm/s)	Hatch spacing (mm)	Energy density (J/mm <sup>3</sup> )	UTS (MPa)	TYS (MPa)	Bib. ref.		
Aluminium	AlSi10Mg	200-370	500-1650	0.105-0.5	27-65	285-460	160-330	[13]		
	Al6061	300-400	1000-1400	0.1-0.19	20.41-123.3	133-396.5	66-246			
Titanium	Ti6Al4V	200	600-1250	0.03-0.12	40-400	1323-1904	896-1468	[97]		
						UCS	CYS			
Nickel	90° rotation (vectors parallel and perpendicular to the reference direction)									
	IN738LC	150-400	800-3500	0.05-0.12	-	-	108-196	[101]		
	90° rotation (vectors at ±45° to the reference direction)									
	IN738LC	150-400	800-3500	0.05-0.12	-	-	164-228			
67° rotation (around the reference direction)										
IN738LC	150-400	800-3500	0.05-0.12	-	-	-	134-210			

## Scanning factors on hardness

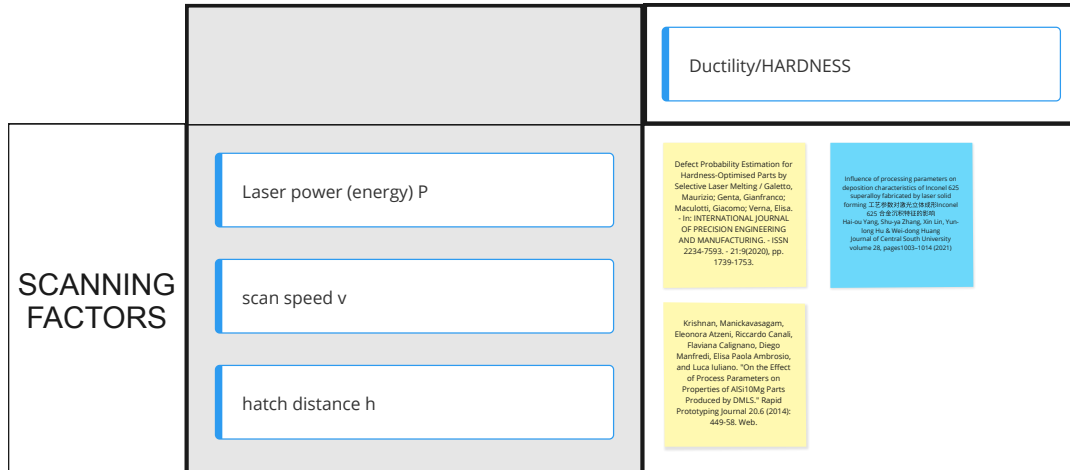


Figure 73: Scanning factors on mechanical properties.

## Al-alloys

Analyzing the effect of laser scanning parameters on the hardness of AlSi10Mg specimens manufactured via selective laser melting the following considerations can be made [13][102][104]:

- Laser parameters have a greater influence on the hardness along Z direction than along XY plane (Fig. 74).
- Micro-hardness is higher along XY plane (115-118 HV ) than along Z direction (86-103 HV) (Fig. 74).
- Maximum micro-hardness along Z direction (103 HV) is obtained at 27 J/mm<sup>3</sup> energy density (Fig. 74 a)).
- Micro-hardness increases for increasing hatch distance and scanning speed while it decreases for increasing laser power and energy (Fig. 74 and Fig. 75).
- Scan speed and hatch distance are the parameters that have a greater influence on hardness (Fig. 75) (energy density not considered being a combination of the three).
- For DMLS a processing window (1.2-1.8 J/mm<sup>2</sup>) has been found at  $h_d=0.17$  mm, values at which a scanning speed increase until 900 mm/s has no effect on the properties [104]. Then, if one parameter changes also the others have to change according to the energy density equation that links them [104].

- In general, an increase in porosity has a detrimental effect on hardness but the set of parameters resulting in minimum porosity may not also give the maximum hardness, even if the differences are very small (for DMLSed specimens [104]).
  - Highest density of 99.07% at 195 W, 700 mm/s and 0.17 mm (Hardness = 112 HB).
  - Highest hardness of 113 HB at 180 W, 700 mm/s and 0.1 mm (Relative density = 98.61%).
- Higher hardness values are often attributed to smaller micro-structural grains.
- AlSi10Mg specimens exhibit in general higher hardness compared to Al6061 ones due to the higher Si content.
- Hardness of AlSi10Mg as-built samples is usually higher than the hardness of the corresponding cast alloys that is around 75 HV.

In case of Al6061 it can be seen that the effects of scanning parameters are in general greater than in case of AlSi10Mg. Hatch spacing has a much more considerable effect, and it can be seen that the lines representing the different values of the hatching distance intersect in certain points, meaning that a careful choice of the hatch spacing needs to be done because the assumption of a direct linear correlation can lead to undesired outcomes (Fig. 77).

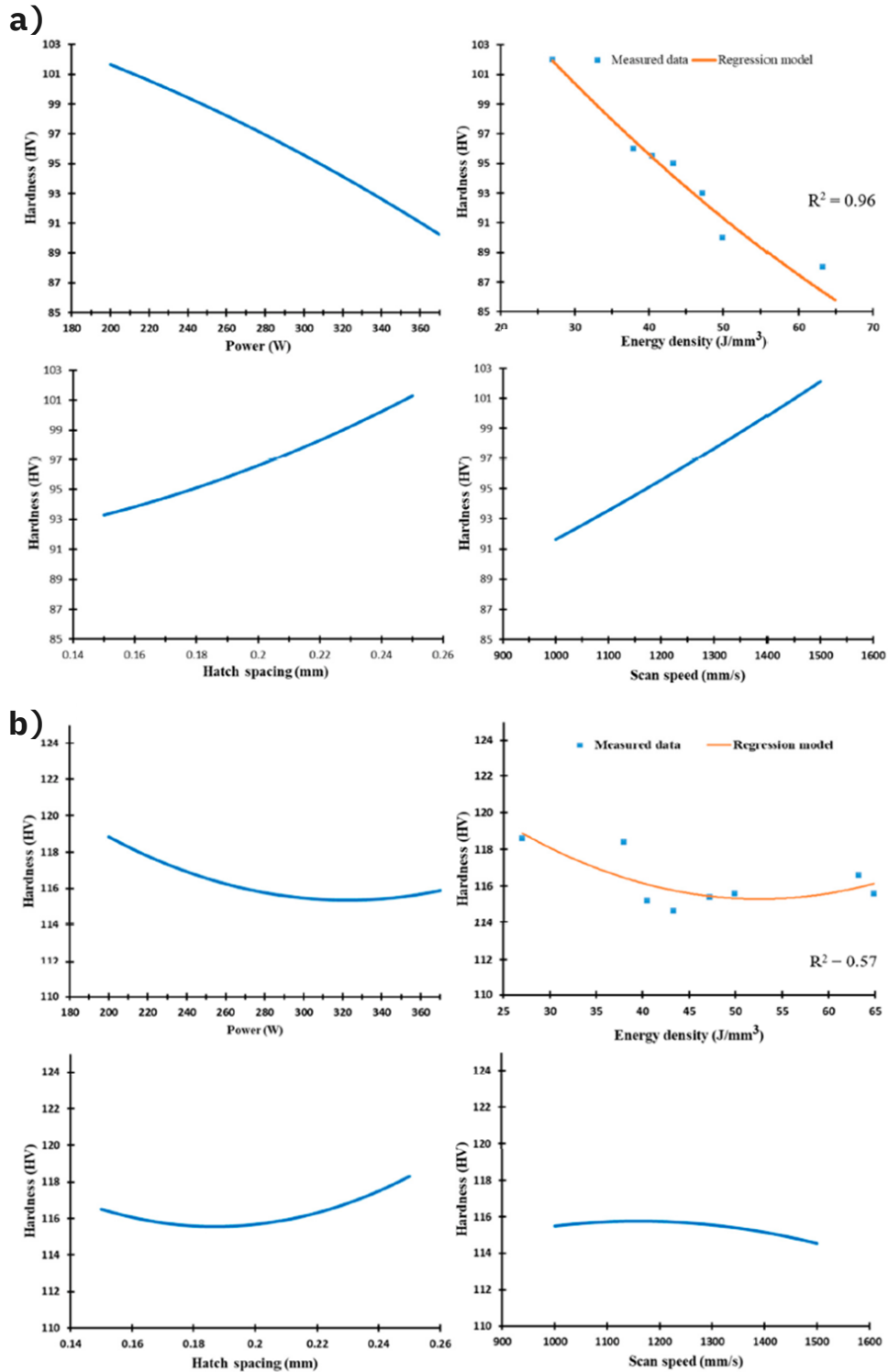


Figure 74: SLMed as-built AlSi10Mg specimens. Effects of laser power, energy density, hatch spacing and scan speed on micro-hardness along the X direction a) and along the XY plane [13].

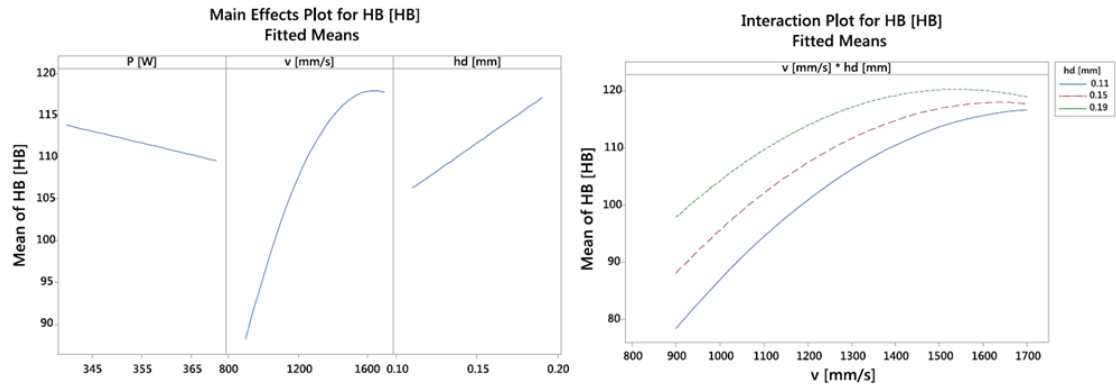


Figure 75: SLMed AlSi10Mg specimens. Main effects (laser power, scan speed and hatch distance) and interaction plots for hardness (HB) [102].

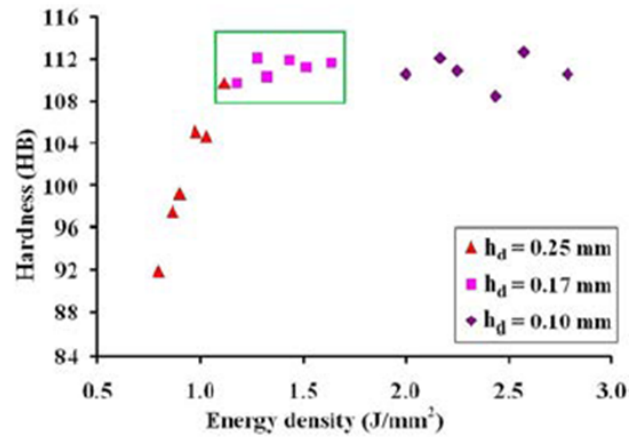


Figure 76: DMLSed AlSi10Mg specimens. Energy density on hardness, identification of a processing window ( $h_d$ : hatching distance) [104].

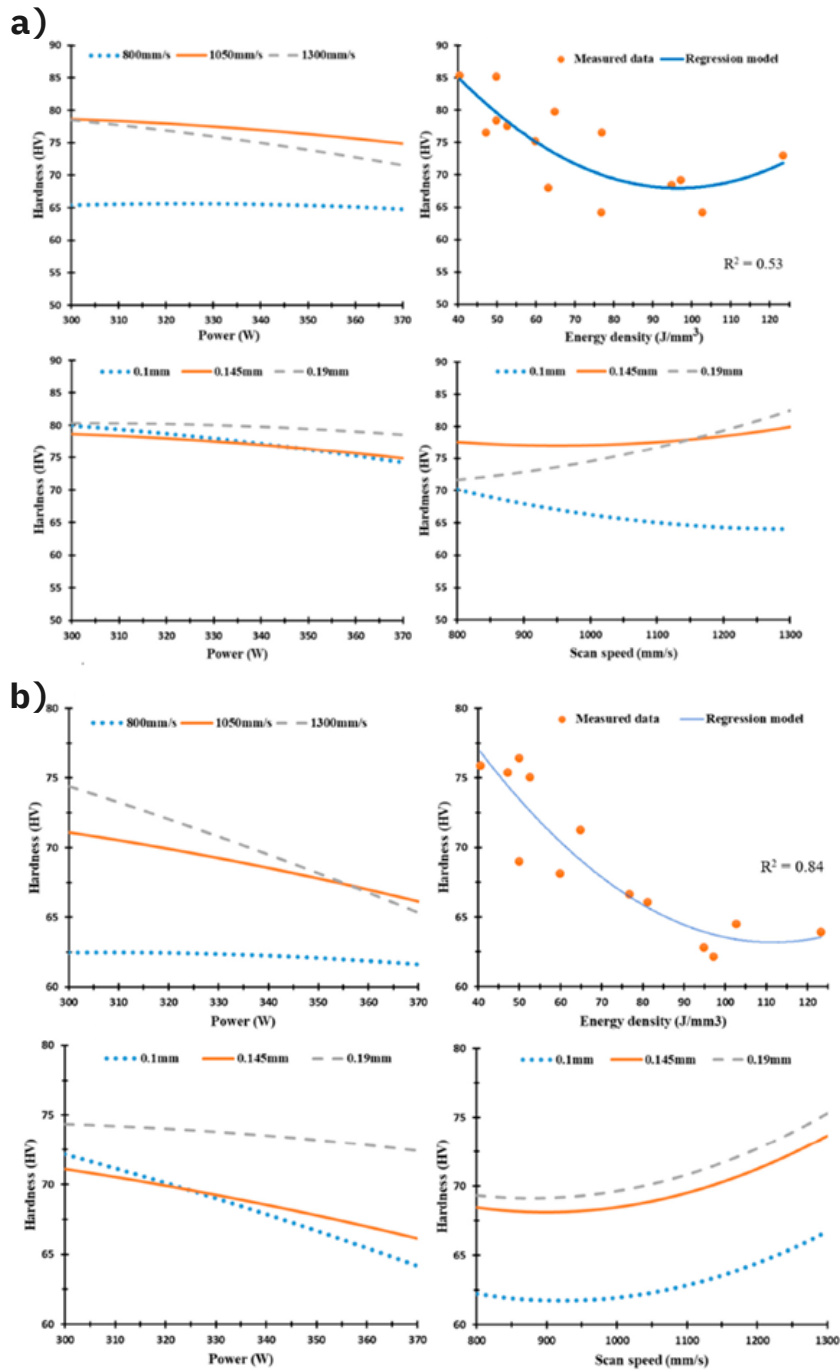


Figure 77: SLMed as-built Al6061 specimens. Effects of laser power, energy density, hatch spacing and scan speed on micro-hardness along the Z direction a), and along the XY plane b) [13] .

## Ni-alloys

Experiments focused on single tracks scanning revealed that the maximum values of hardness for Ni-superalloy 247LC are obtained for the highest values of energy density. The scan speed resulted to be secondary and the void content (porosity) to be strictly correlated with the hardness. In contrast, no connections between micro-hardness and crack density have been found [14].

The influence of laser exposure time and point distance have been observed by keeping the laser power and the hatch distance fixed (200 W and 0.1 mm). Consequently the energy supplied varies as well. There is a slight increase in hardness (from 290 to 320 HV) for the SLMed Alloy 718 manufactured specimens even if the results are quite scattered and a clear relation cannot be delineated (Fig. 78) [94].

The same alloy fabricated by EBM technique showed no significant differences between macro and micro-hardness along all the directions except from a slight increase between the core and the external part of the component. The average hardness resulted to range between 350 HV and 377 HV, and it seems to be dependent upon the focus offset that has the major effect on the formation of  $\gamma'$  and  $\gamma''$  precipitates [15].

Ni-alloys produced via laser solid forming have been investigated too. It is the case of Inconel 625 single track clads for which the highest hardness has been obtained for 1 kW laser power, 1200 mm/s scanning speed and 25 g/min powder feed rate [103].

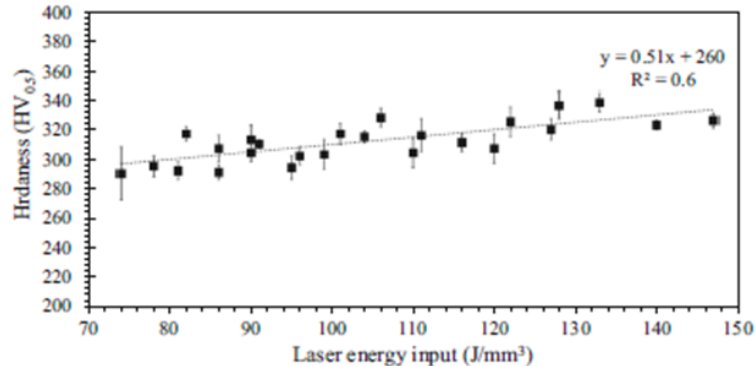


Figure 78: SLMed as-built Alloy 718 specimens. Effects of laser energy on hardness [94].

## Scanning factors on porosity

		Porosity (relative density)
SCANNING FACTORS	Laser power (energy) P	<p>H. Gong, (2013). Generation and detection of defects in metallic parts fabricated by selective laser melting and electron beam melting and their effects on mechanical properties, Dissertation, Doctor of Philosophy, Department of Industrial Engineering, University of Louisville, Louisville, Kentucky.</p> <p>Wolff, Sarah J., Stephen Lin, Eric J. Faenuss, Weig Kem Liu, Gregory J. Wagner, and Jun Cao. "A Framework to Link Localized Cooling and Properties of Directed Energy Deposition (DED) processed Ti-6Al-4V." <i>Acta Materialia</i> 132 (2017): 106-17. Web.</p>
	scan speed v	<p>Radek Vrāna et al. "Selective Laser Melting Strategy for Fabrication of Thin Struts Usable in Lattice Structures". In: <i>Materials</i> 11.9 (2018), p. 1763. doi: 10.3390/ma11091763.</p>
	hatch distance h	<p>The influence of the process parameters on the densification and microstructure development of laser powder bed fused Inconel 939 / Marchese, G., Parisio, S., Sabboni, A., Manfredi, D., Lombardi, M., Fino, P., Ugues, D., Biamino, S., - In: <i>METALS - ISSN 2075-4701 - ELECTRONICO</i>, 1088(2020), pp. 1-19.</p>
	Spot size and geometry	<p>Karimi Neghani, Paria, Tahira Raza, Joel Andersson, and Lars Erik Svensson. "Influence of Laser Exposure Time and Point Distance on 75-µm-thick Layer of Selective Laser Melted Alloy 718." <i>The International Journal of Advanced Manufacturing Technology</i> 94.5-6 (2018): 2199. Web.</p>

Figure 79: Scanning factors on porosity.

## Al-alloys

Considering the peculiar alloy  $TiB_2/AlSi10Mg$  it has been noted that for fixed laser power (320 W) and hatch distance (0.15 mm) the relative density increases for increasing scan speed from 98.5% (at 900 mm/s) to 99.5% (at 1500 mm/s) [73]. Nevertheless, an increase in scan speed not always reduces porosity, as it is shown in Figure 80, where a decrease is present and it is very rapid for scanning speed higher than 1250 mm/s, regardless of the method used to produce the AlSi10Mg raw powder [30]. Analyzing single laser tracks applied to AlSi10Mg a processing window has been identified for: 8-10 J input energy, 0.25-0.4 J/mm linear energy, 225-300 W laser power, 1250-1750 mm/s laser scanning speed, 20%-30% weld overlap [108]. Probably the scan speed is the most influencing parameters but its relation with porosity

has yet to be fully understood.

Considering bulk specimens it can still be affirmed that:

- Scan speed has the greatest impact among the various laser scanning parameters.
- The presence of entrapped vapor or gas pores is always present in Al-Si alloys.
- The building orientation do not modify the general trend of the “porosity – linear energy” function (Fig. 81).
- Lower values of the energy are preferable to obtain low porosity and low roughness (Fig. 81).
- A too high (> 50%) or too low (< 10%) weld overlap does not guarantee an improve in hardness.

Porosity of lattice struts does not vary linearly with the energy density or the laser scanning speed (Fig. 82), in this case optimal values of laser power and scan speed are around 250 W and 4000 mm/s [96].

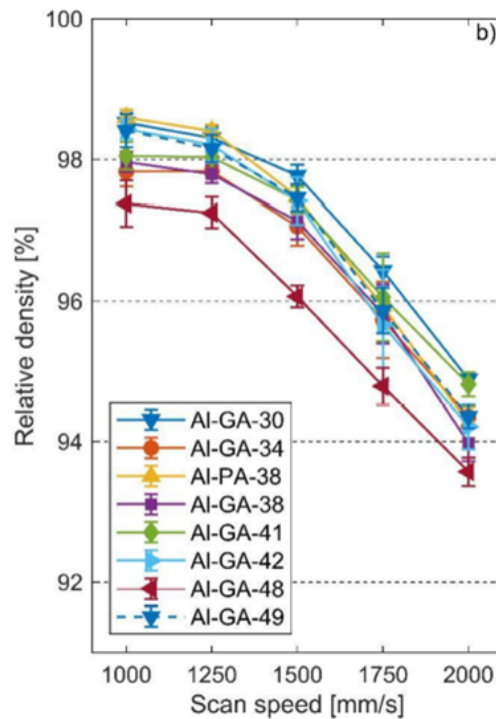


Figure 80: SLMed  $TiB_2/AlSi10Mg$  samples. Scan speed vs. relative density for different raw powders [30].

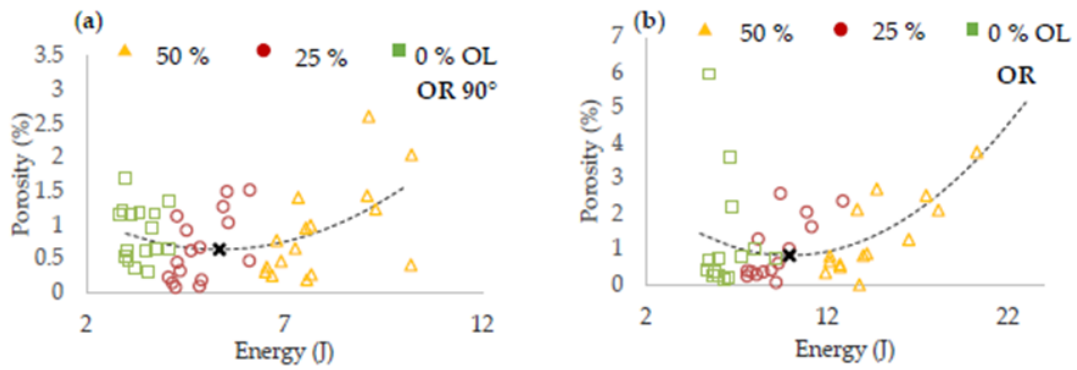


Figure 81: Energy input (J) vs. porosity for 90° (a) and 35.26° (b) inclination (OL = weld overlap) [108].

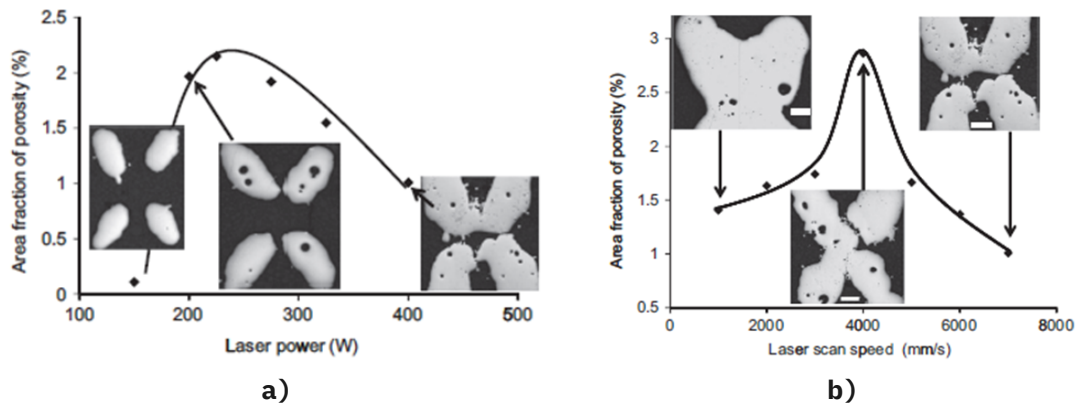


Figure 82: SLMed AlSi10Mg lattice struts. a): laser power vs. area fraction of porosity at fixed scan speed (7000 mm/s). b): scan speed vs. area fraction of porosity at fixed laser power (400 W) [96].

## Ti-alloys

SLM manufactured specimens with low porosity have been fabricated by various researchers. The common aim is to find a suitable processing windows and considering Ti6Al4V alloy two analysis seem to be relevant to this purpose.

In the first case the ranges of scanning parameters are: 200 W constant laser power, scanning speed 600-1250 mm/s and hatching distance 30-120  $\mu\text{m}$  [97]. From the dependence of porosity upon energy density (Fig. 83) emerged that:

- Minimal porosity has been reached at 110  $\text{J}/\text{mm}^3$  energy density.
- Porosity decreases for increasing energy density (porosity <1% for energy density >90  $\text{J}/\text{mm}^3$ ).
- A processing window for low porosity (around 0.6%) has been identified for energy densities from 92.6 to 137.3  $\text{J}/\text{mm}^3$ .

A similar study not investigating the effect of the hatch distance but varying the laser power ( 40-160 W laser power and 120-1560 mm/s scan speed) found that [106]:

- A good processing window has been identified from 720 to 1200 mm/s scan speed at constant laser power (160 W). Other windows are also available but they are narrower (Fig. 85 a) ).

The two processing windows are not in perfect agreement meaning that the effects of the energy density range around 90  $\text{J}/\text{mm}^3$  (roughly between 60 and 130  $\text{J}/\text{mm}^3$ ) need further investigations, and also that the scanning parameters are not the only relevant factors in tuning porosity.

Common considerations can still be formulated:

- Pores are not very sensitive to manufacturing imperfections [75].
- Lower energy density causes lack of fusion defects, while too high levels of energy cause keyholes voids, that collapsing leave voids of vapor, and also small pores caused by the inert gas [107].
- Energy density and porosity are not directly correlated.
- High porosity generally comes together with large defects size.

Observing instead the effects of the scanning parameters on porosity for EBM Ti6Al4V manufactured specimens some evidence emerges clearly [106]:

- The speed function index has the greatest effect, the line offset and the focus offset are still important while the max current is the least relevant.

- In general, the effects of the four scanning parameters can be identified (Fig. 85 b) ):
  - Porosity decreases for increasing max current.
  - Porosity increases for increasing line offset (especially above 0.18 mm).
  - Porosity increases for increasing focus offset (especially above 0.16 mm).
  - Porosity decreases for increasing speed function index.

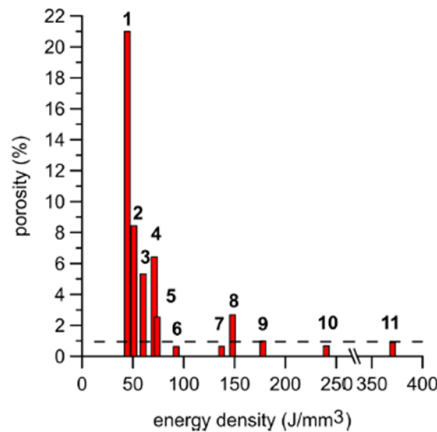


Figure 83: Energy density vs. porosity for constant 200 W laser power, 600-1260 mm/s scan speed and 30-120  $\mu$ m hatching distance (SLM, Ti6Al4V) [97] .

The effects of two different scanning strategies have been analyzed. EBMed specimens have been produced with a raster scan strategy while SLMed ones with stripes of 3 mm (Fig. 84). It emerged that the porosity content for EBM was lower regardless of the scanning strategy adopted, indeed this was attributed to the higher energy supplied and to the higher temperatures characterizing the EBM process. The pores generally formed at the turning points, this is the additional reason why porosity is, in this particular case, higher for SLM and, accordingly, the areas with higher porosity for the EBMed specimens are those near the edges [83]. Hence, the proper scanning strategy can be used to tune the porosity distribution inside the manufactured components.

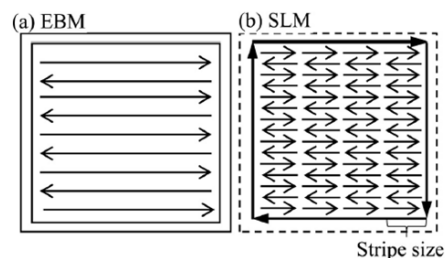


Figure 84: Scanning strategies for EBM (a) and SLM (b) Ti6Al4V manufactured specimens [83].

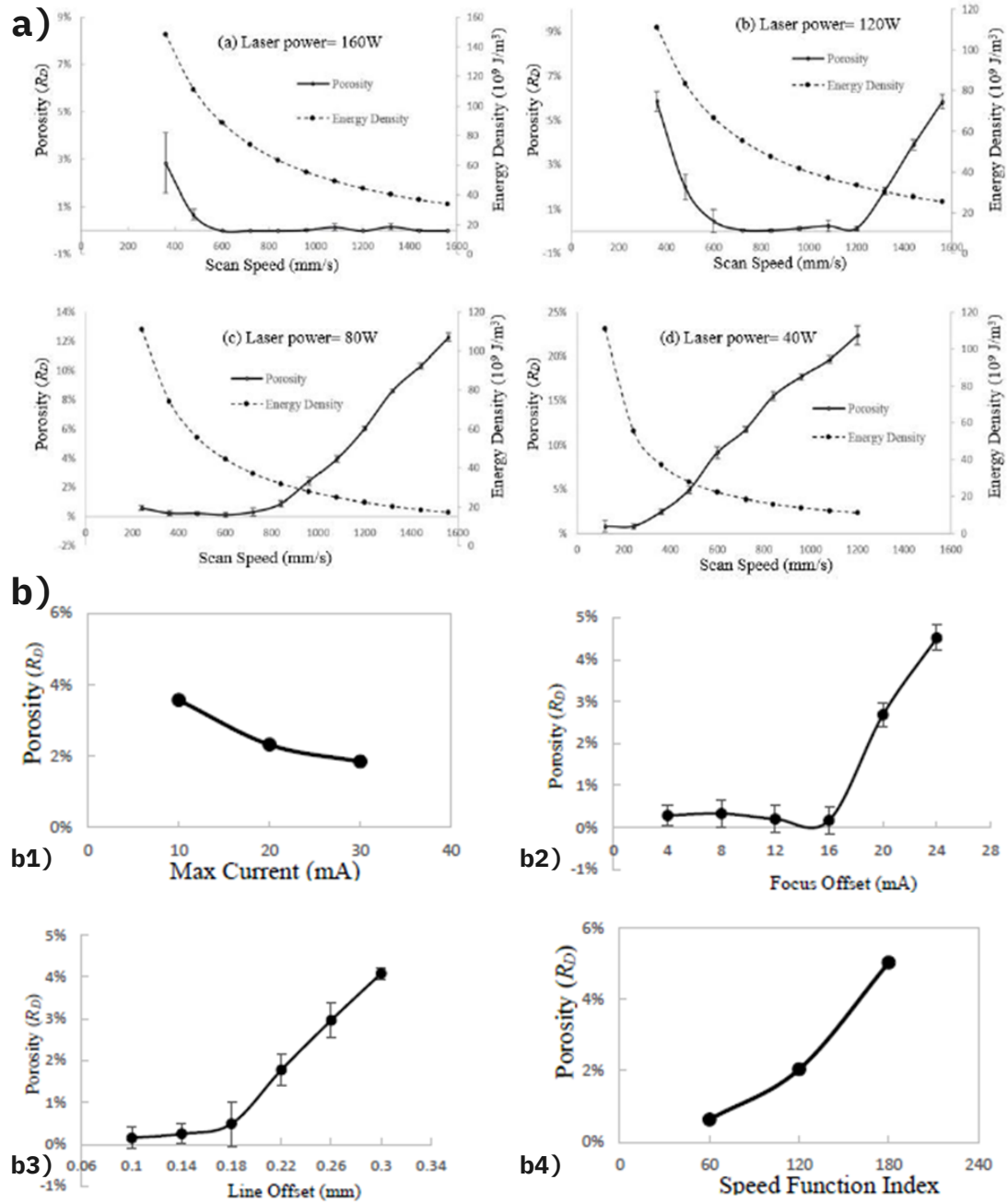


Figure 85: a) Porosity vs. scanning factors for SLMed Ti6Al4V samples. b) Porosity vs. scanning factors for EBMed Ti6Al4V samples (b1) and b4) result from Taguchi experimental factors) [106].

## Ni-alloys

Porosity of SLM manufactured Hastelloy X has been analyzed as a function of laser power and scanning speed for three different values of the hatching distance [92].

- The effects of scan speed and laser power are greater for higher values of the hatching distance, in particular at:
  - $h_d = 0.11$  mm: high porosity regardless of the laser scan speed and power (Fig. 86 (c)).
  - $h_d = 0.08$  mm: lower porosity for 185 W regardless of the scan speed (Fig. 86 (b)).
  - $h_d = 0.05$  mm: apart from points far from the trend, the scan speed is more important for increasing laser power (Fig. 86 (a)).
- The lowest porosity (around 0.065%) obtained for a  $h_d = 0.05$  mm, a power of 195 W and a scan speed of 1000 mm/s (Fig. 86 (a)).
- Generally higher porosity is obtained for larger hatching distance.

Similar results emerged from the analysis of Inconel 939 (IN939) specimens manufactured via LPBF [105]. Keeping the spot size and the laser power constant at 50  $\mu\text{m}$  and 95 W with a layer thickness of 20  $\mu\text{m}$ , it resulted that:

- A low hatch distance of 0.03 mm represents the best trade-off, in particular:
  - At scan speed = 1000 mm/s: the porosity level is very low (around 0.14%) in favor to a higher cracking density (approx. 0.8 mm/mm<sup>2</sup>).
  - At scan speed = 1800 mm/s: the cracking density (around 0.08 mm/mm<sup>2</sup>) is reduced to a minimum but porosity increases (around 0.67%)

In this case a compromise should be found considering also the possibility to apply a post-process heat treatment, such as hot isostatic pressing, that can have a beneficial effect on crack density, this can be a case in which a higher crack density after the manufacturing phase is desirable.

A set of samples have been fabricated in Alloy 718 by SLM technique for various levels of point distance and exposure time (constant power (200 W) and hatch distance (0.1 mm)) [94].

- In general, the porosity decreases for high values of the exposure time regardless of the point distance (Fig. 86).
- Low porosity can be obtained with low point distances (40-53  $\mu\text{m}$ ) and high exposure times (200-220  $\mu\text{m}$ ), upper right corner in Figure. 86.

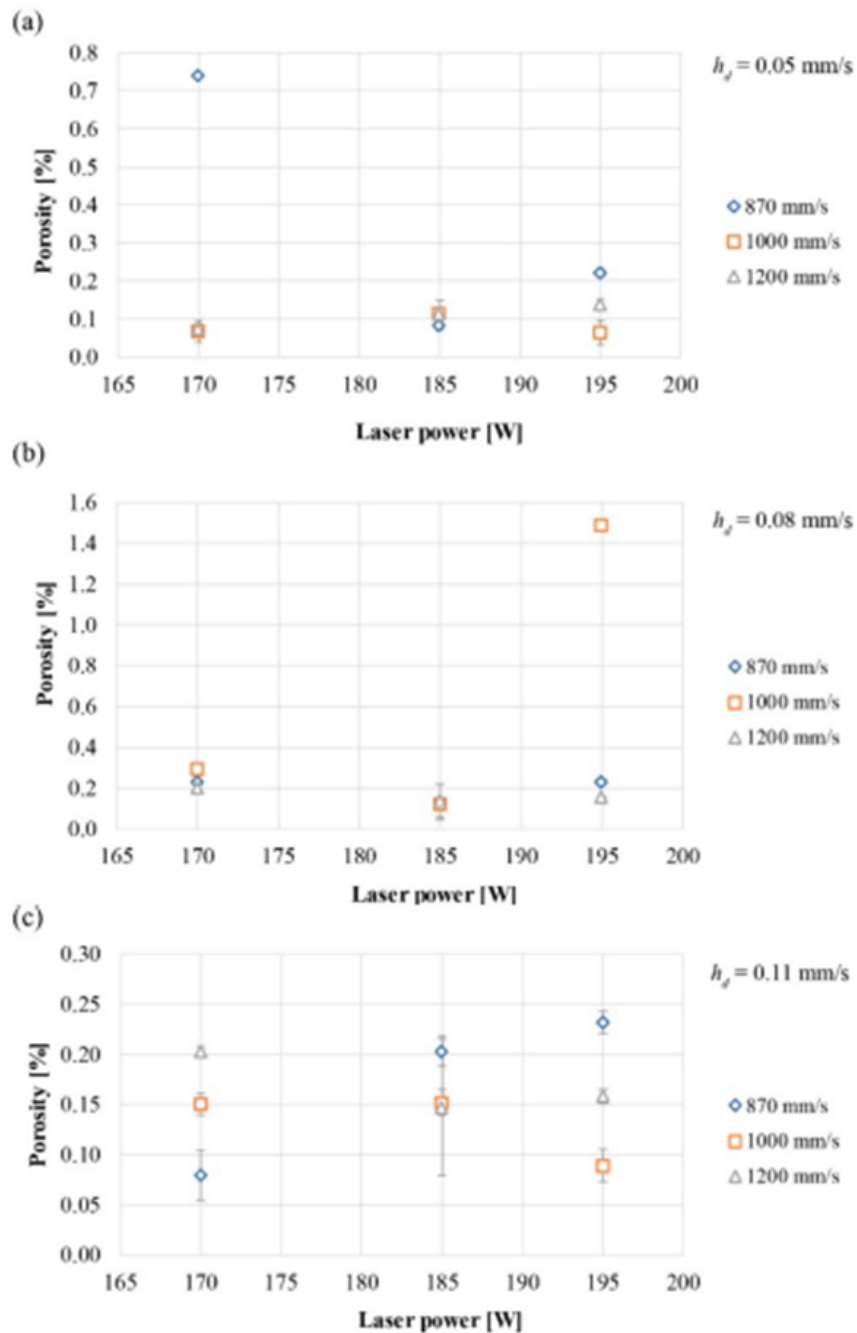


Figure 86: Dependence of porosity on laser power for 870, 1000 and 1200 mm/s scan speed at 3 hatching distances: a) 0.05 mm, b) 0.08 mm and c) 0.11 mm (SLM, Hastelloy X) [92] .

- $122 \text{ J/mm}^3$  laser energy input corresponds to the lowest porosity value.
- Higher point distances induce larger lack of fusion defects.

- 75  $\mu\text{m}$  layer thickness is better than 50  $\mu\text{m}$  especially for small point distances.

Data on on a different type of Ni-alloy (Alloy 230) can be found in [122].

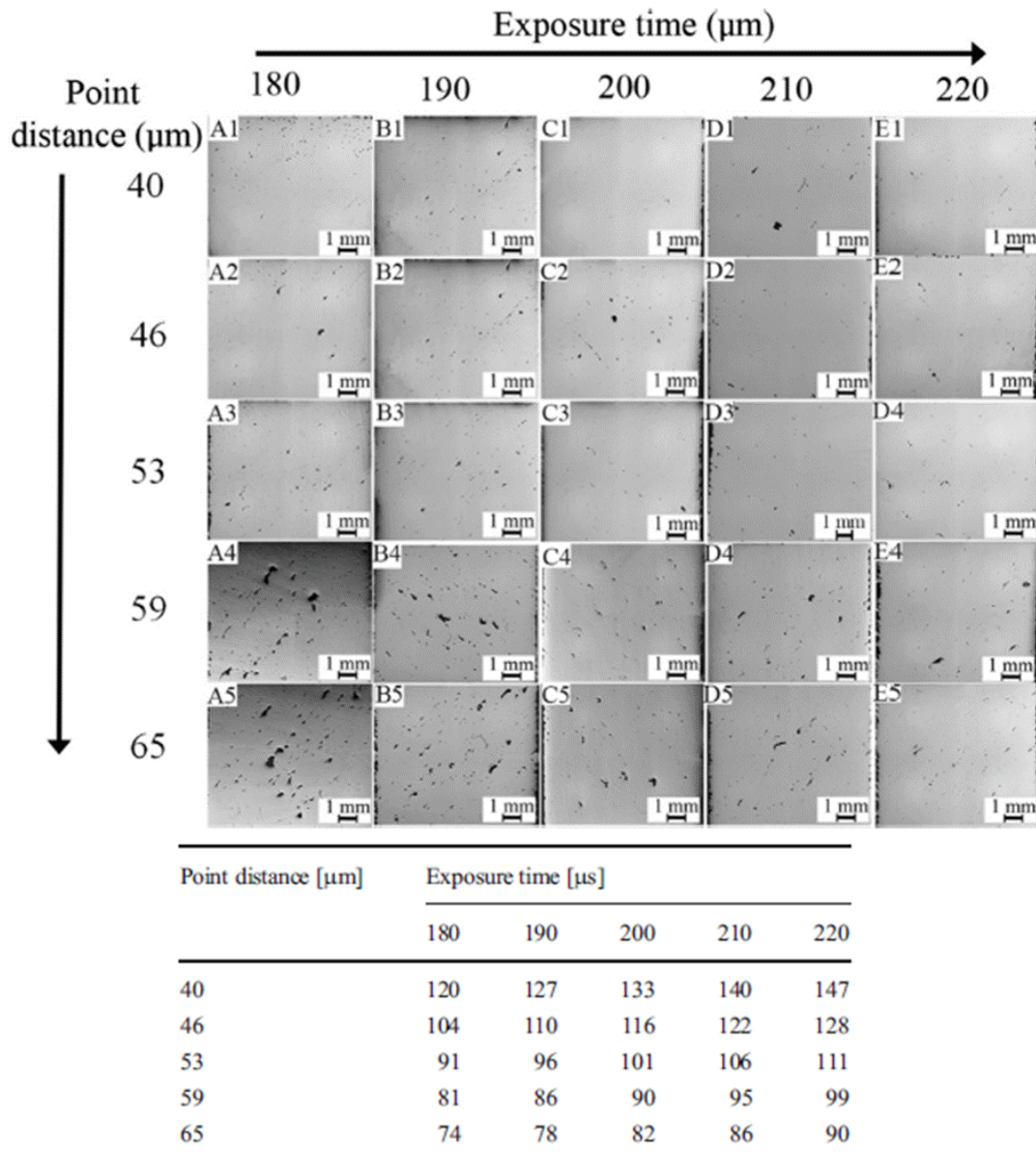


Figure 87: Optical microscopy images for different laser exposure time ( $\mu\text{s}$ ) and point distance ( $\mu\text{m}$ ) with relative values of the laser energy input ( $\text{J}/\text{mm}^3$ ) (SLM, Alloy 718) [94].

## Scanning factors on porosity - Process windows

Table 9: Scanning factors on porosity - process windows.

Material	Alloy type	Laser power (W)	Scan speed (mm/s)	Hatch spacing (mm)	Energy density (J/mm <sup>3</sup> )	Porosity (%)	Bib. ref.
	TiB <sub>2</sub> /AlSi10Mg	320	900-1500	0.15	50-70	$\rho > 99.9\%$	[73]
Aluminium	AlSi10Mg	225-300	1250-1750	20%-30% overlap	-	optimal	[108]
	AlSi10Mg Lattice	250	4000	-	-	optimal	[96]
	AlSi10Mg	-	-	-	50-60	optimal	[13]
	AlSi10Mg (DMLS)	195	700	0.17	-	optimal	[104]
Titanium	Ti6Al4V	200	600-1250	0.03-0.12	92.6-137.3	approx. 0.6	[97]
	Ti6Al4V	160	720-1200	-	-	optimal	[106]
Nickel	Hastelloy X	195	1000	0.05	-	approx. 0.065	[92]
	IN939	95	1000-1800	0.03	-	0.14-0.67	[105]
	Alloy 718	200	800-3500	0.1	122	optimal	[94]

## Scanning factors on geometrical properties and defects

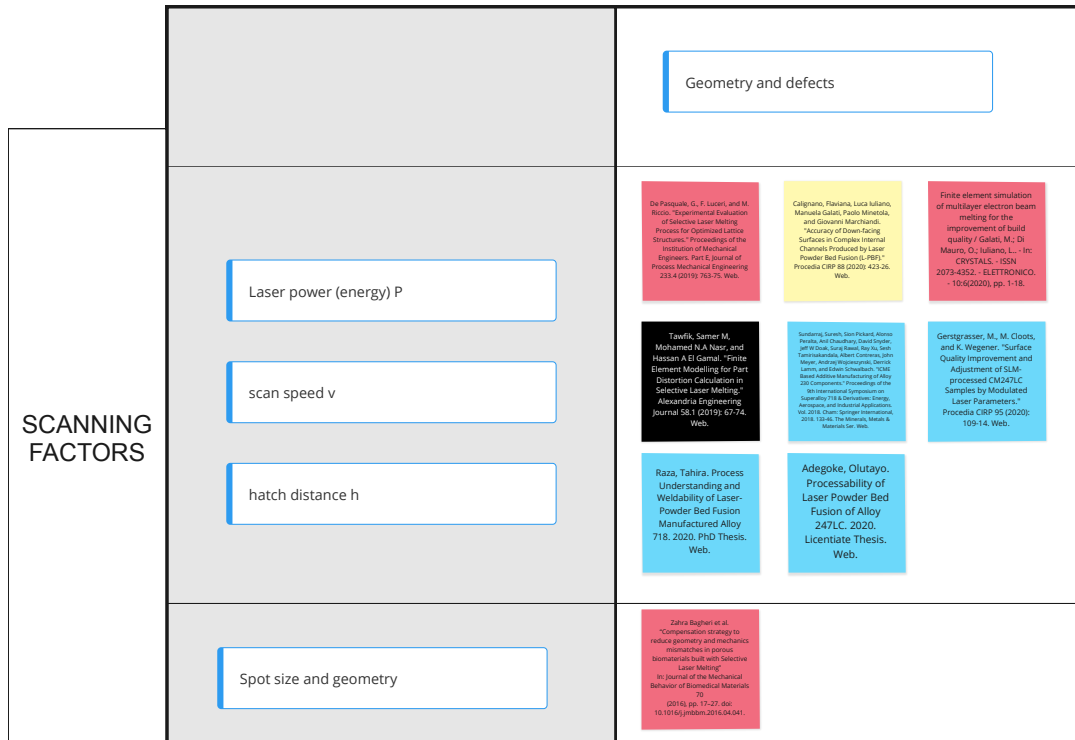


Figure 88: Scanning factors on geometrical properties and defects.

## Al-alloys

AlSi10Mg is among the most used aluminium alloys. SLMed lattice struts resulted to be generally over-sized with respect to the nominal design, thus the effects of laser power and scanning speed on the struts diameter have been investigated [96].

- Increasing the laser scanning speed (at 400 W constant power) the strut diameter decreases until a value of the speed around 3000 mm/s after which its effect becomes almost negligible (Fig. 89 a).
- Strut diameter is directly proportional to laser power (Fig. 89 b).

These are attributed to the amount of energy supplied resulting in a certain melt pool behavior. It is common to have over-sized diameters due to increase in the melt pool width.

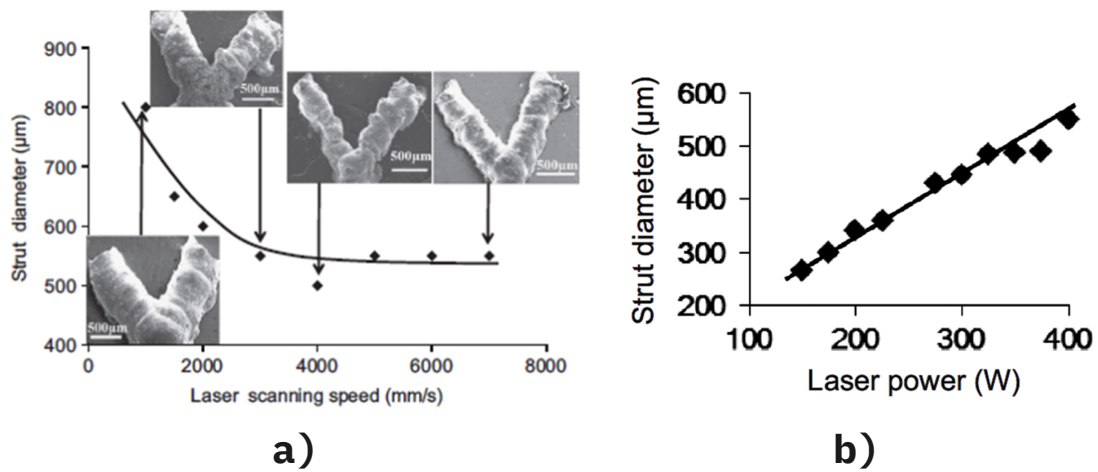


Figure 89: Dependence of the strut diameter on: a) laser scanning speed (power = 400 W); b) laser power (scan speed = 7000 mm/s). Nominal diameter = 300 μm [96].

The fabrication of internal channels is also explored and compared to the ideal CAD model. Optimized parameters resulted in a dimensional accuracy of 0.04-0.07 mm. Three different energy density levels have been found: 70, 79 and 47.4 J/mm<sup>3</sup>, for the down-skin, up-skin and the core, respectively. In general, a good range can be identified between 60 and 80 J/mm<sup>3</sup> [110].

### Ti-alloys

Geometric defects are mainly investigated with the aim of finding suitable compensation strategies to avoid common errors such as larger or smaller geometric mismatches and stair case effects, or to find an optimal set of parameters [111].

For SLMed Ti6Al4V samples the minimum possible diameter has been found to be 200 μm [75], while a suitable volumetric energy density range seems to be approximately between 15 and 17 J/mm<sup>3</sup> [87].

### Ni-alloys

Strategies to reduce the surface roughness of the superior surface of SLMed Hastelloy X lattice structures, that imply an increase in the laser spot and a reduction in the scan speed, have the opposite effect on the surface roughness of lateral surfaces that, in contrast, is improved by reducing the laser spot overlap and increasing the scan speed. A compromise has been found for high peak powers that avoid balling, uniform the melt pool and improve the wettability [89].

The raising of the edges in L-PBF produced Hastelloy X samples is also investigated and its cause is not attributed to the proper choice of the scanning parameters but to the high

temperature gradients related to this production technique that triggers internal residual stresses. In particular the layer exposed to the laser absorbs heat and expands while the previous one, being colder, goes under contraction. Stresses at the interface between the two subsequent layers are supposed to be the cause of the raising of the edges. Surface roughness is also investigated and it seems to be caused by two phenomena [92]:

- The spatters of liquid from the melt pool.
- Partially melted particles adhered to the part surface.

The best surface finish ( $R_a = 1.51 \pm 0.01 \mu\text{m}$ ) is given by 195 W laser power, 870 mm/s scan speed and 0.08 mm hatch distance.

Experiments using single laser tracks on the Ni-superalloy 247LC revealed that the voids content is strictly related to the energy density. A threshold has been identified at  $81 \text{ J/mm}^3$  below which the void content rapidly increases. Values above the threshold give a low amount of voids and are desirable but not higher than  $163 \text{ J/mm}^3$ , value at which the crack density increases [14]. Deeper surface investigations using a larger amount of surface parameters can be necessary [114] but, due to limited time, can not be done in the present work.

Focus offset seems to play the major role in EBMed Alloy 718 specimens. Keeping the focus offset low can guarantee both a fully dense part and a low surface roughness [15]. The same alloy type produced via L-PBF contains mainly lack of fusion defects and gas porosity. The former can be avoided by selecting the proper set of laser scanning parameters that are equally all relevant, while gas porosities can never be fully avoided. Alloy 718 also revealed to be sensitive to cracking during welding. The risk of HAZ cracking can be reduced by applying the proper heat treatment and by welding along the direction parallel to the grain orientation [12].

### Other alloys

AISI 304 stainless steel is subject to a slight deformation that depends on the scanning speed and on the number of layers deposited. The higher the scanning speed and the more pronounced is the part distortions. These distortions basically consists of vertical displacements that depend on the gradients of temperatures formed on the upper surface of the component during the fabrication. Increasing the scanning speed the part do not have time to dissipate the heat accumulated before the following layer is deposited resulting in higher deformation [115].

## Melt pool analysis

		Melt pool morphology and temperature
SCANNING FACTORS	Laser power (energy) P	Arif, Payman, Adil Farhan, Fakhri, Saib Vezhaga, Roghaidh Almarri, Ghaf, Cank Akca, and Moin U Salam, "Selective Laser Melting of 316L Austenitic Stainless Steel: Detailed Process Understanding Using Multiphysics Simulation and Experimentation," <i>Metals (Basel)</i> 11:7 (2021): 1076. Web.
	scanning path or deposition pattern	Masoomi, Mohammad, Scott M Thompson, and Nina Shamsaei, "Laser Powder Bed Fusion of Ti-6Al-4V Parts: Thermal Modeling and Mechanical Implications," <i>International Journal of Machine Tools &amp; Manufacture</i> 118:119 (2017): 73-90. Web.
MATERIAL FACTORS	base powder (Feedstock type, form, condition and properties)	Chen, Zhenhan, Xiaohu Zeng and Xiaohui Zhang, "Analysis of the Temperature Field during the Selective Laser Melting Process Based on a Finite Element Model," <i>International Journal of Manufacturing Research</i> 14:4 (2019): 305-12. Web. Galati, Marcella, Luca Iuliano, Alessandro Salvi, and Eleonora Abate, "Modeling Energy Source and Powder Properties for the Development of a Thermal FE Model of the EBM Additive Manufacturing Process," <i>Additive Manufacturing</i> 14 (2017): 49-59. Web. Cao, Yang, Xin Liu, Nan Kang, Liang Ma, Jun Wei, Min Zhang, Jun Yu, Donglan Pang, and Weidong Huang, "A Novel High-efficient Finite Element Analysis Method of Powder Bed Fusion Additive Manufacturing," <i>Additive Manufacturing</i> 46 (2021): Additive Manufacturing, 2021-10, Vol.46. Web.

Figure 90: Design parameters on melt pool morphology.

MELT POOL CHARACTERIZATION	Mechanical properties	Melt pool morphology and temperature
melt pool morphology	Smith, Jacob, Kiong, Wei, Cao, Jun, Liu, Wang, Kim, 2017b, "Thermodynamically consistent microstructure prediction of additively manufactured materials," <i>Computational Mechanics</i> , 57(3): 355-370. doi:10.1007/s00466-015-1243-1	Papadogiou, E.I., M.E. Karakostas, and A.P. Maniopoulos, "A Comprehensive Study on Thermal Modeling of EBM Process under Conduction Mode Using FEM," <i>International Journal of Advanced Manufacturing Technology</i> 111:9-10 (2008): 2019-2025. Web.

Figure 91: Melt pool on properties.

The thermal phenomena taking place during the fabrication phase, the melt pool (MP) morphology, the defects and the resulting properties of the manufactured part are all correlated and are commonly studied considering their mutual relations. This is the reason why it has been decided to inspect these aspects (Fig. 90 and Fig. 91) in one section only.

There are three basic thermal phenomena transferring heat from the energy source (Fig. 92 a): radiation, convection and conduction. Their magnitude can depend on the

properties of the powder, such as the energy absorption capacity, as well as on the parameters characterizing the energy source.

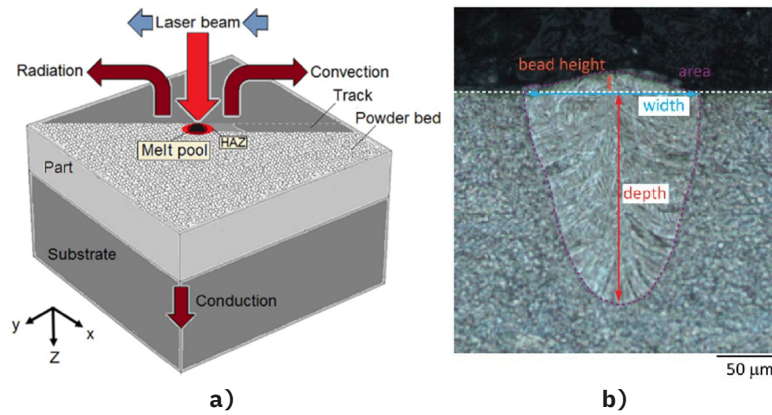


Figure 92: a) Schematic of the thermal phenomena occurring during L-PBF process [17]. b) Vertical section of the melt pool with nomenclature [136].

## Ti-alloys

FEM analysis seems to be a promising method to simulate the behavior of the melt pool. Estimations validated by experimental activities take into consideration the three ways of energy transfer just mentioned, as well as the fact that the material properties change with temperature and also with the material state (powder, liquid and solidified metal). Examples related to SLM of Ti6Al4V powder can be found in literature [117] [17] and identified for this particular case a peak temperature around 2500 °C, a peak and a semi-continuous cooling around 106 °C and 103 °C, and a maximum temperature gradient of 50 °C.

## 316L stainless steel

The effects of the laser scanning parameters resulting from a multi-physics numerical model have been plotted for 316L austenitic stainless steel (Fig. 94 and Fig. 93). The two red horizontal lines define the range of temperatures. If the MP temperature goes above the evaporation temperature there is a mixing between liquid metal and vapors resulting in defects like spatters, holes and overcooking. If, instead, the temperature of the melt pool goes below the melting temperature defects (lack of fusion, unmelted particles) are present. In Figure 93 A) it can be observed how the MP shape, modeled as a Gaussian curve, changes as a function of the spot size diameter: the higher the spot diameter the wider the MP bead. Attention should be put on the MP width that does not follow the same trend, in Figure 93 A) (b) the MP width is around 5 nanometers for 100 μm spot

size, while in Figure 93 A) (c) a lower width (approx. 5 nanometers) is obtained for a greater spot size diameter (150  $\mu\text{m}$ ) [116].

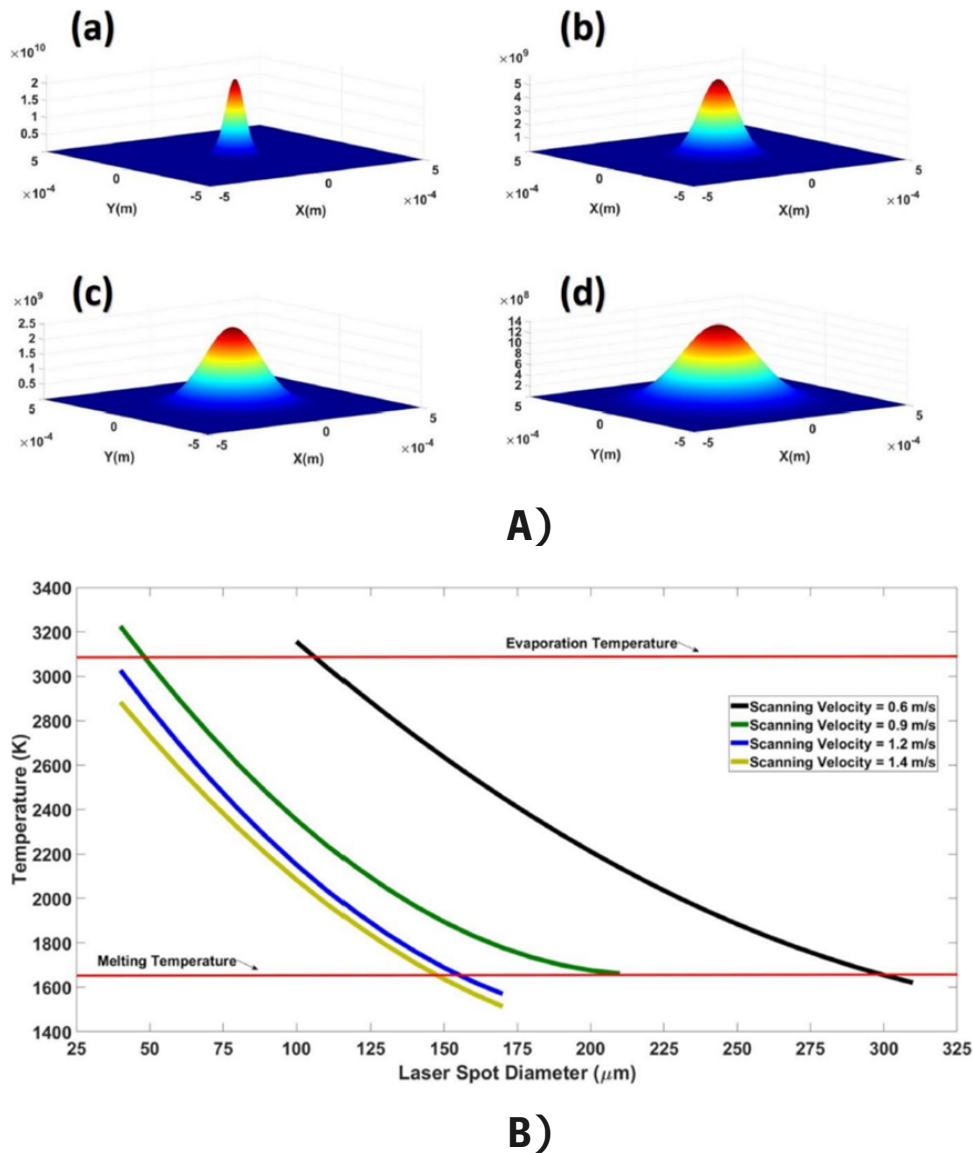


Figure 93: A) Gaussian distribution of heat for laser spot diameter of (a) 50  $\mu\text{m}$ , (b) 100  $\mu\text{m}$ , (c) 150  $\mu\text{m}$  and (d) 200  $\mu\text{m}$ . B) Melt pool temperature vs. laser spot diameter for various scan speed at 150 W laser power (SLM, 316L SS) [116].

The melt pool temperature increases for increasing power (Fig. 94) and decreasing speed (Fig. 93 B) ), this obviously means that it is directly proportional to the energy density. Simulations on single tracks revealed a uniform melt pool for a volumetric energy density (VED) of 97  $\text{J}/\text{mm}^3$ . Decreasing the VED to 81  $\text{J}/\text{mm}^3$  resulted in ellipsoid

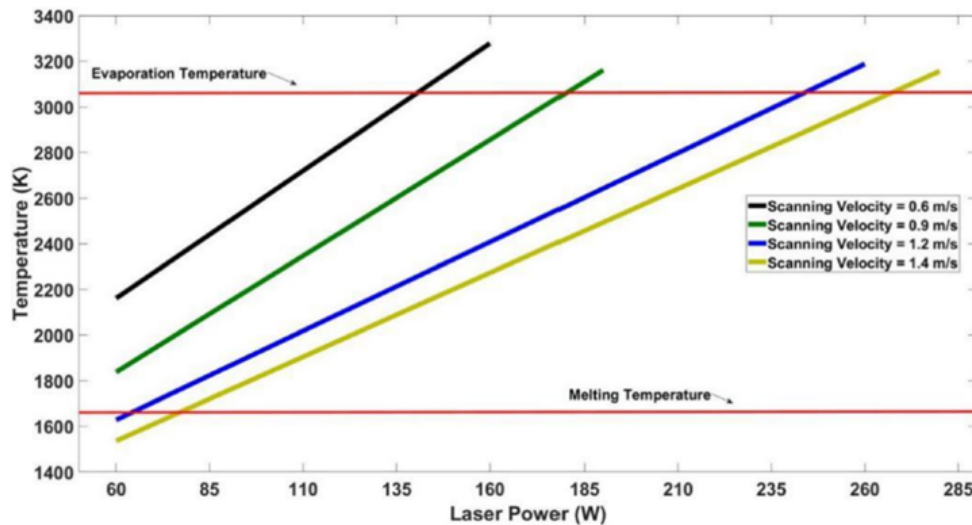


Figure 94: Melt pool temperature vs. laser power for various scan speed at 80  $\mu\text{m}$  spot diameter (SLM, 316L SS) [116].

formations, that are followed by a narrowing of the MP when the VED is again reduced to  $48 \text{ J/mm}^3$  [79].

FE simulations related to EBM production technique ([118]) or to other heat transfer analysis ([86]) can also be found in literature.

## Al-alloys

Some aspects similar to those described in the previous section have been observed also in the case of Al-alloys .

- Too high MP temperatures can trigger the Marangoni effect causing the MP to trap gas particles (usually hydrogen and Ar) that generate round gas pores.
- Too high laser power makes the MP unstable resulting in metal droplets splashing and then solidifying in small spherical particles (balling effect).
- If the energy density is too low the powder is not sufficiently melted and the liquid metal do not reach all the empty spaces before solidifying.
- When the hatch distance is too low insufficient melting has been observed.

In both cases the defects generated increase the porosity level. So the proper scanning parameters has been identified with those giving the lowest porosity (Table 9), both in case of  $\text{TiB}_2/\text{AlSi10Mg}$  [73] and  $\text{AlSi10Mg}$  [96].

Moreover, during melting the melt pool evolves and from being narrow gradually increases in size becoming more and more unstable, then the molten metal droplets splashes outside of the melt pool and then the MP becomes narrower and stable again. This “stability-to-instability” cycle repeats constantly [96]. Applying a gradually increasing energy density to an AlSi10Mg powder bed different defects appear:

- 27 J/mm<sup>3</sup>: key-holes pores due to lack of fusion.
- 38 J/mm<sup>3</sup>: key-holes pores decrease and MP size increases.
- 50 J/mm<sup>3</sup>: key-holes pores disappear and the microstructure becomes coarser.
- 65 J/mm<sup>3</sup>: regions where hydrogen pores appear, the microstructure is coarse and the MP boundaries are visible, and regions characterized by homogeneous microstructure consisting of elongated columnar grains parallel to the building direction.

It is now evident that the energy density plays a fundamental role in determining the MP behavior, and an energy density around 50 J/mm<sup>3</sup> seems to be optimal for both AlSi10Mg and Al6061. However, Al6061 has a higher reflectivity with respect to AlSi10Mg and is more prone to hot cracks, so further investigations should be conducted [13]. Hatch distance - energy density relations have been analyzed in case of DMLS process for the AlSi10Mg powder. The width of the scan track decreases for increasing energy values (Fig. 95 a) ) while the relation between the height of the scan track and the energy density is not clear (Fig. 95 b) ). It has already been noted that the influence of the scanning speed is more visible for higher values of the hatching distance [104]. An example of FEA method applied to PBFed AlSi10Mg alloy powder is also provided in [119].

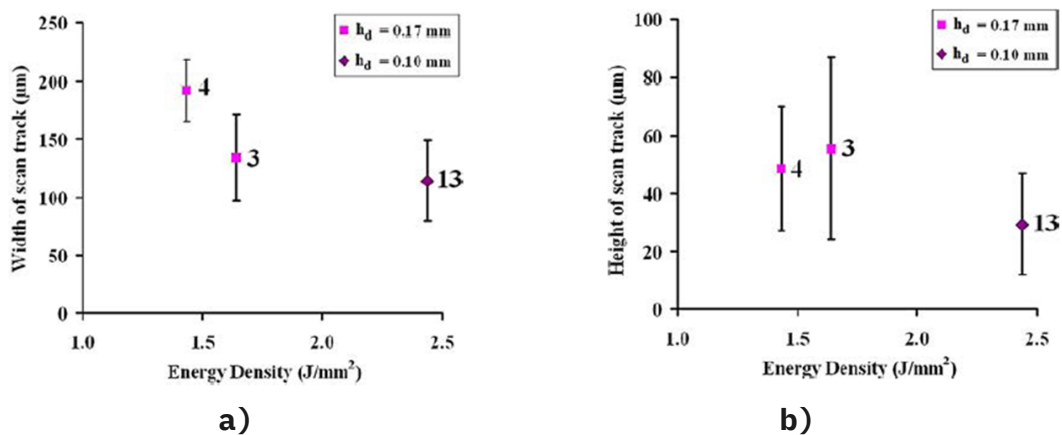


Figure 95: a) energy density vs. width of the scan track and b) energy density vs. height of the scan track for 3 different specimens (DMLS, AlSi10Mg) [104].

In the previous sections it has been observed that the vertical lattice struts are closer to the ideal 3D CAD model with respect to the oblique or horizontal ones. This can also be explained looking at the melt pool. During the building of vertical struts the MP pool is in contact with the previously melted layer while in case of oblique struts the MP is in contact also with the raw powder, that undergoes a partial melting and sticks to the strut causing geometrical mismatches and increasing the surface roughness [81]. Irregularities of the strut diameters are also caused, at higher powers and lower scanning speed, by the violent interaction between the laser and the melt pool resulting in a wider scanning track that produces larger strut diameters. These violent interactions between the laser beam and the melt pool led to increased surface roughness and defects and are again responsible for the increase of internal porosity. For SLMed AlSi10Mg lattice struts, suitable values of the laser power and the scanning speed are 150 W and 7000 mm/s, respectively [96].

### Ni-alloys

SLM of Alloy 718 showed that for longer exposure times the influence of the point distance on the melt pool morphology is almost null. Decreasing the exposure time the point distance becomes more relevant until a minimum value of 180  $\mu\text{s}$  when: for a smaller point distance the MP is narrower and deeper, and for a larger point distance the MP beads are wider like those obtained for long exposure times. In particular the width of the MP increased from  $150\pm 16\ \mu\text{m}$  to  $290\pm 18\ \mu\text{m}$  [94].

Considering the EBM production technique, the phenomena occurring at high MP temperatures are similar to those seen for SLM: molten jet spattering and smoking (Fig. 96).

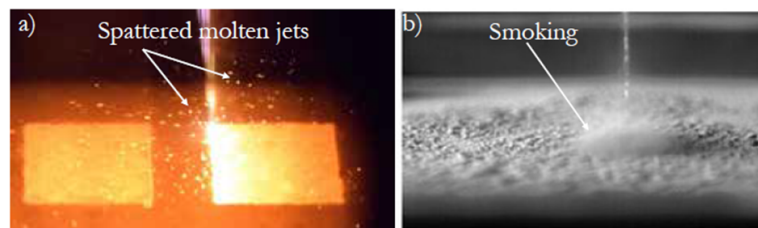


Figure 96: Interactions between the electron beam and the powder: a) spattered molten jets and b) smoking [15].

In addition it has been observed that [15]:

- The speed function, that is the relationship between the scanning speed and the beam current, plays an important role, and is strongly connected to the other scanning parameters.
- If the MP length-to-diameter ratio is greater than 2:1 the MP shape changes from a weld bead to a melt ball.

- Build plate preheating influence the MP geometry making it larger and creates more continuous scan tracks.
- Increasing the focus offset the MP becomes shorter and wider (Fig. 97).
- The melt pool height should be higher than the layer thickness to ensure welding between two consecutive layers (Fig. 97).

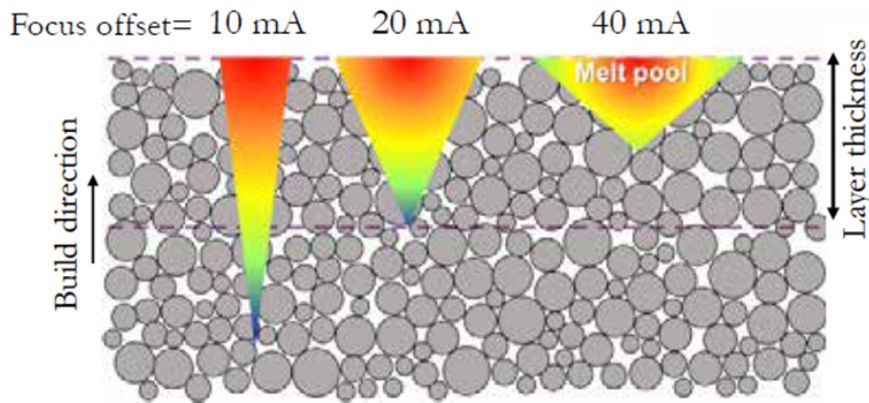


Figure 97: Focus offset vs. melt pool shape [15].

## Heat treatments

### Heat treatments on mechanical properties, ductility and hardness

		Compressive Properties	Yield, UTS, elongation, fracture toughness
HEAT TREATMENT AND POSTO-PROCESSING	Heat treatment parameters	<p>Salari, Morteza; Akhavan-Labori, Sara; Mariani, Eleonora; Caporaso, Marcellino; Cristofari, Giovanni; Marchionni, Paolo; Mariani, Paolo; Peng, Jun; and Liao, Jiahua. "Effect of Laser Heat Treatment on Mechanical Properties." <i>Processes</i> 10(2022): 411-16. Web.</p> <p>Abstract: Laser heating of Ti-6Al-4V alloy... mechanical properties... laser heat treatment... 10.3390/proc10020411</p>	<p>Thien, Perumal et al. "Enhancing the tensile properties of Ti6Al4V parts: Effect of HIP and chemical milling." <i>Materials</i> 14(2021): 143. doi:10.3390/ma14020143</p> <p>Chemical milling... 143 Materials 2021, 14(2), 143. doi:10.3390/ma14020143</p>
		Ductility/HARDNESS	<p>Yield, UTS, elongation, fracture toughness</p> <p>Thien, Perumal et al. "Enhancing the tensile properties of Ti6Al4V parts: Effect of HIP and chemical milling." <i>Materials</i> 14(2021): 143. doi:10.3390/ma14020143</p>
		<p>Yield, UTS, elongation, fracture toughness</p> <p>Thien, Perumal et al. "Enhancing the tensile properties of Ti6Al4V parts: Effect of HIP and chemical milling." <i>Materials</i> 14(2021): 143. doi:10.3390/ma14020143</p>	

Figure 98: Heat treatments on mechanical properties, ductility and hardness.

## Al-alloys

In general heat treatments (HT) have a softening effect that decreases the strength and hardness and increases the ductility of the component. The influence of heat treatments on mechanical properties has been quantitatively analyzed to create process windows (Table 11) composed of various ranges of the mechanical properties that depend on the HT applied (Table 10) [91][137].

Table 10: Heat treatments (from [137]).

Nomenclature	Temperature (°C)	Time (min)	Cooling method	Pressure (psi)
SR1	285	120	Air	–
SR2	190	120	Air	–
HIP	515	180	Inert gas	14,500
HIP + T6	530	360	Quench	–

The ranges proposed in Table 11 are obtained considering the widest possible intervals from the data analyzed. Such ranges can appear even too large due to the fact that they refer to different aging times (from 0 to 1000 hours). It is then suggested to

observe the table together with the charts proposed in Figure 99, that compare the mechanical properties for various heat treatments and, for each HT, the four aging times are considered. However, it can be noted that the aging treatment mainly affects the mechanical properties of those specimens that have undergone the HIP+T6 treatment. In all the other cases such a large variation of the mechanical properties is not present. So, considering also the fact that the heat treatments have can have considerable costs, the designer should evaluate if they are really worth the price.

Table 11: Heat treatments on mechanical properties - process windows for AlSi10Mg (elaborated from [91] and [137]).

Condition	UTS (MPa)	YS (MPa)	$\epsilon$ (%)	Modulus of elasticity (GPa)	Hardness (HV)
Vertical direction Z (building direction)					
As-built	460±20	240±10	9±2	70±10	–
As-built	386-466	217-245	3.6-8.6	–	123-140
Anneal 2 h at 300 °	350±10	230±10	11±2	60±10	–
SR1	239-275	145-177	12.8-23.4	–	82-107
SR2	383-459	215-262	3.5-6.4	–	121-139
HIP	126-145	79-95	27.434.6	–	46-61
HIP + T6	138-313	90-248	13-31.6	–	57-120
Horizontal direction XY					
As-built	460±20	270±10	9±2	75±10	–
As-built	457-368	244-284	8.6-13.7	–	124-147
Anneal 2 h at 300 °	345±10	230±10	12±2	70±10	–
SR1	239-276	151-184	19.3-25.5	–	83-99
SR2	350-388	229-256	9-13.2	–	118-131
HIP	129-147	81-99	28.6-38.6	–	44-61
HIP + T6	147-288	99-235	11.5-31.3	–	58-111

Note: the property ranges provided in the form "min.value-max.value" are referred to different aging treatments at 177 °C (in addition to the heat treatments already applied) that last from 0 to 1000 hours. The "annealing time-properties" relation is not always linear.



Figure 99: Effect of heat treatments (Table 10) on properties of AlSi10Mg SLMed samples for different aging times at 177 °C along Z and XY directions: (a) and (d) YS; (b) and (e) UTS; (c) and (f) elongation (from [137]).

## Ti-alloys

The data in Table. 12 and the following considerations are referred to the Ti6Al4V alloy.

- HIP increases ductility, elongation and resistance to fatigue and decreases YS and UTS. The effect is much more evident in SLM than EBM [83] [125].
- Chemical etching improves YS, UTS, elongation and ductility. It reduces the negative effect of a poor surface finish but, removing material on the surface, makes the sub-surface porosities emerge (EBM, Ti6Al4V) [125].
- HIP can close or reduce the internal pores.
- “HIP + chemical etching” can then be a good combination.
- HIP below the  $\beta$ -transus temperature gives better properties than that above the  $\beta$ -transus [125].
- Lattice specimens exhibit a brittle behavior in the as-built state that can become ductile after HT [123] [124] .
- As-built EBMed lattice specimens can sustain a higher compressive load until a certain level of strain (6-7%) after which there is a drop. Heat treated specimens show a more gradual increase in the stress-strain curve (Fig. 100).
- The relative density of the unit cell is still strictly correlated with the compressive properties.

Hot isostatic pressing treatments seems to be widely used with Ti6Al4V samples both in case of lattice and bulk pieces. In general, the softening effect (increase in ductility and elongation and decrease in strength) it is also valid for for Ti6Al4V as it was for Al-alloys and, usually, it is valid for the majority of the alloys. Following this reasoning it can be affirmed that the machined specimens exhibit the highest strength. Lattice specimens and thin parts can not be machined but an improvement of the surface finish, that results to be beneficial for the performances, can be obtained by applying a chemical etching followed by a HIP treatment (Fig. 101). The above mentioned guidelines can be useful but obviously there can be exceptions. It has also been observed that SLM manufactured lattice specimens can keep their compressive strength and stiffness also after the HT. However, the changes in mechanical properties are much more affected by changes in size and shape of the unit cell than HT [124].

The designer should then be aware of selecting the proper geometrical parameters characterizing the unit cell because, if the resulting properties do not satisfy the requirements, not much can be done by post-heat treatments. It is also interesting to note that the HIP treatments above the  $\beta$ -transus temperature (above 850 °C) have slight effects

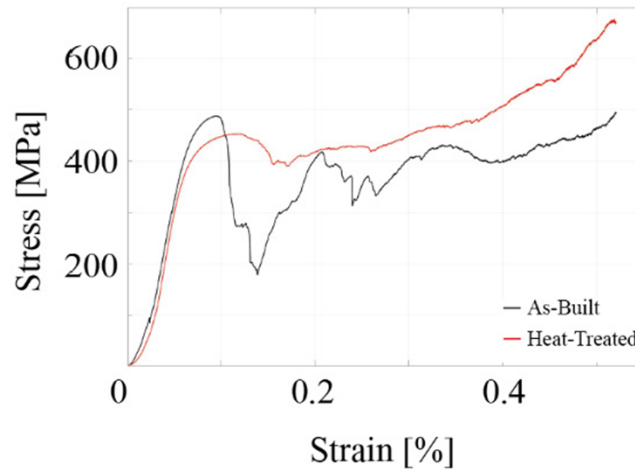


Figure 100: Compressive stress-strain curves for as-built and heat treated Ti6Al4V lattice specimens (4 mm cell size)[123].

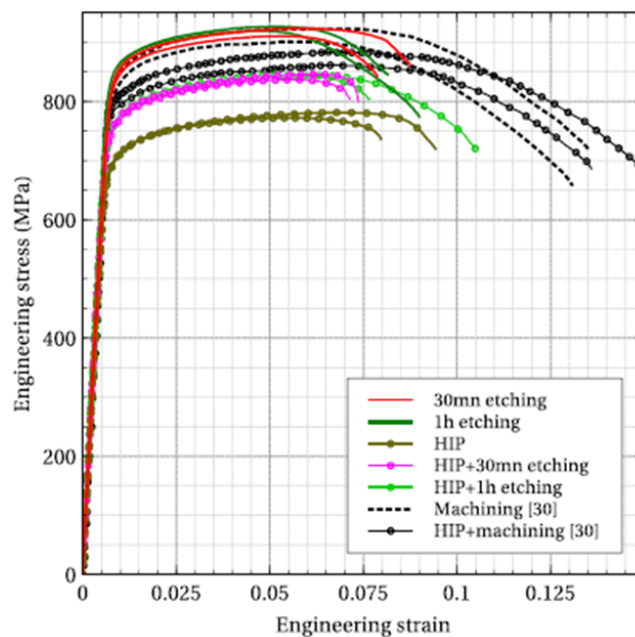


Figure 101: Tensile stress-strain curves for EBMed Ti6Al4V specimens after various heat treatments [125].

on the YS and UTS while are really degrading the elongation (more than halved). In contrast, the HIP treatments below the  $\beta$ -transus temperature have a beneficial effect on elongation but decrease the UTS (approximately of less than 30%). The yield strength and the hardness are however only slightly affected by the choice of the HIP treatment temperature [126].

Table 12: Heat treatments on mechanical properties for Ti6Al4V alloy.

Heat treatment	T (°C)	Time (min)	Pressure (MPa)	Cooling (MPa)	YS (MPa)	UTS (MPa)	$\epsilon$ (%)	Hardness (HRC)
Anneal	704±14	120±15	-	Air or furnace	1185±15	1217±13	8.7±1.3	43.9±1.36
HIP	881-970	180±60	100	Inert atm. < 425 °C	1025±17	1083±13	17.7±0.8	40.7±0.93
Anneal + HIP		see previous 2 lines			1039±9	1089±9	16.1±1.1	40.4±0.97
As-built	-	-	-	-	753±4	824±5	6.1±0.8	-
Etched	-	30	-	-	842±8	918±6	8.3±0.4	-
Etched	-	60	-	-	754±3	923±4	8.6±0.4	-
HIP		rise at 300 °C + anneal 2 h at 920 °C + furnace cooling (T<150 °C after 3 h)			697	77±5	8.8±0.8	-
HIP + Etched (30 min)		see previous line			757±4	841±5	7.3±0.2	-
HIP + Etched (60 min)		see previous line			763±2	844±1	9.1±1.4	-
				Cooling rate (°C/min)				
As-built	-	-	-	-	940	1020	12.3	12.3
HIP above $\beta$ -transus	920	120	103	100	900	990	5.1	36
HIP above $\beta$ -transus	1050	120	103	1000	910	1040	3.4	40
HIP above $\beta$ -transus	1200	120	103	1000	870	1030	4.2	39
HIP above $\beta$ -transus	1050	240	103	1000	910	1040	2.7	41
HIP above $\beta$ -transus	1050	120	103	100	830	930	7	39
HIP below $\beta$ -transus	800	120	207	100	910	990	11.5	39
HIP below $\beta$ -transus	800	240	207	100	840	980	13.6	39
HIP below $\beta$ -transus	800	120	207	1000	750	970	11.6	38
HIP below $\beta$ -transus	850	120	207	100	900	1000	14.3	37

## Ni-alloys

The effects of the following heat treatments on mechanical properties and hardness (Table 13) of L-PBF Inconel 718 and DEDed Inconel 625 have been investigated.

### L-PBF Inconel 718 [130]:

- SR (stress-relief anneal): 1065 °C for 90 min.
- HIP (hot isostatic pressing): 1120 °C for 240 min.
- HIP\* (hot isostatic pressing): 1163 °C for 180 min at 15000 psi (approx. 103 MPa).
- SA (stress relief anneal): 720 °C for 480 min.
- SA\* (stress relief anneal): 1060 °C for 20 min at 12000 psi (approx. 83 MPa).
- Aging: 620 °C for 480 min.

### DED Inconel 625 [120]:

- ST (solution treatment): 1200 °C for 30 min.
- Aging: 650 °C for 3000 min (50 hours).
- HIP\*\* (hot isostatic pressing): 1150 °C for 180 min at 160 MPa.

From Table 13 it can be noted that, for Inconel 718, the maximum hardness corresponds to the minimum elongation and vice-versa. The connection between heat treatments and the mechanical properties passes through the component microstructure. In the present work the microstructure characteristics are not deepened, however it can be mentioned that the equiaxed twinned grain structures containing carbides have the most important effect on the mechanical properties of Inconel 718 [130] [127].

Another proof of the “heat treatment - microstructure - properties” relation can be found in Figure. 102 where an opposite trend between the hardness and the lattice parameter of the  $\gamma$  phase is evident. Looking individually at the left chart (Fig. 102 (a) ) a non-linear relation between the HT temperature and the hardness value is present and this is also attributed to the presence of carbides [131].

The dependency of hardness upon heat treatments is totally different in the case of L-PBF manufactured Ni-superalloy 247LC, indeed, the hardness in the as-built state resulted almost equal to that of the heat treated samples [14].

Beneficial effects on anisotropy have also been found for the heat treated Ni-base superalloy IN738LC subjected to: recrystallization above the  $\gamma'$ -solvus temperature (1250 °C, 3 hours), HIP (1200 °C, 4 hours, 100 MPa), post-HIP solution (1120 °C, 2 hours) and final precipitation hardening (850 °C, 20 hours) [101].

Table 13: Heat treatments on mechanical properties - process windows for L-PBF Inconel 718 and DED Inconel 625 (elaborated from [130] and [120]).

Alloy	Mech. property	Ranges		Heat treatments
L-PBF Inconel 718	YS (MPa)	Max	1260	SR + SA + Aging
		min	600	SR
	UTS (MPa)	Max	1400	SR + SA + Aging
		min	920	SR
	$\epsilon_{\max}$ (%)	Max	43.1	SR
		min	11.4	SR* + HIP* + SA* + Aging
	Hardness (HRC)	Max	54	SR + SA + Aging
		min	33	SR
DED Inconel 625	YS (MPa)	Max	756	SA + aging + water-quenching
		min	436	ST
	UTS (MPa)	Max	1087	SA + aging + water-quenching
		min	893	ST
	$\epsilon_{\max}$ (%)	Max	55	HIP** + furnace cooling
		min	25	SA + aging + water-quenching
	E (MPa)	Max	237	SA + aging + water-quenching
		min	193	ST

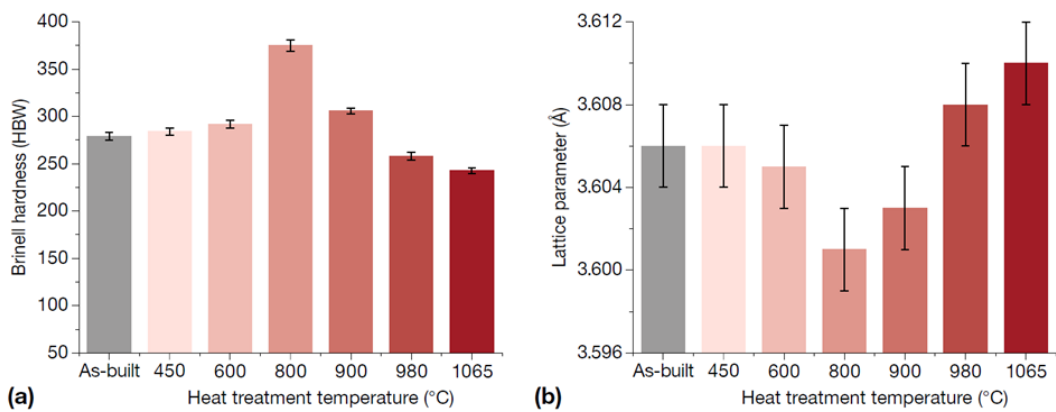


Figure 102: Effect of heat treatment temperature on (a) hardness and on (b) lattice parameter of  $\gamma$  phase of L-PBF Inconel 718 [131].

## Heat treatment on porosity, geometry, and defects

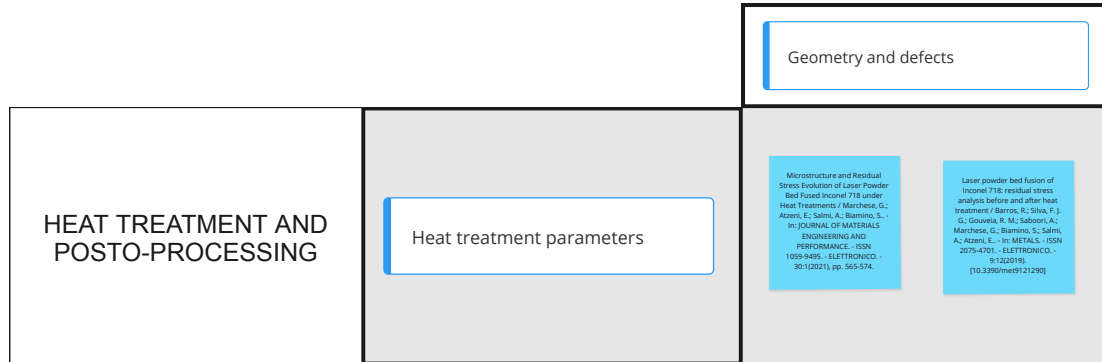


Figure 103: Heat treatments on mechanical properties, ductility and hardness.

### Al-alloys

Solution heat treatment followed by aging improves the strength affecting the mechanical properties but has no effect on the morphology of AlSi10Mg lattice specimens [76].

### Ti-alloys

As already mentioned in the section related to the building orientation, the flatness of the down-skin surface is more affected by heat treatments (Fig. 56) than by the wire EDM cutting operated to remove the part from the build plate. A closer observation to the Ti6Al4V specimens allows to see that the heat treatment had been able to remove the small surface waves but the large ones are still present (Fig 104 (a) ) [74]. Chemical etching is able to both reduce the sub-surface defects (porosity < 1%) of EBM manufactured Ti6Al4V specimens (Fig 104 (b) ), that for certain types of load like bending fatigue are very detrimental for the component life, and improve the surface finish (Fig 104 (c) ). With chemical etching a notable reduction of the sub-surface pores can be achieved, while the porosity at the core of the component can be reduced by hot isostatic pressing treatment, that is actually able to reduce the porosity of the whole component (close to 0%) [125]. It has to be pointed out that the chemical etching treatment resulted to be not homogeneous, the particles stucked to the component are removed before the other defects, and convex surfaces are more impacted than concave ones [125]. The quantitative effects of chemical etching and HIP on surface roughness ( $R_t$  and  $R_a$ ) are summarized in Table 14. The previous parameters values in case of as-built component are given as a reference:  $R_t = 42.6 \mu\text{m}$  and  $R_a = 405 \mu\text{m}$ .

Table 14: Effect of HIP and chemical etching on surface finish (EBM, Ti6Al4V) (elaborated from [125]).

Alloy		Ranges		Heat treatments
EBM Ti6Al4V	$R_t$ ( $\mu\text{m}$ )	Max	390	HIP
		min	232	1 hour Etching
	$R_a$ ( $\mu\text{m}$ )	Max	43.3	HIP
		min	26.4	1 hour Etching

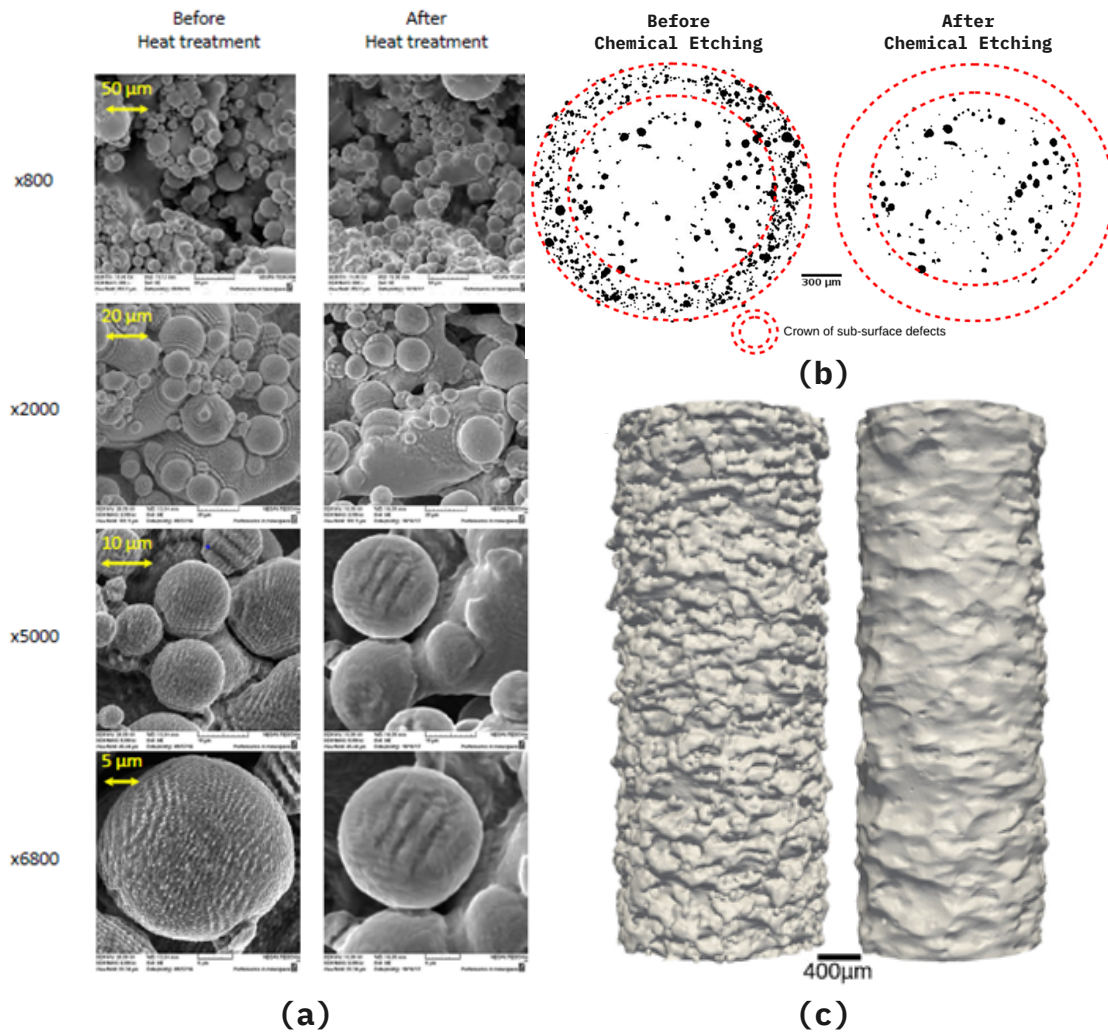


Figure 104: (a) effect of the heat treatment on the surface waviness at nanoscale [74]. Effect of chemical etching (30 min) on porosity (b) and surface roughness (c) (Ti6Al4V). [75].

## Ni-alloys

The discussion about the influence of heat treatments on Ni-alloys mainly focuses on the effects of such treatments on the crack susceptibility and residual stresses of PBF Alloy or Inconel 718.

Referring to the internal cracks it has been noted that the average crack length and the average maximum crack length decreases from the as-built condition to the HIPed specimens, that exhibit values comparable to those of wrought alloys. Instead, the average total amount of cracks is minimum in the as-built state and decreases for various heat treatments until the maximum level is reached in the HIP treated samples, that is again comparable to the amount of cracks present in wrought alloys (Fig. 105). These trends can be explained in simple terms by saying that the heat treatments are able to reduce the size of the cracks (approximately from 300 to less than 200  $\mu\text{m}$ ) that, in contrast, are higher in number. The standard deviations are however quite relevant and very precise conclusions can not be deducted [12].

The heat treatments reported in Figure 105 are:

- Hot isostatic pressing (HIP): 1160 °C for 3 hours.
- Standard solution heat treatment (SHT): 954 °C for 1 hour.
- 2-step aging (AGED): 760 °C for 5 hour + 649 °C for 1 hour.

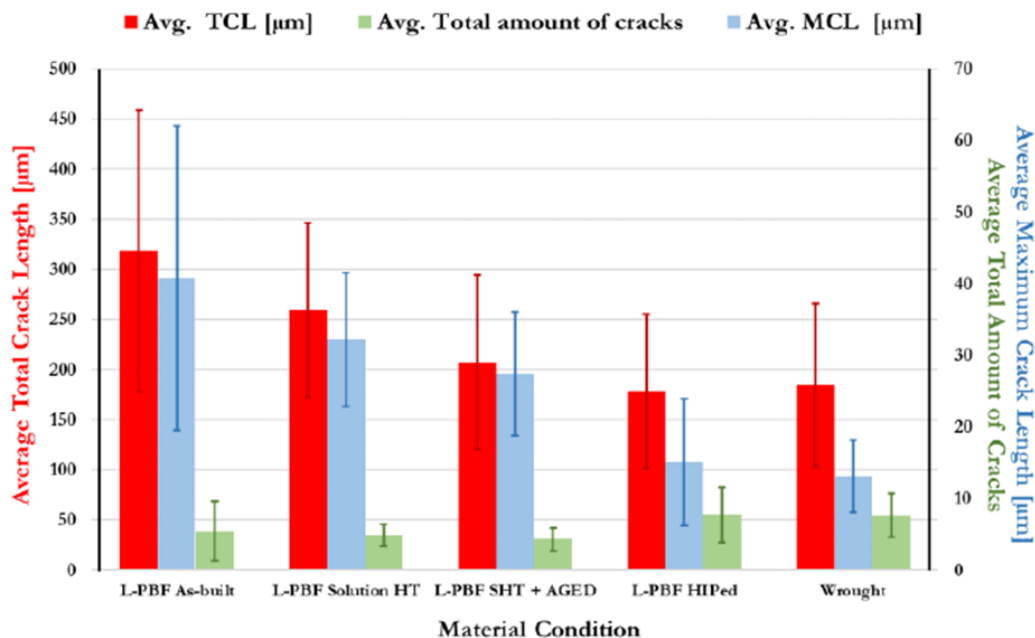


Figure 105: Effects of heat treatments on the length and amount of cracks for PBF Alloy 718 [12].

The HT temperature seems to play a crucial role in case of sub-surface residual stresses (RS). The threshold level has been identified around 700 °C, heat treatments at low temperature (at 450 and 600 °C) mitigate the residual stresses causing apparently negligible changes to the microstructure, while heat treatments at high temperature (from 800 to 1065 °C) are effective in reducing the residual stresses but also trigger modifications in the microstructure that are also evident from the change in hardness (already analyzed in the previous sections). Moreover, differences in the order of magnitude of the RS have been found between the top surface and the lateral surfaces highlighting a significant degree of anisotropy (Fig. 106) [131, 132].

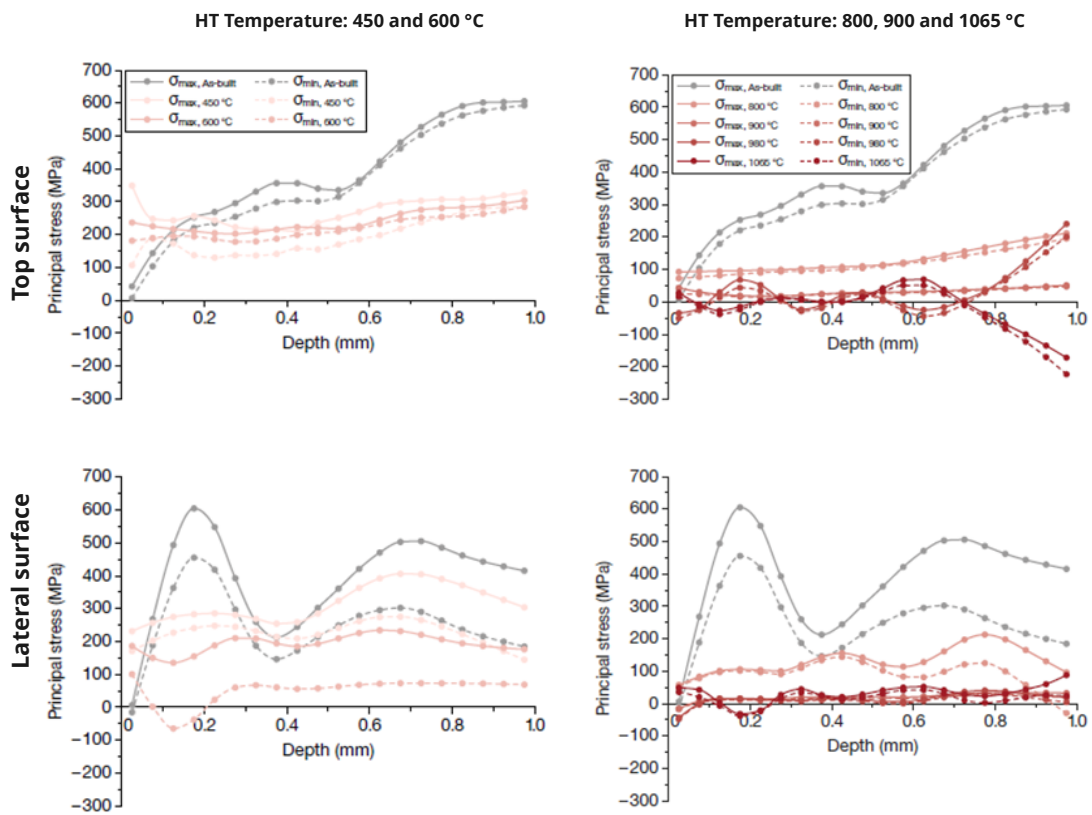


Figure 106: Effects of HT temperatures on sub-surface principal stresses for L-PBF Inconel 718 (from [131]).

## Defects

Different types of defects have already been explored in previous sections. Here a further investigation will be done by mentioning some attempts aiming at including the defects inside the finite elements models to make numerical simulations closer to real cases, and by briefly showing the defects that can lead to failure in case of AlSi10Mg and TiB<sub>2</sub>/AlSi10Mg).

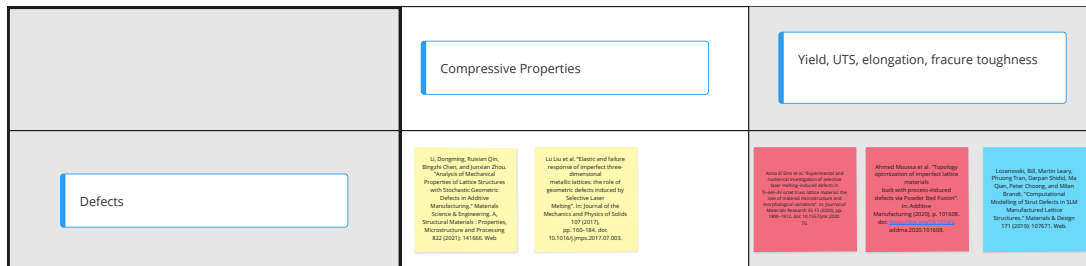


Figure 107: Defects on mechanical properties

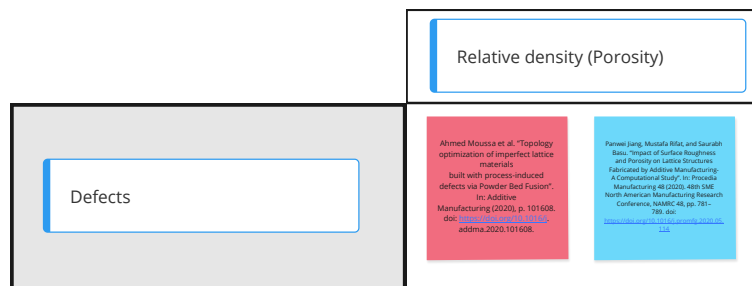


Figure 108: Defects on porosity.

The modification of the AlSi10Mg alloy with TiB<sub>2</sub> have notable effects on the mechanical properties that have already been mentioned. In addition, effects on the fracture mechanism have also been observed. The crack can start propagating from the melt pool boundary where the microstructure is typically coarse, and also from the distributed TiB<sub>2</sub> particles that can form small agglomerates (Fig. 109). The component can fail in different ways and the failure mechanism is hardly predictable. The choice of TiB<sub>2</sub>/AlSi10Mg alloy has for sure advantages in terms of mechanical properties but the engineer has also to consider the further level of complexity that would be added to the component design [73].

The incorporations of defects inside numerical models can be very convenient. Various attempts have been made in this direction. The statistical FEM showed to be closer to the experimental results than the ideal FEM, and through the statistical FEM the impacts

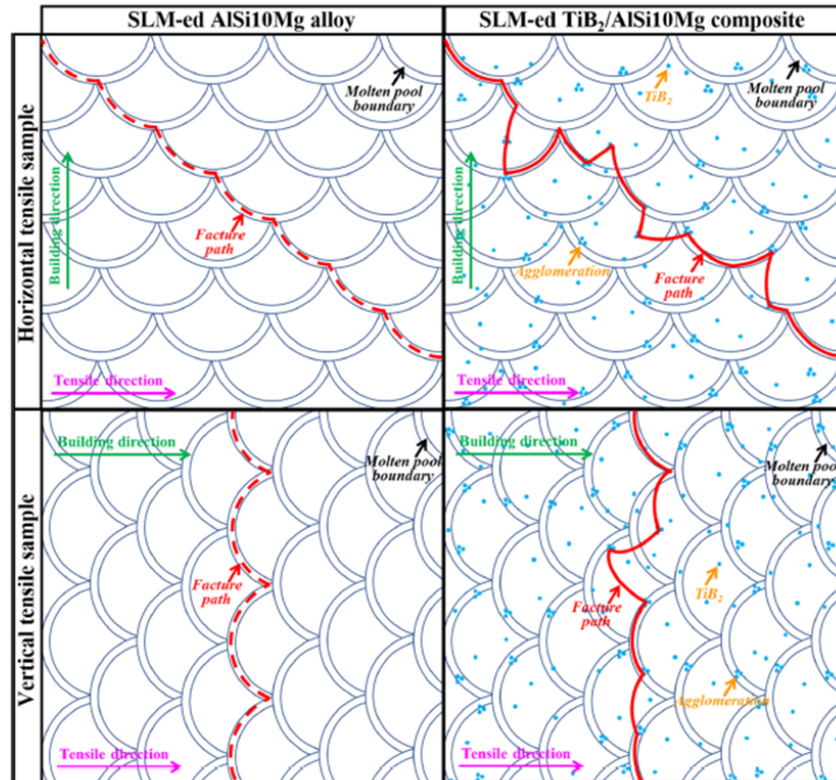


Figure 109: Fracture path and defects comparison for  $\text{TiB}_2/\text{AlSi10Mg}$  and  $\text{AlSi10Mg}$  [73].

of struts geometrical mismatches on the SEA coefficient, that represent the specific energy absorption capability, have been evaluated for a  $\text{AlSi10Mg}$  FCC lattice cell. It resulted that the thickness of the diagonal struts can increase the energy absorption capacity, while the thickness of vertical struts and the surface waviness can decrease it [76].

A similar work to foresee the Young's modulus and the compressive strength of regular octet and rhombicuboctahedron lattice cells has also been conducted considering again strut undersizing, strut thickness variation and strut waviness [133].

Equivalently, efforts have been invested to analyze  $\text{Ti6Al4V}$  alloy both numerically ([113][64]) and experimentally ([106]), and examples of FEM simulations applied to Inconel 625 ([134]) and Inconel 718 ([135]) are also present in the literature.

The analysis of FE models is not the main objective of the present work, still it can be affirmed that successful progresses have been achieved to make the outcomes of the simulations closer to those obtained experimentally, nonetheless further research is necessary.



# AM economics

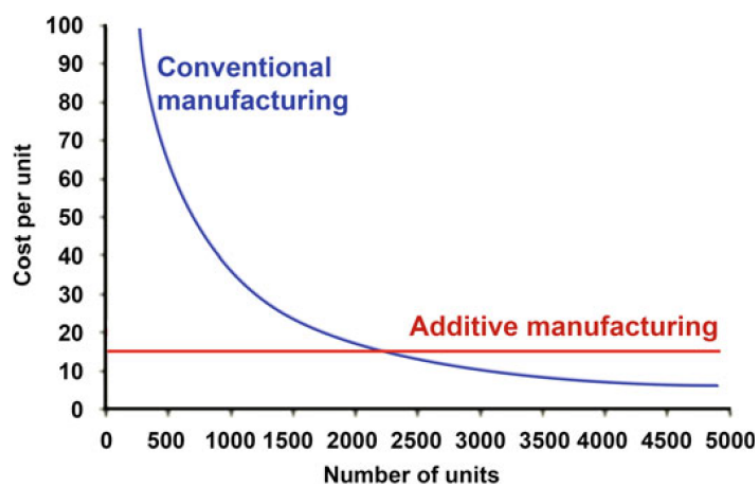


Figure 110: Cost of per unit of parts produced with conventional and additive manufacturing [1].

The information provided in the chart above (Fig. 110) induces to think that producing a single part, or a small batch, using additive manufacturing technologies instead of traditional manufacturing methods is much cheaper. This is generally wrong. The error made is not exclusively related to the money that can be saved but the real mistake is the wrong approach to the design for additive manufacturing. To exploit the many advantages that AM can offer the engineer must understand that the design, or the re-design, of a part has to be totally different. The choice of adopting AM to produce a component that normally would have been produced with CNC or other traditional technologies in most of the cases will increase the cost of such component.

The price of an additive manufacturing system ranges between \$500 000 and \$1 200 000 depending on its specifications, and the resulting hourly cost between \$37.45 and \$89.89. Assuming that the average cost is \$65/h and considering that the average time to produce a part not designed for AM ranges from 40 to more than 100 hours, it is easy to understand that AM cannot be economically competitive if compared to traditional manufacturing techniques that require much less time. The gap becomes even wider taking into account that the support structures, and the material needed to anchor the component to the

building platform (approximately 10% of the total material amount) have to be removed after manufacturing but still take time to be printed. Moreover, the time needed by the machine to produce the part has to be added to that involving pre- and post- process activities which can represent 70% of the total cost.

It becomes very easy to understand that approaching AM as a mere substitute for traditional manufacturing in almost all the cases leads to unsatisfactory results.

The most important advantage is the design freedom provided by AM, almost any shape can be realized and, especially comparing it to conventional manufacturing, an increase in complexity imply a negligible increase in cost (Fig. 111).

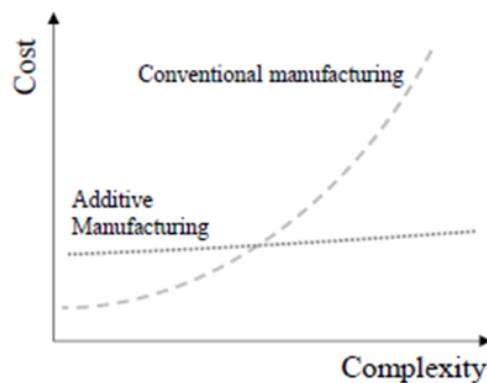


Figure 111: Complexity vs. cost for conventional and additive manufacturing [139].

It is then crucial to invest a considerable amount of time and resources in the design phase so that all the potentials of AM can be exploited.

Consequently, all the design and manufacturing steps need to be accounted in the prediction of the total costs (examples for various AM techniques can be found in [140] [141] [142] [143] [144], also considering environmental costs [145]).

Reducing time means reducing costs, thus the engineer can design the part trying to find a trade off between two objectives:

1. Reduce printing time
2. Reduce support structures

The re-coating time needed to supply new powder layers is estimated between 20% and 30% of the total time used by the machine to produce the workpiece. This can only be reduced by reducing the number of layers to be deposited that means changing the building orientation of the part. However, a different orientation may require the addition of support structure (additional material to be printed) and, as it has been pointed out analyzing the part design factors in *Step 3*, it also affects the surface roughness, the surface flatness and the roundness of the holes. In a similar case a post-process machining operation can be useful to improve the surface roughness but it can only

be applied as long as such surface can be reached by machining tools. So, the building orientation should be carefully chosen considering both the constraints of the problem, and the fact that the anisotropy direction of the mechanical properties strongly depends upon such orientation.

Reducing the number of support structures obviously implies a direct saving of material. When they can not be avoided, due to overhangs or to the need of reducing sub-surface stresses, it is suggested to incorporate them inside the final shape of the part. By doing so the component will result stiffer and the time that would have been employed to remove the supports is totally saved [1].

In conclusion, before starting the design a set of priorities must be clarified considering all the different requirements, the constraints, and the resources available.

A proper design can add a considerable value to the manufacturing and consequently to the whole production chain [146].

Moreover, the design freedom allowed by additive manufacturing can simplify the pursuit of sustainability in the production processes, promoting the implementation of the circular economy and having positive social impacts [147][148].



## Case study - reverse engineering approach

To show a practical application of all the guidelines provided along the previous chapters, it has been decided to analyze an aerospace bracket made of Ti6Al4V alloy [138]. In this paper the authors analyzed the component using a numerical modeling technique, re-designed it through a topological optimization and, after a preliminary characterization of the material, they produced the bracket via EBM and SLM. The key-points that can be useful to apply a reverse engineering approach are the following:

- **Preliminary characterization of the material:**

16 specimens have been manufactured via EBM and DMLS along different building directions, machined and tested. Yield strength, UTS and elongation are reported in Figure 112.

Material process		Yield (MPa) min÷max	UTS (MPa) min÷max	Elong. % min÷max
DMLS	X	1199÷1214	1322÷1339	7.0÷9.4
	Y	1201÷1217	1320÷1326	5.6÷8.0
EBM	X	1000÷1057	1077÷1127	13.2÷13.5
	Y	1007÷1107	1077÷1169	11.1÷13.7
	Z	973÷1029	1044÷1081	10.4÷11.2

Figure 112: Tensile test results for material characterization [138].

- **Topology optimization:**

The optimization shown in Figure 113 led to a 80% mass reduction.

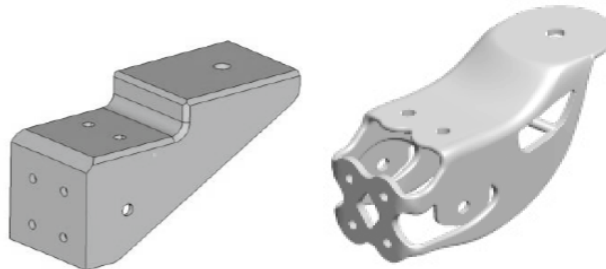


Figure 113: Original (left) and optimized (right) designs [138].

- **EBM manufactured bracket** (Fig. 114 (a) ) :
  - As built (no heat treatment or surface finishing).
  - High number of pores and low-density areas.
  - Low surface finish (Fig. 114 (c) ).
  - External defects localized on certain edges. (Fig. 114 (e) ).
- **SLM manufactured bracket** (Fig. 114 (b) ) :
  - Heat treatment and tumble finishing applied.
  - Low number of internal defects (justified by the heat treatment applied).
  - Higher surface finish (justified by the tumble finishing applied) (Fig. 114 (d) ).
  - Warping (justified by the high thermal gradients of SLM) (Fig. 114 (f) ).
- The interfaces of the bracket have been machined in all the cases.

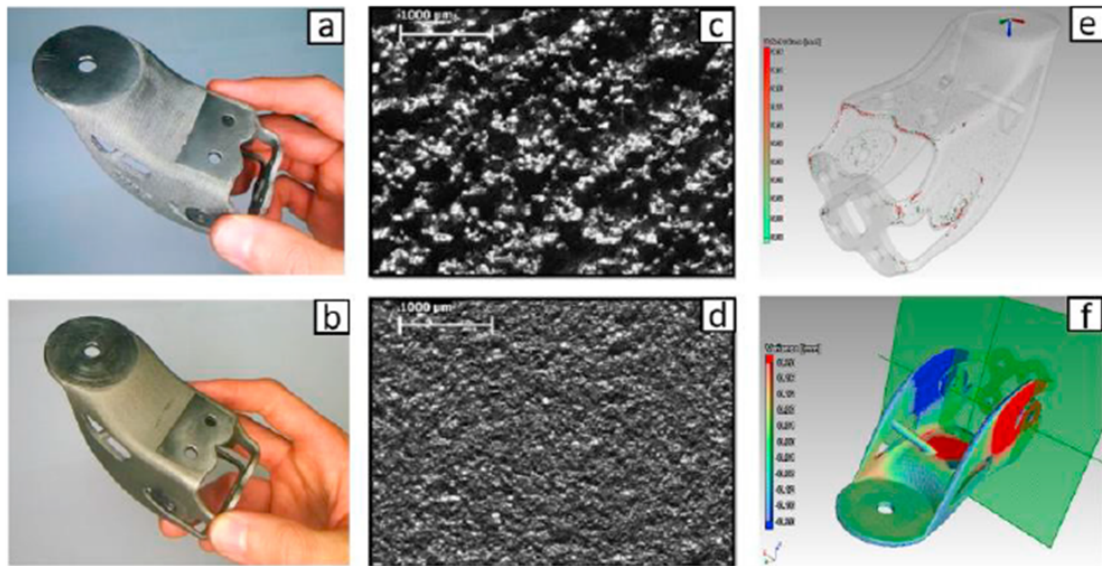


Figure 114: EBM (a) and SLM (b) AMed aerospace bracket. Surface roughness of the EBM (c) and SLM (d) parts. Defects detection from tomographic analysis of EBM component (e), dimensional control on the SLM bracket (f) [138].

Unfortunately, estimates about the mechanical properties of the bracket cannot be done accordingly to the guidelines seen until now due to its complex shape.

## **Analysis**

Considering all the elements mentioned above it can be supposed that the re-design of the bracket has been done complying with few basic requirements:

- Lightness
- Reliability
- Complexity reduction

The bracket is produced for aerospace applications (Lightness). It is a component that belongs to a much bigger aerospace system where complex elements, such as the engine, are present, so adding levels of complexity in re-designing the bracket would be counter-productive (Complexity reduction). And, being a structural element, it also must not fail (Reliability).

### **Step 1**

Ti6Al4V is a well know alloy especially in the aerospace field, many researches and a considerable amount of data is available in the literature so a low amount of time and resources is necessary to characterize it, and the probability of finding unexpected anomalies in the material behavior is also reduced. All this means lower risks, complexity and costs.

In addition, it is well known that Ti6Al4V alloy has a high strength-to-weight ratio that results in a light but reliable component.

A first estimate of the mechanical properties can be done looking at the chart in Figure 31:

- DMLS (as-built state): YS approx. 1100-1200 MPa, UTS slightly above 1200 MPa; elongation around 7.5 %.
- EBM (as-built state): YS approx. 900-1000 MPa, UTS slightly above 1000 MPa; elongation around 10 %.

These values are similar to those referred to the specimens mentioned before (Fig. 112).

### **Step 2**

The topology optimization applied is of the type previously defined as “macro-topology” optimizations. The TO implemented guarantees a notable mass reduction and it is obviously the one to be used for bulk parts. A topology optimization at a ”microscopic level” is, instead, appropriate for lattice structure. In this case a re-design of the bracket to obtain a lattice structure would be extremely demanding. The computational power

required to perform a numerical simulation, applying the proper mesh to each single unit cell of the whole part, would be so high to make a FEA impossible. In addition, the estimation of the component behavior is much easier for bulk pieces.

### **Step 3**

The characteristics of the metal powder adopted can hardly be guessed for the SLMed part because the heat treatment and the surface finish modified both the internal and the external characteristics. The EBMed bracket has a high level of porosity and low-density areas which can be traced back to the use of a coarse powder with a wide PSD. Usually, EBM manufactured parts have a reasonably low porosity level and do not necessarily need further heat treatments. However, a coarser powder, having a higher surface-to-volume ratio, holds a lower absorption capacity that could result in insufficient melting. It generates defects that are usually higher in number but smaller in size compared to a fine powder. Moreover a powder characterized by a wide PSD has the tendency to form separated agglomerates of fine and coarse powder and, at their interfaces, is present a considerable amount of voids. Referring to the powder properties, the latter are the two main reason that can justify the high level of defects detected in the EBM bracket. Typical ranges of the PSD for the Ti6Al4V alloy are (Table tab:Powder sizes for different materials):

- SLM: 20-50  $\mu\text{m}$ ;
- EBM: 40-100  $\mu\text{m}$ ;

Looking at the surface roughness in Figure 114 (c) and (d) one could assume that EBM naturally gives a lower surface quality compared to SLM that, in contrast, is a slower process. This is generally true but not in this case where a surface finishing has been applied to the SLMed part making such a comparison meaningless.

The specimens used to characterize the material have been machined. Machined samples usually exhibit slightly higher strength than as-built ones. The difference for Al-alloys has been identified in the range 20-50 MPa but a similar information is not available for Ti6Al4V, however it can be considered negligible with respect to the ranges proposed here.

Referring to SLM, the energy density value is supposed to be between the value resulting in the lowest porosity ( $110 \text{ J/mm}^3$ ) and the one giving the maximum mechanical properties ( $150 \text{ J/mm}^3$ ). The other parameters have been identified from Table 8 and Table 9.

So, the laser scanning parameters for the SLMed bracket are supposed to be:

- Laser power: 160-200 W;
- Laser scanning speed: 600-1250 mm/s;

- Hatching distance: 30-120  $\mu\text{m}$ ;
- Volumetric energy density: 110-140  $\text{J}/\text{mm}^3$ ;

The energy density value has been estimated comparing the above mentioned values (110-150  $\text{J}/\text{mm}^3$ ) with those of the process windows in Table 9 (93-137  $\text{J}/\text{mm}^3$ ).

Due to the few data available similar ranges of the scanning parameters cannot be proposed for the EBM case. However, looking at Figure 114 (e) the location of the defects can be traced back to the building orientation. According to this reasoning the colored edges result to be downward surfaces where partially melted particles are more likely to adhere. The orientation of the bracket on the building platform can also be identified simply by looking at its shape, nonetheless this is not always so immediate and a similar consideration can be useful in case of other geometries.

Considering that the colored areas are not so large (low partially melted particle adhesion) and that the number of internal defects is high, probably the energy provided by the electron beam was too low. This choice could have been intentional if the higher amount of internal pores and voids was preferred to the higher partially melted particle adhesion deriving from higher energy inputs.

The warping occurring in the SLM manufactured bracket (Fig. 114 (f) ) is justified by the authors recurring to the high thermal gradients involved in the SLM process. This is reflected in the present work, in particular the deformed portions (the colored areas) of the surfaces are those constrained on three sides. This is also in agreement with the observations in the previous chapters saying that the "more closed the geometry of a part is and the more the part will be prone to deform" because of the sub-surface residual stresses caused by the large temperature gradients.



# Conclusion

In the past AM was considered as a useful technology for rapid prototyping and to produce small batches, mainly due to the economic advantages with respect to traditional manufacturing techniques. Progressively increases in research changed this common opinion and AM is now approached as disruptive technology that can guarantee a design freedom not reachable with traditional manufacturing techniques. Therefore, it is expected to grow even faster in the future.

Many resources are invested trying to find the best compromise among all the available possibilities and many efforts are still needed. A wider adoption of AM technologies is mainly hindered by the limited data available and by the many areas that still have to be well understood.

In the present work a further step is made. In the introduction, where a collection of many parameters, methods and techniques are collected and classified, the high degree of complexity can be perceived. The core of this work can be defined as a three steps guideline that analyzes the whole production process, starting from the choice and the analysis of the raw metal powder and concluding with the selection of the proper final heat treatment. These three steps aim at proposing various options to answer to different questions, thanks to which the engineer, analyzing such options, is able to find a suitable trade off that allows him to create well tailored solution:

- **Step 1:** Which type of powder is more suitable and how to characterize it?
  - Traditional powders: Al, Ti or Ni alloys.
  - Innovative solutions: powder additives, compositionally graded materials or hybrid materials.
  - The main properties are listed together with the necessary standards.
- **Step 2:** How to approach topology optimization?
  - A basic idea of how it works is provided.
  - Macroscopic topology optimization approaches (set of examples).
  - Microscopic topology optimization approaches (set of examples).

- **Step 3:** How to tune the design parameters (or factors) to achieve the objective?
  - Guidelines, process windows and properties ranges are provided after the analysis of the following relations.
    - \* Material factors - properties
    - \* Part design factors - properties
    - \* Process machine and environmental factors - properties
    - \* Scanning factors - properties
    - \* Melt pool - properties
    - \* Heat treatments - properties

The above mentioned properties do not only refer to the mechanical behavior of the component but also to geometrical features, defects and other aspects, such as the failure mode or the support structures that are less explored in the literature.

The most extended part is that related to the third step. After the collection of data from many experiments it has been possible to provide ranges of the most common parameters reported in Figure 115 and Figure 116 (graphical anomalies are due to few data available), even if the reader should refer to the relative step for a much more detailed analysis that also include general trends and considerations, advantages and disadvantages, many tables and charts, that are all the result of the correlation between many and various experimental results.

Considering the high number of factors having an influence on the final component it can be questioned the adoption of three steps only. This is especially valid for the third step where a long analysis is reported. It has been decided to include a relevant number of variables inside one step only because they are all interconnected so they should not be considered as independent elements. As a matter of fact, this is the important conceptual result of the present work, which is able to demonstrate that a holistic approach is essential to obtain conscious and successful outcomes.

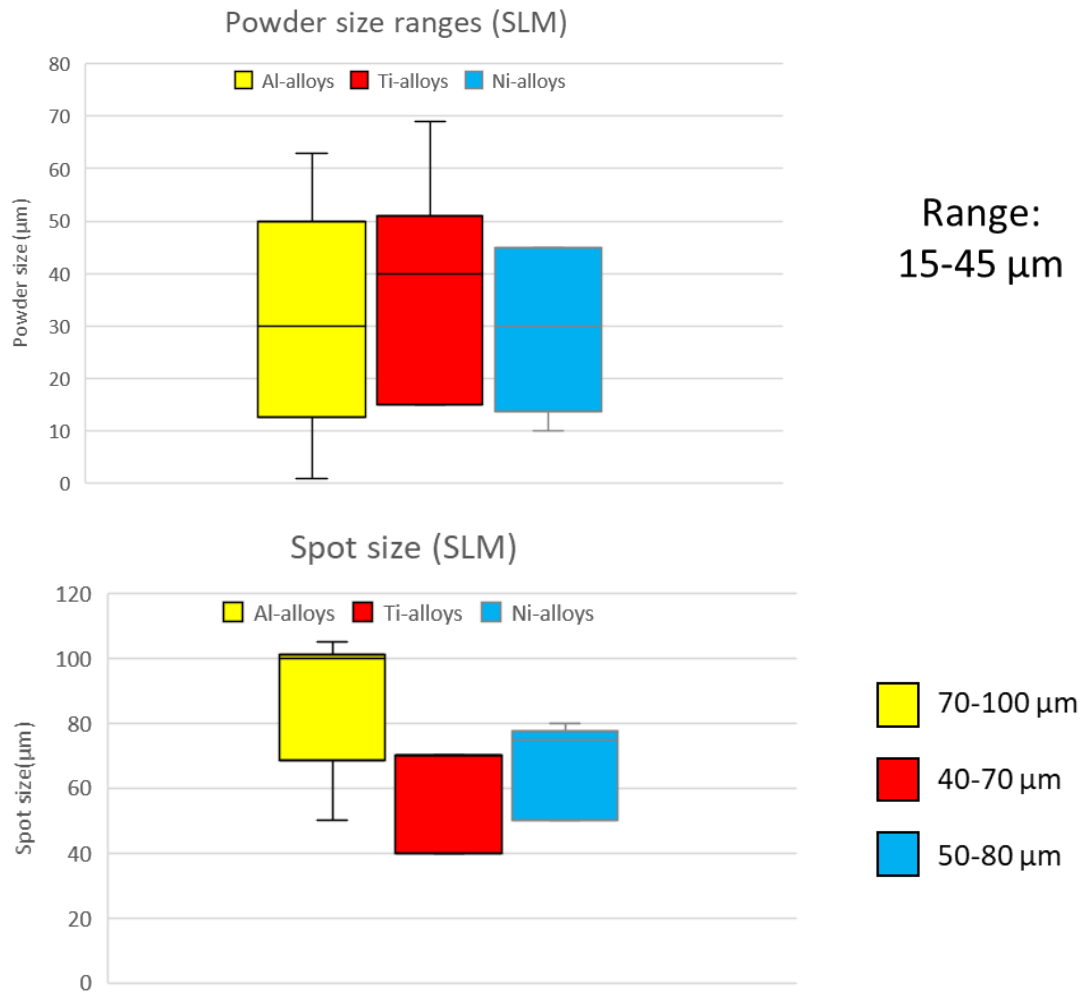


Figure 115: Powder size and spot size ranges for SLMed Al, Ti and Ni alloys [73, 76, 74, 80, 81, 83, 89, 91, 92, 30, 96, 97, 13, 98, 99, 101, 102, 104, 105, 75, 87, 14].

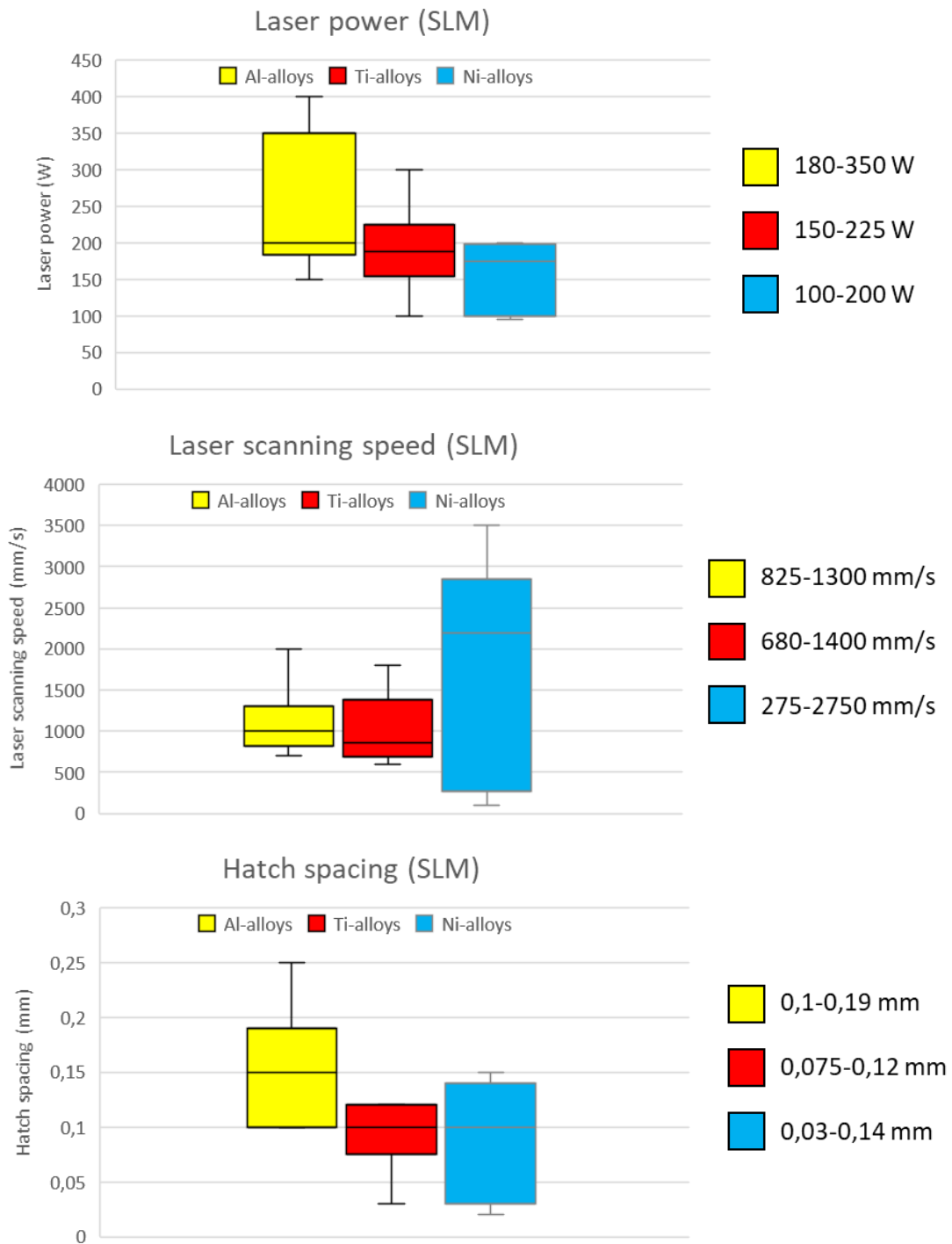


Figure 116: Laser power, scanning speed and hatch spacing ranges for SLMed Al, Ti and Ni alloys [73, 76, 74, 80, 81, 83, 89, 91, 92, 30, 96, 97, 13, 98, 99, 101, 102, 104, 105, 75, 87, 14].





# Bibliography

- [1] Diegel O., Nordin A., and Motte D., *A Practical Guide to Design for Additive Manufacturing*, Singapore, Springer, 2019.
- [2] Gibson I., Rosen D., Stucker, Brent. *Additive Manufacturing Technologies*, 2 ed., New York, Springer, 2015.
- [3] D’Antonio, Gianluca, Frédéric Segonds, Floriane Laverne, Joel SAUZA BEDOLLA, and Paolo Chiabert. “A Framework for Manufacturing Execution System Deployment in an Advanced Additive Manufacturing Process.” In: *INTERNATIONAL JOURNAL OF PRODUCT LIFECYCLE MANAGEMENT*, v. 10, No. 1, 2017.
- [4] Anton Wiberg, Johan Persson and Johan Ölvander. “Design for additive manufacturing – a review of available design methods and software.” In: *Rapid Prototyping Journal*, v.25 n.6, p.1080-1094, 2019.
- [5] Elshaer Amr, Nair Sawmya, Hassanin Hany. “Near Net Shape Manufacturing of Dental Implants Using Additive Processes”, Cham, Switzerland, Springer International Publishing, 2019.
- [6] <https://www.smartechanalysis.com/news/2019-additive-manufacturing-market-growth/>
- [7] Development of AM Technologies for Metals in the Sector of Medical Implants - Scientific Figure on ResearchGate. Available from: [https://www.researchgate.net/figure/The-distribution-of-additive-manufacturing-AM-in-different-sectors-1\\_fig1\\_341619882](https://www.researchgate.net/figure/The-distribution-of-additive-manufacturing-AM-in-different-sectors-1_fig1_341619882).
- [8] Verhoef Leendert A, Bart W Budde, Cindhuja Chockalingam, Brais García Nodar, and Ad J.M Van Wijk. “The Effect of Additive Manufacturing on Global Energy Demand: An Assessment Using a Bottom-up Approach.” In: *Elsevier Ltd*, Energy Policy, v.112, p:349-60,2018.

- [9] F. Facchini, A. De Chirico, G. Mummolo. “Comparative Cost Evaluation of Material Removal Process and Additive Manufacturing in Aerospace Industry.” In: *Industrial Engineering and Operations Management*, p.47-59, Cham, Springer International Publishing, 2019.
- [10] Yan, W., Lin, S., Kafka, O.L. et al. “Modeling process-structure-property relationships for additive manufacturing.” *Front. Mech. Eng.* v.13, p.482–492, 2018. DOI: <https://doi.org/10.1007/s11465-018-0505-y>.
- [11] Bian Linkan, Shamsaei Nima , Usher John M. “Laser-Based Additive Manufacturing of Metal Parts: Modeling, Optimization, and Control of Mechanical Properties”, CRC Press, 1 ed., Boca Raton, CRC Press, 2017. DOI: <https://doi.org/10.1201/9781315151441>.
- [12] Raza, Tahira. “Process Understanding and Weldability of Laser-Powder Bed Fusion Manufactured Alloy 718”. PhD Thesis. 2020.
- [13] Maamoun, Ahmed H, Yi F Xue, Mohamed A Elbestawi, and Stephen C Veldhuis. “The Effect of Selective Laser Melting Process Parameters on the Microstructure and Mechanical Properties of Al6061 and AlSi10Mg Alloys.” In: *Materials*, v.12, p.12, 2018. DOI: <https://doi.org/10.3390/ma12010012>
- [14] Adegoke Olutayo. “Processability of Laser Powder Bed Fusion of Alloy 247LC.” Licentiate Thesis, 2020.
- [15] Karimi Neghlani Paria. “Electron Beam-powder Bed Fusion of Alloy 718: Effect of process parameters in microstructure evolution”. PhD Thesis. 2020.
- [16] Froes F., Boyer R. *Additive Manufacturing for the Aerospace Industry*, San Diego, Elsevier, 2019.
- [17] Masoomi, Mohammad, Scott M Thompson, and Nima Shamsaei. “Laser Powder Bed Fusion of Ti-6Al-4V Parts: Thermal Modeling and Mechanical Implications.” In: *International Journal of Machine Tools & Manufacture* , v.118-119, p:73-90, 2017. DOI: <https://doi.org/10.1016/j.ijmachtools.2017.04.007>.
- [18] Chua, Chee Kai, Chee How Wong, and Wai Yee Yeong. *Standards, Quality Control, and Measurement Sciences in 3D Printing and Additive Manufacturing*. San Diego, Elsevier Science & Technology, 2017.

- [19] Kasperovich G., Haubrich J., Gussone, J., Requena G. “Correlation between porosity and processing parameters in TiAl6V4 produced by selective laser melting” In: *Materials & Design*, v.105, p:160-170, 2016. DOI: <https://doi.org/10.1016/j.matdes.2016.05.070>.
- [20] Mohammadpour P., Plotkowski A., Phillion A. “Revisiting solidification microstructure selection maps in the frame of additive manufacturing.” In: *Additive Manufacturing*, v.31 (C), p.100936, 2020. DOI: <https://doi.org/10.1016/j.addma.2019.100936>.
- [21] Badiru, Adedeji B, Vhance V Valencia, and David Liu. *Additive Manufacturing Handbook: Product Development for the Defense Industry* 1st ed, Oakville, CRC Press, 2017.
- [22] Ossola, Enrico. “Design of Additive Manufactured Structural Shells for Harsh Environment Probes”. PhD Thesis. 2021.
- [23] Pakkanen, Jukka Antero. “Designing for Additive Manufacturing - Product and Process Driven Design for Metals and Polymers”. PhD Thesis, 2018.
- [24] <https://www.pim-international.com/analysis-of-additive-manufacturing-materials-from-wohlers-and-senvol-database/>
- [25] A.Ünal. “Production of Rapidly Solidified Aluminium Alloy Powders by Gas Atomisation and Their Applications” In: *Powder Metallurgy* , 33:1, p:52-64, 1990. DOI: <https://doi.org/10.1179/pom.1990.33.1.53>.
- [26] Canakci A., Varol T. “A Novel Method for the Production of Metal Powders without Conventional Atomization Process.” In: *Journal of Cleaner Production* , v.99, p:312-319, 2015. DOI: <https://doi.org/10.1016/j.jclepro.2015.02.090>.
- [27] Trevisan, Francesco. “Study and characterisation of different metal alloys processed through Laser Powder Bed Fusion”. Thesis, 2018.
- [28] ASM International. *Titanium: A Technical Guide*. ASM, Materials Park, OH, 1988.
- [29] Haferkamp Lukas, Spierings Adriaan, Rusch Marco, Jermann Dominik , Spurek Marvin, Wegener Konrad. “Effect of Particle size of monomodal 316L powder on powder layer density in powder bed fusion.” In: *Progress in Additive Manufacturing* , v.6, p:367-374, 2021. DOI: <https://doi.org/10.1007/s40964-020-00152-4>.

- [30] Haferkamp L., Haudenschild L., Spierings A., Wegener K., Riener K., Ziegelmeier S., Leichtfried G.J. “The Influence of Particle Shape, Powder Flowability, and Powder Layer Density on Part Density in Laser Powder Bed Fusion.” In: *Metals*, v.11, 418, 2021. DOI: <https://doi.org/10.3390/met11030418>.
- [31] Young Benjamin, Joseph Heelan, Sean Langan, Matthew Siopis, Caitlin Walde, and Aaron Birt. “Novel Characterization Techniques for Additive Manufacturing Powder Feedstock.” In: *Metals*, v.11, 720, 2021. DOI: <https://doi.org/10.3390/met11050720>.
- [32] Dutta B., and Francis H Froes. “24 - The Additive Manufacturing (AM) of Titanium Alloys.” In: *Titanium Powder Metallurgy*, Elsevier, p:447-468, 2015. DOI: <https://doi.org/10.1016/B978-0-12-800054-0.00024-1>.
- [33] Ozgur Poyraz. “Additive Manufacturing with Nickel Feedstock”, 13-01-2021. link: <https://www.epma.com/dm-industry-news/1044-cu030-lecture-2/file>
- [34] Günther Johannes, Brenne Florian, Droste M., Wendler Marco, Volkova O., Biermann H., Niendorf T. “Design of novel materials for additive manufacturing - Isotropic microstructure and high defect tolerance.” In: *Scientific Reports*, v.8, 2018. DOI: <https://doi.org/10.1038/s41598-018-19376-0>.
- [35] Omoniyi O. A, R. Mansour, M. J Cardona, M. L Briuglia, R. L O’Leary, and J. F. C Windmill. “Fabrication and Characterization of a Novel Photoactive-based (0–3) Piezocomposite Material with Potential as a Functional Material for Additive Manufacturing of Piezoelectric Sensors.” In: *Journal of Materials Science: Materials in Electronics*, v.32, p:11883–11892, 2021. DOI: <https://doi.org/10.1007/s10854-021-05818-5>.
- [36] Y. Wang, S. Y. Liu, and J. S. Meng. “Advanced materials for additive manufacturing.” In: *IOP Conf. Ser.: Mater. Sci. Eng.*, v.479, p:012088, 2019. DOI: <https://doi.org/10.1088/1757-899x/479/1/012088>.
- [37] Neng Li, Shuai Huang, Guodong Zhang, Renyao Qin, Wei Liu, Huaping Xiong, Gongqi Shi, Jon Blackburn. “Progress in additive manufacturing on new materials: A review.” In: *Journal of Materials Science & Technology*, v.35(2), p:242-269, 2019. DOI: <https://doi.org/10.1016/j.jmst.2018.09.002>.
- [38] Yunlong Li, Xin Lin, Yunlong Hu, Jun Yu, Junguo Zhao, Hongbiao Dong, Weidong Huang. “Synergistic effect of Mo and Zr additions on microstructure and mechanical properties of Nb-Ti-Si-based alloys additively manufactured by laser

- directed energy deposition.” In: *Journal of Materials Science & Technology*, v.103, p:84-97, 2022. DOI: <https://doi.org/10.1016/j.jmst.2021.06.027>.
- [39] Oropeza, Daniel, Douglas C Hofmann, Kyle Williams, Samad Firdosy, Punnathat Bordeenithikasem, Maximillian Sokoluk, Maximilian Liese, Jingke Liu, and Xiaochun Li. “Welding and Additive Manufacturing with Nanoparticle-enhanced Aluminum 7075 Wire.” In: *Journal of Alloys and Compounds*, v.834, p:154987, 2020. DOI: <https://doi.org/10.1016/j.jallcom.2020.154987>.
- [40] Canziani, Herbert, Salvatore Chiera, Thomas Schuffenhauer, Sebastian-Paul Kopp, Florian Metzger, Andreas Bück, Michael Schmidt, and Nicolas Vogel. “Bottom-Up Design of Composite Supraparticles for Powder-Based Additive Manufacturing.” In: *Small*, v.16, 2020. DOI: <https://doi.org/10.1002/smll.202002076>.
- [41] Reichardt Ashley, Shapiro Andrew A., Otis Richard, Dillon R., Peter Borgonia, John Paul, McEnerney Bryan W., Hosemann Peter, Beese Allison M. “Advances in additive manufacturing of metal-based functionally graded materials.” In: *International Materials Reviews*, v.66, 2020. DOI: <https://doi.org/10.1080/09506608.2019.1709354>.
- [42] Bobbio Lourdes, Bocklund Brandon, Reichardt Ashley, Otis Richard, Borgonia John Paul, Dillon Robert, Shapiro Andrew, McEnerney, Bryan, Hosemann Peter, Liu Zi-Kui, Beese, Allison “Analysis of formation and growth of the  $\sigma$  phase in additively manufactured functionally graded materials.” In: *Journal of Alloys and Compounds*, v.814, 2019. DOI: <https://doi.org/10.1016/j.jallcom.2019.151729>.
- [43] Firdosy Samad, Ury Nicholas, Kustas Andrew, Carroll Jay, Pathare Priya, Casias Zachary, Tung Daniel, Susan D., Bobbitt N., Chandross Michael, Borgonia John Paul, Ravi Vilupanur, Dillon Robert. “Compositionally graded joints between magnetically dissimilar alloys achieved through directed energy deposition.” In: *Scripta Materialia*, v.202, p:114005, 2021. DOI: <https://doi.org/10.1016/j.scriptamat.2021.114005>.
- [44] A. Ben-Artzy, A. Reichardt, J.-P. Borgonia, et al. “Compositionally graded SS316 to C300 Maraging steel using additive manufacturing.” In: *Materials & Design*, v.201, p:109500, 2021. DOI: <https://doi.org/10.1016/j.matdes.2021.109500>.
- [45] Cakmak, Ercan and Sridharan, Niyanth and Venkata krishnan, Singanallur and Bilheux, Hassina and Santodonato, Louis and Shyam, Amit and Babu, Sudarsanam. “Feasibility Study of Making Metallic Hybrid Materials Using Additive Manufacturing.” In: *Metallurgical and Materials Transactions A*, v.49, 2018. DOI: <https://doi.org/10.1007/s11661-018-4741-x>.

- [46] Chueh Yuan-Hui, Zhang Xiaoji, Ke Jack, Li Qian, Wei Chao, Lin Li. “Additive manufacturing of hybrid metal/polymer objects via multiple-material laser powder bed fusion.” In: *Additive Manufacturing*, v.36, p:101465, 2020. DOI: <https://doi.org/10.1016/j.addma.2020.101465>.
- [47] De Pasquale Giorgio, Sibona Stefano. “Hybrid materials based on polymer-filled AM steel lattices with energy absorption capabilities.” In: *Mechanics of Advanced Materials and Structures*, p:1-13, 2021. DOI: <https://doi.org/10.1080/15376494.2020.1871536>.
- [48] Chueh Yuan-Hui. “Laser-based additive manufacturing of hybrid metal/polymer components”, PhD Thesis, University of Manchester, 2021.
- [49] Di Caprio Francesco, Acanfora Valerio, Franchitti Stefania, Sellitto Andrea, Riccio Aniello. “Hybrid Metal/Composite Lattice Structures: Design for Additive Manufacturing.” In: *Aerospace*, v.6, p:71, 2019. DOI: <https://doi.org/10.3390/aerospace6060071>.
- [50] Varela, Jaime and Arrieta, Edel and Paliwal, Muktesh and Marucci, Mike and Sandoval, Jose H. and Gonzalez, Jose A. and McWilliams, Brandon and Murr, Lawrence E. and Wicker, Ryan B. and Medina, Francisco. “Investigation of Microstructure and Mechanical Properties for Ti-6Al-4V Alloy Parts Produced Using Non-Spherical Precursor Powder by Laser Powder Bed Fusion.” In: *Materials*, v.14, 2021. DOI: <https://www.mdpi.com/1996-1944/14/11/3028>.
- [51] Gao J., Xiao M., Zhang Y. et al. “A Comprehensive Review of Isogeometric Topology Optimization: Methods, Applications and Prospects.” In: *Chin. J. Mech. Eng.*, v.33, 87, 2020. DOI: <https://doi.org/10.1186/s10033-020-00503-w>.
- [52] Tyflopoulos Evangelos, Flem David, Steinert Martin, Olsen Anna. “State of the art of generative design and topology optimization and potential research needs. ”, 2018.
- [53] Bendsoe, Martin P. and Ole Sigmund. *Topology Optimization Theory, Methods, and Applications*, 2 ed., corrected printing, Berlin, Springer, 2003.
- [54] Ribeiro T.P., Bernardo L.F.A., Andrade J.M.A., “Topology Optimisation in Structural Steel Design for Additive Manufacturing.” In: *Applied Sciences*, v.11, 2112, 2021. DOI: <https://www.mdpi.com/2076-3417/11/5/2112>.
- [55] Tianxia Zhan. “Progress on different topology optimization approaches

- and optimization for additive manufacturing: a review.” In: *Journal of Physics: Conference Series*, v.1939, p:012101 , 2021. DOI: <https://doi.org/10.1088/1742-6596/1939/1/012101>.
- [56] Sima M. Jwad, Shanga S. Abdulkareem, Tavan A. Awaxy, Sara M. Omer. “A Comprehensive Literature Survey of the Application of Modeling and Optimization Techniques in Additive Manufacturing Processes.” Thesis. 2018.
- [57] Zhu Jihong, Zhou Han, Wang Chuang, lu Zhou, Yuan Shangqin, Zhang Weihong. “A review of topology optimization for additive manufacturing: Status and challenges.” In: *Chinese Journal of Aeronautics.*, v.34, 2020. DOI: <https://doi.org/10.1016/j.cja.2020.09.020>.
- [58] Reddy S., Ferguson I., Frecker M., Simpson T., Dickman C. “Topology optimization software for additive manufacturing: A review of current capabilities and a real-world example.” In: *Proceedings of the ASME 2016 International Design Engineering Technical Conferences and Computers and Information in Engineering Conference. Volume 2A: 42nd Design Automation Conference.* Charlotte, North Carolina, USA. August 21–24, 2016. V02AT03A029. ASME. DOI: <https://doi.org/10.1115/DETC2016-59718>.
- [59] Bartsch Katharina, Lange Fritz, Gralow Melanie, Emmelmann Claus. “Novel approach to optimized support structures in laser beam melting by combining process simulation with topology optimization.” In: *Journal of Laser Applications*, 31, 022302, 2019. DOI: <https://doi.org/10.2351/1.5096096>.
- [60] Saadlaoui Yassine, Milan Jean-Louis, Rossi Jean-Marie, Chabrand Patrick. “Topology optimization and additive manufacturing: Comparison of conception methods using industrial codes.” In: *Journal of Manufacturing Systems*, v.43, p:178-186, 2017. DOI: <http://dx.doi.org/10.1016/j.jmsy.2017.03.006>.
- [61] Shabani Betim and Dukovski Vladimir. “Integration of Reverse Engineering and Topology Optimization with Additive Manufacturing.” In: *Computer-Aided Design and Applications*, v.19, p:164-175, 2021. DOI: <https://doi.org/10.14733/cadaps.2022.164-175>.
- [62] Seabra Miguel, Azevedo José, Araújo Aurélio, Reis Luís, Pinto Elodie, Alves Nuno, Santos Rui, Pedro Mortágua João. “Selective laser melting (SLM) and topology optimization for lighter aerospace components.” In: *Procedia Structural Integrity*, v.1, p:289-296, 2016. DOI: <https://doi.org/10.1016/j.prostr.2016.02.039>.
- [63] Yang, Kai Ke; Zhu, Ji Hong; Wang, Chuang; Jia, Dong Sheng; Song, Long Long;

- Zhang, Wei Hong. "Experimental validation of 3D printed material behaviors and their influence on the structural topology design." In: *Computational Mechanics*, v.61, 2018. DOI: <https://doi.org/10.1007/s00466-018-1537-1>.
- [64] Moussa Ahmed, David Melancon, Asma El Elmi, and Damiano Pasini. "Topology Optimization of Imperfect Lattice Materials Built with Process-induced Defects via Powder Bed Fusion." In: *Additive Manufacturing*, v.37, 101608, 2021. DOI: <https://doi.org/10.1016/j.addma.2020.101608>.
- [65] Bertolino Giulia, Marco Montemurro, and Giorgio De Pasquale. "Multi-scale Shape Optimisation of Lattice Structures:an Evolutionary-based Approach." In: *International Journal on Interactive Design and Manufacturing* , v.13, p:1565–1578, 2019. DOI: <https://doi.org/10.1007/s12008-019-00580-9>.
- [66] Zefeng Xiao, Yongqiang Yang, Ran Xiao, Yuchao Bai, Changhui Song, Di Wang. "Evaluation of topology-optimized lattice structures manufactured via selective laser melting." In: *Materials & Design*, v.143, p:27-37, 2018. DOI: <https://doi.org/10.1016/j.matdes.2018.01.023>.
- [67] van Woensel Remco, van Oirschot Teun, Burgmans Mats, Mohammadi Masi, Hermans Kristel. "Printing Architecture: An Overview of Existing and Promising Additive Manufacturing Methods and Their Application in the Building Industry." In: *The International Journal of the Constructed Environment*, v.9, p:57-81, 2018. DOI: <https://doi.org/10.18848/2154-8587/CGP/v09i01/57-81>.
- [68] Evolution of Polymer 3D Printing Hardware Revenues from Use in Professional Environments 2017 vs. 2027, by Polymer Print Technology Group. Source: SmarTech Publishing - Additive Manufacturing with Polymer and Plastics 2018. Link: <https://ml.globenewswire.com/Resource/Download/71214f13-6adf-4825-b998-fe344b42ac7f>.
- [69] Zaman Uzair Khaleeq Uz, Rivette Mickael, Siadat A., Mousavi Seyed. "Integrated product-process design: Material and manufacturing process selection for additive manufacturing using multi-criteria decision making." In: *Robotics and Computer-Integrated Manufacturing*, v.51, p:168-180, 2018. DOI: <https://doi.org/10.1016/j.rcim.2017.12.005>.
- [70] François Cardarelli, *Materials Handbook*, 2 ed., London, Springer, 2008.
- [71] Pantarelli, Anna. "Trattamenti termici della lega AlSi10Mg realizzata mediante Additive Manufacturing: microstruttura e proprietà meccaniche". Thesis, 2019.

- [72] Link: <https://www.globalsino.com/EM/page2222.html>.
- [73] Feng Z., Tan H., Fang Y., Lin X., Huang W. "Selective laser melting of TiB<sub>2</sub>/AlSi10Mg composite: Processability, microstructure and fracture behavior." In: *Journal of Materials Processing Technology*, v.299, p. 117386, 2022. DOI: <https://doi.org/10.1016/j.jmatprotec.2021.117386>.
- [74] F. Cabanettes, A. Joubert, G. Chardon, V. Dumas, J. Rech, C. Grosjean, Z. Dimkovski. "Topography of as built surfaces generated in metal additive manufacturing: a multi scale analysis from form to roughness." In: *Precision Engineering*, v.52, p. 249-265, 2018. DOI: <https://doi.org/10.1016/j.precisioneng.2018.01.002>.
- [75] Zahra Bagheri et al. "Compensation strategy to reduce geometry and mechanics mismatches in porous biomaterials built with Selective Laser Melting." In: *Journal of the Mechanical Behavior of Biomedical Materials*, v.70, p. 17-27, 2016. DOI: <https://doi.org/10.1016/j.jmbbm.2016.04.041>.
- [76] Li Dongming, Ruixian Qin, Bingzhi Chen, and Junxian Zhou. "Analysis of Mechanical Properties of Lattice Structures with Stochastic Geometric Defects in Additive Manufacturing." In: *Materials Science and Engineering: A*, v.822, p. 141666, 2021. DOI: <https://doi.org/10.1016/j.msea.2021.141666>.
- [77] Koříněk M., Halama R., Fojtík F., Pagáč M., Krček J., Krzikalla D., Kocich R., Kunčická L. "Monotonic Tension-Torsion Experiments and FE Modeling on Notched Specimens Produced by SLM Technology from SS316L." In: *Materials*, v. 14, p. 33, 2021. DOI: <https://dx.doi.org/10.3390/ma14010033>.
- [78] Wang Z., Lin X., Wang L., Cao Y., Zhou Y., Huang, W. "Microstructure evolution and mechanical properties of the wire arc additive manufacturing Al-Cu alloy." In: *Additive Manufacturing*, v. 47, p. 102298, 2021. DOI: <https://dx.doi.org/10.1016/j.addma.2021.102298>.
- [79] Papazoglou Emmanouil-Lazaros, Karkalos Nikolaos, Markopoulos Angelos. "A comprehensive study on thermal modeling of SLM process under conduction mode using FEM." In: *The International Journal of Advanced Manufacturing Technology*, v. 111, p. 1-17, 2020. DOI: <https://dx.doi.org/10.1007/s00170-020-06294-7>.
- [80] De Pasquale G., Luceri F., Riccio M. "Experimental Characterization of SLM and EBM Cubic Lattice Structures for Lightweight Applications." In: *Experimental Mechanics*, v. 59, p. 469-482, 2019. DOI: <https://dx.doi.org/10.1007/s11340-019-00481-8>.

- [81] Ferro Carlo, Varetti Sara, Maggiore Paolo, Lombardi Mariangela, Biamino Sara, Manfredi Diego, Calignano Flaviana. "Design and characterization of trabecular structures for an anti-icing sandwich panel produced by additive manufacturing." In: *Journal of Sandwich Structures & Materials* , v. 22, p. 109963621878051, 2018. DOI: <http://dx.doi.org/10.1177/1099636218780513>.
- [82] De Pasquale, Giorgio, and Alberto Tagliaferri. "Modeling and Characterization of Mechanical and Energetic Elastoplastic Behavior of Lattice Structures for Aircrafts Anti-icing Systems." In: *Proceedings of the Institution of Mechanical Engineers* , v. 235, p. 1829-1839, 2021. DOI: <http://dx.doi.org/10.1177/0954406219853857>.
- [83] Xiaoli Zhao, Shujun Li, Man Zhang, Yandong Liu, Timothy B. Sercombe, Shaogang Wang, Yulin Hao, Rui Yang, Lawrence E. Murr. "Comparison of the microstructures and mechanical properties of Ti-6Al-4V fabricated by selective laser melting and electron beam melting." In: *Materials & Design* , v. 95, p. 21-31, 2016. DOI: <https://doi.org/10.1016/j.matdes.2015.12.135>.
- [84] Shamsaei Nima, Yadollahi Aref, Bian Linkan, Thompson Scott. "An Overview of Direct Laser Deposition for Additive Manufacturing; Part II: Mechanical Behavior, Process Parameter Optimization and Control." In: *Additive Manufacturing* , v. 8, p. 12-35, 2015. DOI: <https://doi.org/10.1016/j.addma.2015.07.002>.
- [85] Del Guercio Giuseppe, Galati Manuela, Saboori Abdollah. "Innovative Approach to Evaluate the Mechanical Performance of Ti-6Al-4V Lattice Structures Produced by Electron Beam Melting Process." In: *Metals and Materials International* , v. 27, p. 55-67, 2021. DOI: <https://doi.org/10.1007/s12540-020-00745-2>.
- [86] Smith Jacob, Xiong Wei, Cao Jian, Liu Wing. "Thermodynamically consistent microstructure prediction of additively manufactured materials." In: *Computational Mechanics* , v. 57, p. 1-12, 2016. DOI: <https://doi.org/10.1007/s00466-015-1243-1>.
- [87] De Pasquale G., Luceri F., Riccio M. "Experimental Evaluation of Selective Laser Melting Process for Optimized Lattice Structures." In: *Proceedings of the Institution of Mechanical Engineers, Part E: Journal of Process Mechanical Engineering* , v. 233, p. 763-775 , 2019. DOI: <https://doi.org/10.1177/0954408918803194>.
- [88] Smith M., Z. Guan, W.J Cantwell. "Finite Element Modelling of the Compressive Response of Lattice Structures Manufactured Using the Selective Laser Melting Technique." In: *International Journal of Mechanical Sciences* , v. 67, p. 28-41 , 2013.

- DOI: <https://doi.org/10.1016/j.ijmecsci.2012.12.004>.
- [89] Alghamdi Ahmad, David Downing, Matthew McMillan, Milan Brandt, Ma Qian, and Martin Leary. "Experimental and Numerical Assessment of Surface Roughness for Ti6Al4V Lattice Elements in Selective Laser Melting." In: *International Journal of Advanced Manufacturing Technology* , v. 105, p. 1275-1293 , 2019. DOI: <https://doi.org/10.1007/s00170-019-04092-4>.
- [90] Galati Manuela, Minetola Paolo, Rizza Giovanni. "Surface Roughness Characterisation and Analysis of the Electron Beam Melting (EBM) Process." In: *Materials* , v. 12, p. 1-13 , 2019. DOI: <https://doi.org/10.3390/ma12132211>.
- [91] Salmi A., Atzeni E. "Residual stress analysis of thin AlSi10Mg parts produced by Laser Powder Bed Fusion." In: *Materials* , v. 15, p. 1-13 , 2019. DOI: <https://doi.org/10.1080/17452759.2019.1650237>.
- [92] Calignano Flaviana and Minetola Paolo. "Influence of Process Parameters on the Porosity, Accuracy, Roughness, and Support Structures of Hastelloy X Produced by Laser Powder Bed Fusion." In: *Materials* , v. 12, p. 3178 , 2019. DOI: <https://doi.org/10.3390/ma12193178>.
- [93] Aversa Alberta, Saboori Abdollah, Librera Erica, Chirico Michele, Biamino Sara, Lombardi Mariangela, Fino Paolo. "The Role of Directed Energy Deposition Atmosphere Mode on the Microstructure and Mechanical Properties of 316L Samples." In: *Additive Manufacturing* , v. 34, p. 101274 , 2020. DOI: <https://doi.org/10.1016/j.addma.2020.101274>.
- [94] Karimi Neghlani Paria, Tahira Raza, Joel Andersson, and Lars-Erik Svensson. "Influence of Laser Exposure Time and Point Distance on 75- $\mu$ m-thick Layer of Selective Laser Melted Alloy 718." In: *The International Journal of Advanced Manufacturing Technology* , v. 94, p. 2199 , 2018. DOI: <https://doi.org/10.1007/s00170-017-1019-1>.
- [95] Soltani Tehrani Arash, Habibnejad-Korayem Mahdi, Shao Shuai, Haghshenas Meysam, Shamsaei Nima. "Ti-6Al-4V Powder Characteristics in Laser Powder Bed Fusion: The Effect on Tensile and Fatigue Behavior." In: *Additive Manufacturing* , v. 51, p. 102584 , 2021. DOI: <https://doi.org/10.1016/j.addma.2021.102584>.
- [96] Qiu Chunlei, Sheng Yue, Nicholas J.E Adkins, Mark Ward, Hany Hassanin, Peter D Lee, Philip J Withers, and Moataz M Attallah. "Influence of Processing Conditions on Strut Structure and Compressive Properties of Cellular Lattice Structures Fabricated by Selective Laser Melting." In: *Materials Science & Engineering. A*,

- Structural Materials : Properties, Microstructure and Processing* , v. 628, p. 188-197 , 2015. DOI: <https://doi.org/10.1016/j.msea.2015.01.031>.
- [97] Roudnicka Michaela, Jiri Bigas, and Dalibor Vojtech. “Tuning Porosity and Mechanical Properties of Ti6Al4V Alloy Additively Manufactured by SLM.” In: *Key Engineering Materials* , v. 865, p. 1-5, 2020. DOI: <https://doi.org/10.4028/www.scientific.net/kem.865.1>.
- [98] Brandt Milan. *Laser Additive Manufacturing.*, Cambridge, Elsevier Science & Technology, 2016.
- [99] Terrazas-Najera, C.A. and Mayoral, F.L. and Garcia, O.F. and Hossain, M.S. and Espalin, D. and Fernandez, A. and Murr, Lawrence and Wicker, R.B. “Effects of process interruptions on microstructure and mechanical properties of three face centered cubic alloys processed by laser powder bed fusion.” In: *Journal of Manufacturing Processes* , v. 66, p. 397-406, 2021. DOI: <https://doi.org/10.1016/j.jmapro.2021.04.013>.
- [100] Wang Zihong, Lin Xin, Kang Nan, Wang Yanfang, Yu Xiaobin, Tan Hua, Yang Haiou, Huang Weidong. “Making selective-laser-melted high-strength Al–Mg–Sc–Zr alloy tough via ultrafine and heterogeneous microstructure.” In: *Scripta Materialia* , v. 203, p. 114052, 2021. DOI: <https://doi.org/10.1016/j.scriptamat.2021.114052>.
- [101] Geiger Fabian, Karsten Kunze, and Thomas Etter. “Tailoring the Texture of IN738LC Processed by Selective Laser Melting (SLM) by Specific Scanning Strategies.” In: *Materials Science & Engineering. A, Structural Materials : Properties, Microstructure and Processing* , v. 661, p. 240-46, 2016. DOI: <https://doi.org/10.1016/j.msea.2016.03.036>.
- [102] Galetto Maurizio, Genta Gianfranco, Maculotti Giacomo, Verna Elisa. “Defect Probability Estimation for Hardness-Optimised Parts by Selective Laser Melting.” In: *International Journal of Precision Engineering and Manufacturing* , v. 21, p. 1739-1753, 2020. DOI: <https://doi.org/10.1007/s12541-020-00381-1>.
- [103] Yang Ho., Zhang Sy., Lin X. et al. “Influence of processing parameters on deposition characteristics of Inconel 625 superalloy fabricated by laser solid forming.” In: *Journal of Central South University* , v. 28, p. 1003-1014, 2021. DOI: <https://doi.org/10.1007/s11771-021-4675-0>.
- [104] Krishnan Manickavasagam, Atzeni Eleonora, Canali Riccardo, Calignano Flaviana, Manfredi Diego, Ambrosio Elisa, Iuliano Luca. “On the effect of process parameters

- on properties of AlSi10Mg parts produced by DMLS.” In: *Rapid Prototyping Journal* , v. 20, p. 449-458, 2014. DOI: <https://doi.org/10.1108/RPJ-03-2013-0028>.
- [105] Marchese G., Parizia S., Saboori A., Manfredi D., Lombardi M., Fino P., Ugues D., Biamino S. ”The influence of the process parameters on the densification and microstructure development of laser powder bed fused Inconel 939.” In: *Metals* , v. 10, p. 1-19, 2020. DOI: <https://doi.org/10.3390/met10070882>.
- [106] H. Gong. “Generation and detection of defects in metallic parts fabricated by selective laser melting and electron beam melting and their effects on mechanical properties.” Dissertation, Doctor of Philosophy, Department of Industrial Engineering, University of Louisville, Louisville, Kentucky, 2013.
- [107] Wolff Sarah J, Stephen Lin, Eric J Faierson, Wing Kam Liu, Gregory J Wagner, and Jian Cao. “A Framework to Link Localized Cooling and Properties of Directed Energy Deposition (DED)-processed Ti-6Al-4V.” In: *Acta Materialia* , v. 132 , p. 106-117, 2017. DOI: <https://doi.org/10.1016/j.actamat.2017.04.027>.
- [108] Vrána Radek, Daniel Koutný, David Paloušek, Libor Pantělejev, Jan Jaroš, Tomáš Zikmund, and Jozef Kaiser. “Selective Laser Melting Strategy for Fabrication of Thin Struts Usable in Lattice Structures.” In: *Materials* , v. 11 , p. 1763, 2018. DOI: <https://doi.org/10.3390/ma11091763>.
- [109] Minetola, Paolo, Manuela Galati, Flaviana Calignano, Luca Iuliano, Giovanni Rizza, and Luca Fontana. “Comparison of Dimensional Tolerance Grades for Metal AM Processes.” In: *Procedia CIRP* , v. 88 , p. 399-404, 2020. DOI: <https://doi.org/10.1016/j.procir.2020.05.069>.
- [110] Calignano, Flaviana, Luca Iuliano, Manuela Galati, Paolo Minetola, and Giovanni Marchiandi. “Accuracy of Down-facing Surfaces in Complex Internal Channels Produced by Laser Powder Bed Fusion (L-PBF).” In: *Procedia CIRP* , v. 88 , p. 423-426, 2020. DOI: <https://doi.org/10.1016/j.procir.2020.05.073>.
- [111] Galati, Manuela, Oscar Di Mauro, and Luca Iuliano. “Finite Element Simulation of Multilayer Electron Beam Melting for the Improvement of Build Quality.” In: *Crytals* , v. 10 , p. 532, 2020. DOI: <https://doi.org/10.3390/cryst10060532>.
- [112] Xue Aitang, Xin Lin, Lilin Wang, Xufei Lu, Hanlin Ding, and Weidong Huang. “Heat-affected Coarsening of  $\beta$  Grain in Titanium Alloy during Laser Directed Energy Deposition.” In: *Scripta Materialia* , v. 205 , p. 114180, 2021. DOI: <https://doi.org/10.1016/j.scriptamat.2021.114180>.

- [113] Asma El Elmi et al. “Experimental and numerical investigation of selective laser melting–induced defects in Ti–6Al–4V octet truss lattice material: the role of material microstructure and morphological variations.” In: *Journal of Materials Research* , v. 35 , p. 1-13, 2020. DOI: <https://doi.org/10.1557/jmr.2020.75>.
- [114] Gerstgrasser M., M. Cloots, and K. Wegener. “Surface Quality Improvement and Adjustment of SLM-processed CM247LC Samples by Modulated Laser Parameters.” In: *Procedia CIRP* , v. 95 , p. 109-114, 2020. DOI: <https://doi.org/10.1016/j.procir.2020.01.175>.
- [115] Tawfik Samer M., Mohamed N.A. Nasr, and Hassan A. El Gamal. “Finite Element Modelling for Part Distortion Calculation in Selective Laser Melting.” In: *Alexandria Engineering Journal* , v. 58, p. 67-74, 2019. DOI: <https://doi.org/10.1016/j.aej.2018.12.010>.
- [116] Ansari Peyman, Asif Ur Rehman, Fatih Pitir, Salih Veziroglu, Yogendra Kumar Mishra, Oral Cenk Aktas, and Metin U Salamci. “Selective Laser Melting of 316L Austenitic Stainless Steel: Detailed Process Understanding Using Multiphysics Simulation and Experimentation.” In: *Metals* , v. 11, p. 1076, 2021. DOI: <https://doi.org/10.3390/met11071076>.
- [117] Chen, Zhehan, Xianhui Zong, and Xiaohua Zhang. “Analysis of the Temperature Field during the Selective Laser Melting Process Based on a Finite Element Model.” In: *International Journal of Manufacturing Research* , v. 14, p. 355-372, 2019. DOI: <https://doi.org/10.1504/IJMR.2019.10026082>.
- [118] Galati, Manuela, Luca Iuliano, Alessandro Salmi, and Eleonora Atzeni. “Modelling Energy Source and Powder Properties for the Development of a Thermal FE Model of the EBM Additive Manufacturing Process.” In: *Additive Manufacturing* , v. 14, p. 49-59, 2017. DOI: <https://doi.org/10.1016/j.addma.2017.01.001>.
- [119] Cao Yang, Xin Lin, Nan Kang, Liang Ma, Lei Wei, Min Zheng, Jun Yu, Dongjian Peng, and Weidong Huang. “A Novel High-efficient Finite Element Analysis Method of Powder Bed Fusion Additive Manufacturing.” In: *Additive Manufacturing* , v. 46, p. 102187, 2021. DOI: <https://doi.org/10.1016/j.addma.2021.102187>.
- [120] Hu, Yunlong, Xin Lin, Yunlong Li, Shuya Zhang, Qiang Zhang, Weimin Chen, Wei Li, and Weidong Huang. “Influence of Heat Treatments on the Microstructure and Mechanical Properties of Inconel 625 Fabricated by Directed Energy Deposition.” In: *Materials Science and Engineering: A* , v. 817, p. 141309, 2021. DOI: <https://doi.org/10.1016/j.msea.2021.141309>.

- [121] Wang, Zihong, Xin Lin, Nan Kang, Jing Chen, Hua Tan, Zhe Feng, Zehao Qin, Haiou Yang, and Weidong Huang. "Laser Powder Bed Fusion of High-strength Sc/Zr-modified Al-Mg Alloy: Phase Selection, Microstructural/mechanical Heterogeneity, and Tensile Deformation Behavior." In: *Journal of Materials Science & Technology*, v. 95, p. 40-56, 2021. DOI: <https://doi.org/10.1016/j.jmst.2021.03.069>.
- [122] Sundarraaj, Suresh, Sion Pickard, Alonso Peralta, Anil Chaudhary, David Snyder, Jeff W Doak, Suraj Rawal, Ray Xu, Sesh Tamirisakandala, Albert Contreras, John Meyer, Andrzej Wojcieszynski, Derrick Lamm, and Edwin Schwalbach. "ICME Based Additive Manufacturing of Alloy 230 Components." In: *Proceedings of the 9th International Symposium on Superalloy 718 & Derivatives: Energy, Aerospace, and Industrial Applications.*, Cham: Springer International, v. 2018, p. 133-146, 2018, The Minerals, Metals & Materials. DOI: [https://doi.org/10.1007/978-3-319-89480-5\\_7](https://doi.org/10.1007/978-3-319-89480-5_7).
- [123] Galati, Manuela, Abdollah Saboori, Sara Biamino, Flaviana Calignano, Mariangela Lombardi, Giovanni Marchiandi, Paolo Minetola, Paolo Fino, and Luca Iuliano. "Ti-6Al-4V Lattice Structures Produced by EBM: Heat Treatment and Mechanical Properties." In: *Procedia CIRP*, v. 88, p. 411-416, 2020. DOI: <https://doi.org/10.1016/j.procir.2020.05.071>.
- [124] Del Guercio, G., M. Galati, and A. Saboori. "Electron Beam Melting of Ti-6Al-4V Lattice Structures: Correlation between Post Heat Treatment and Mechanical Properties." In: *The International Journal of Advanced Manufacturing Technology*, v. 116, p. 1-13, 2021. DOI: <https://doi.org/10.1007/s00170-021-07619-w>.
- [125] Théo Persenot et al. "Enhancing the tensile properties of EBM as-built thin parts: Effect of HIP and chemical etching". In: *Materials Characterization*, v. 143, p. 82-93, 2018. DOI: <https://doi.org/10.1016/j.matchar.2018.01.035>.
- [126] Abu-Issa Ahmad, Miguel Lopez, Christina Pickett, Andres Escarcega, Edel Arrieta, Lawrence E Murr, Ryan B Wicker, Magnus Ahlfors, Don Godfrey, and Francisco Medina. "Effects of Altered Hot Isostatic Pressing Treatments on the Microstructures and Mechanical Performance of Electron Beam Melted Ti-6Al-4V." In: *Journal of Materials Research and Technology*, v. 9, p. 8735-8743, 2020. DOI: <https://doi.org/10.1016/j.jmrt.2020.06.019>.
- [127] Zhang Shuya, Xin Lin, Lilin Wang, Xiaobin Yu, Yunlong Hu, Haiou Yang, Liming Lei, and Weidong Huang. "Strengthening Mechanisms in Selective Laser-melted Inconel718 Superalloy." In: *Materials Science & Engineering. A*,

- Structural Materials : Properties, Microstructure and Processing* , v. 812, p. 141145, 2021. DOI: <https://doi.org/10.1016/j.msea.2021.141145>.
- [128] Kořínek, Michal, Radim Halama, František Fojtík, Marek Pagáč, Jiří Krček, David Krzikalla, Radim Kocich, and Lenka Kunčická. “Monotonic Tension-torsion Experiments and Fe Modeling on Notched Specimens Produced by Slm Technology from Ss316l.” In: *Materials* , v. 14, p. 1-15, 2021. DOI: <https://doi.org/10.3390/ma14010033>.
- [129] Segura, I.A, L.E Murr, C.A Terrazas, D. Bermudez, J. Mireles, V.S.V Injeti, K. Li, B. Yu, R.D.K Misra, and R.B Wicker. “Grain Boundary and Microstructure Engineering of Inconel 690 Cladding on Stainless-steel 316L Using Electron-beam Powder Bed Fusion Additive Manufacturing.” In: *Journal of Materials Science & Technology* , v. 35, p. 351-367, 2019. DOI: <https://doi.org/10.1016/j.jmst.2018.09.059>.
- [130] Varela Jaime, Jorge Merino, Christina Pickett, Ahmad Abu-Issa, Edel Arrieta, Lawrence E Murr, Ryan B Wicker, Magnus Ahlfors, Donald Godfrey, and Francisco Medina. “Performance Characterization of Laser Powder Bed Fusion Fabricated Inconel 718 Treated with Experimental Hot Isostatic Processing Cycles.” In: *Journal of Manufacturing and Materials Processing* , v. 4, p. 73, 2020. DOI: <https://doi.org/10.3390/jmmp4030073>.
- [131] Marchese Giulio, Atzeni Eleonora, Salmi Alessandro and Biamino Sara. “Microstructure and Residual Stress Evolution of Laser Powder Bed Fused Inconel 718 under Heat Treatments.” In: *Journal of Materials Engineering and Performance* , v. 30, p. 565-574, 2021 . DOI: <https://doi.org/10.1007/s11665-020-05338-z>.
- [132] Barros Rafael, Francisco J. G Silva, Ronny M Gouveia, Abdollah Sa-boori, Giulio Marchese, Sara Biamino, Alessandro Salmi, and Eleonora Atzeni. “Laser Powder Bed Fusion of Inconel 718: Residual Stress Analysis Before and After Heat Treatment.” In: *Metals* , v. 9, p. 1290, 2021. DOI: <https://doi.org/10.3390/met9121290>.
- [133] Liu Lu, Paul Kamm, Francisco García-Moreno, John Banhart, and Damiano Pasini. “Elastic and Failure Response of Imperfect Three-dimensional Metallic Lattices: The Role of Geometric Defects Induced by Selective Laser Melting.” In: *Journal of the Mechanics and Physics of Solids* , v. 107, p. 160-184, 2017. DOI: <https://doi.org/10.1016/j.jmps.2017.07.003>.
- [134] Lozanovski, Bill, Martin Leary, Phuong Tran, Darpan Shidid, Ma Qian, Peter Choong, and Milan Brandt. “Computational Modelling of Strut Defects in SLM

- Manufactured Lattice Structures.” In: *Materials & Design* , v. 171, p. 107671, 2019. DOI: <https://doi.org/10.1016/j.matdes.2019.107671>.
- [135] Jiang Panwei, Mustafa Rifat, and Saurabh Basu. “Impact of Surface Roughness and Porosity on Lattice Structures Fabricated by Additive Manufacturing- A Computational Study.” In: *Procedia Manufacturing* , v. 48, p. 781-789, 2020. DOI: <https://doi.org/10.1016/j.promfg.2020.05.1141>.
- [136] Soylemez, Emrecan. “Modelling the Melt Pool of the Laser Sintered Ti6Al4V Layers with Goldak’s Double-Ellipsoidal Heat Source.” 2018. Link: [https://www.researchgate.net/figure/Single-bead-cross-section-area-and-visual-definitions-of-the-melt-pool-size\\_fig4\\_328792215](https://www.researchgate.net/figure/Single-bead-cross-section-area-and-visual-definitions-of-the-melt-pool-size_fig4_328792215).
- [137] Merino Jorge, Bryan Ruvalcaba, Jaime Varela, Edel Arrieta, Lawrence E Murr, Ryan B Wicker, Mark Benedict, and Francisco Medina. “Multiple, Comparative Heat Treatment and Aging Schedules for Controlling the Microstructures and Mechanical Properties of Laser Powder Bed Fusion Fabricated AlSi10Mg Alloy.” In: *Journal of Materials Research and Technology* , v. 13, p. 669-685, 2021. DOI: <https://doi.org/10.1016/j.jmrt.2021.04.062>.
- [138] Brusa, Eugenio, Raffaella Sesana, and Enrico Ossola. “Numerical Modeling and Testing of Mechanical Behavior of AM Titanium Alloy Bracket for Aerospace Applications.” In: *Procedia Structural Integrity* , v. 5, p. 753-760, 2017. DOI: <https://doi.org/10.1016/j.prostr.2017.07.166>.
- [139] Hiller Simon, Weber Patrick, Rust Hendrik, Lasi Heiner. “Identifying Business Potentials of Additive Manufacturing as Part of Digital Value Creation in SMEs – An Explorative Case Study.” In: *Procedia CIRP* , v. 33, p. 394-99, 2015. DOI: <https://doi.org/10.24251/HICSS.2020.552>.
- [140] L. Rickenbacher, A. Spierings, and K. Wegener, “An integrated cost model for selective laser melting (SLM)”. In: *Rapid Prototyping J.* , v. 19, p. 208-214, 2013. DOI: <https://doi.org/10.1108/13552541311312201>.
- [141] M. Schröder, B. Falk, R. Schmitt, and X. Boucher. “Evaluation of cost structures of additive manufacturing processes using a new business model”. In: *Procedia CIRP* , v. 30, p. 311–316, 2015. DOI: <https://doi.org/10.1016/j.procir.2015.02.144>.
- [142] Facchini, F., De Chirico, A., Mummolo, G. “Comparative Cost Evaluation of Material Removal Process and Additive Manufacturing in Aerospace Industry”.

- In: *Industrial Engineering and Operations Management I* , Cham: Springer International , p. 47-59, 2019. DOI: [https://doi-org.ezproxy.biblio.polito.it/10.1007/978-3-030-14969-7\\_5](https://doi-org.ezproxy.biblio.polito.it/10.1007/978-3-030-14969-7_5).
- [143] M. Baumers, P. Dickens, C. Tuck, and R. Hague, “The cost of additive manufacturing: Machine productivity, economies of scale, and technology push”. In: *Technological Forecasting Social Change* , v. 102, p. 193–201, 2016. DOI: <https://doi.org/10.1016/j.techfore.2015.02.015>.
- [144] A. Mahadik and D. Masel, “Implementation of additive manufacturing cost estimation tool (AMCET) using break-down approach.” In: *Procedia Manuf.* , v. 17, p. 70–77, 2018. DOI: <https://doi.org/10.1016/j.promfg.2018.10.014>.
- [145] Ingarao G., Priarone P. C., “A comparative assessment of energy demand and life cycle costs for additive- and subtractive-based manufacturing approaches.” In: *JOURNAL OF MANUFACTURING PROCESSES* , v. 56, p. 1219-1229, 2020. DOI: <https://doi.org/10.1016/j.jmapro.2020.06.009>.
- [146] Würtz Günther, Heiner Lasi, and Dominik Morar. “Additive Manufacturing-enabling Technology for Lifecycle Oriented Valueincrease or Value-decrease.” In: *Procedia CIRP* , v. 33, p. 394-99, 2015. DOI: <https://doi.org/10.1016/j.promfg.2018.10.014>.
- [147] Sauerwein, Marita, Eugeni Doubrovski, Ruud Balkenende, and Conny Bakker. “Exploring the Potential of Additive Manufacturing for Product Design in a Circular Economy.” In: *Journal of Cleaner Production* , v. 226 , p. 1138-149, 2019. DOI: <https://doi.org/10.1016/j.jclepro.2019.04.108>.
- [148] Naghshineh, Bardia, Francisco Lourenço, Radu Godina, Celeste Jacinto, and Helena Carvalho. “A Social Life Cycle Assessment Framework for Additive Manufacturing Products.” In: *Applied Sciences* , v. 10 , p. 4459, 2020. DOI: <https://doi.org/10.3390/app10134459>.